N-63-4-3

R-898

DAVIDSON LABORATORY

Report 898

a. Qualified requesters may obtain copies of this report direct from DDC.

PREDICTION OF TRAJECTORIES FOR AN UNDERWATER MISSILE

by

Howard Dugoff

February 1963

R-898

DAVIDSON LABORATORY
REPORT 898

February 1963

PREDICTION OF TRAJECTORIES FOR AN UNDERWATER MISSILE

by

Howard Dugoff

Prepared under sponsorship of
Bureau of Naval Weapons
Contract Now 60-0341-d
DL Project LM 2328

Approved

A. Strumpf

Albert Strumpf
Head, Underwater
Weapons Division

ABSTRACT

Nonlinear motion equations were used to predict vertical planar trajectories of the Basic Finner Missile observed previously in underwater model experiments at California Institute of Technology. Values of the hydrodynamic coefficients appearing in the motion equations were obtained from Basic Finner experiments made previously at CIT, Bureau of Standards, and Davidson Laboratory. Coefficients also were estimated on theoretical grounds. The observed trajectories could not be predicted using experimental coefficients alone. However, theoretical coefficients yielded predictions that agreed well with the observed motions. Computed trajectories were particularly sensitive to independent changes in the values of the hydrodynamic static and damping derivative coefficients. However, when these values were kept consistent with relations expressing their physical interdependence, they could be varied over fairly wide ranges without appreciably affecting the predictions.

TABLE OF CONTENTS

	Page
Abstract	iii
Introduction	1
Equations of Motion	5
Hydrodynamic Coefficients	10
Trajectory Predictions	19
High Speed Vertical Planar Trajectories	19
Straight Horizontal Trajectory	27
Low Speed Vertical Planar Trajectories	31
Straight Vertical Trajectories	33
Conclusions	39
Acknowledgment	42
References	42
Appendix A - Nomenclature	A-1
Appendix B - Evaluation of Hydrodynamic Derivative Coefficients	B-1
Appendix C - Solution of Vertical Planar Motion Equations	C-1
Tables	
Figures	

INTRODUCTION

The main purpose of this study is to determine whether observed underwater trajectories of the Basic Finner Missile can be predicted using equations of motion and hydrodynamic coefficients obtained from experiment or theory. The current work is part of a larger program, sponsored by the Bureau of Naval Weapons, to verify present day trajectory prediction methods.

The Basic Finner Missile (Fig. 1) consists of a cylindrical shaft, pointed at the forward end, and a set of large, wedge-shaped, cruciform tail fins. Although used for research in both aerodynamics and hydrodynamics, it is essentially prototypal of a supersonic aerodynamic missile. Partly because of its blunt base, but primarily because of the great size of its fins, the hydrodynamic reactions it develops in underwater flight are extremely large compared with those on a typical hydrodynamic body (e.g., missiles, torpedoes, submarines) of similar length and cross-sectional area, flying at the same speed and attitude. Consequently, the hydrodynamic derivative coefficients for the Basic Finner not only are very large compared with those of more representative underwater craft,[1] but also are influenced abnormally by the lift and drag characteristics of its fin configuration.

Measurements of the hydrodynamic forces and moments acting on Basic Finner models under various conditions have been made by Kermeen,[2] Kiceniuk,[3,4] Heald and Adams,[5] and Savitsky and Prowse.[6] Extensive model trajectory measurements have been reported by Price.[7] Stubstad,[8] Parrish,[9] and Stubstad and Waugh[10] also have published results of trajectory tests. In addition, some heretofore unpublished Basic Finner trajectory data have been made available to Davidson Laboratory by the Bureau of Naval Weapons.

Some work has been done also in comparing measured Basic Finner trajectory data with results obtained using motion equations. Price[7] and Stubstad and Waugh[10] have employed nonlinear motion equations as models for curve-fits of observed trajectory data, to define hydrodynamic force functions numerically. Stubstad[8] has used the solution of a linear system of motion equations as a basis for curve-fitting observed trajectory data to obtain the numerical values of three physical constants. Caster[11] also has curve-fitted observed trajectory data, by specifying all but one of the hydrodynamic terms appearing in a system of nonlinear motion equations and varying the unspecified term. Parrish[9] has compared observed trajectory data with results computed using a linear system of motion equations. Of all the previous work, however, only Parrish's is an actual comparison of computed and observed trajectories, and this, being a single comparison, is not a sufficient basis for any definite conclusions regarding either the correct forms of the motion equations or the adequacy of the hydrodynamic data.

The model trajectory experiments forming the basis for comparison with the trajectories predicted herein include those reported by Price,[7] and some supplied directly to Davidson Laboratory by the Bureau of Naval Weapons. The experiments were performed at the Controlled Atmosphere Launching Tank of the California Institute of Technology (CIT).[7]

The Price results are vertical planar trajectories in which heavier-than-water models are dropped from rest. Both straight (seven runs) and curved (eight runs) vertical trajectories are included. The results supplied by the Bureau of Naval Weapons are vertical planar trajectories in which heavier-than-water (eight runs), lighter-than-water (two runs), and neutrally buoyant (one run) models are launched with nonzero horizontal velocities.

These results all belong to the class of vertical planar trajectories. For purposes of the present study, they were categorized further according to the number of degrees of freedom of the motion and the type of initial conditions. Four categories were established: high speed vertical planar trajectories, low speed vertical planar trajectories, straight vertical trajectories, and a straight horizontal trajectory.

The first and fourth categories include the trajectories supplied by the Bureau of Naval Weapons; the second and third consist of the results reported by Price. Differentiation between the data from the two sources is based on the prevailing flow conditions. In each trajectory reported by Price, the model is dropped from rest. Hence, the motions run in or, at least, through the laminar flow regime. In the runs supplied by BuWeps, the model is launched at high enough velocity so that the flow is turbulent throughout virtually the entire trajectory. Moreover, the angles of attack attained in the high speed (BuWeps) trajectories are restricted to the range $|\alpha| < 6.5^{\circ}$, whereas attack angles as high as $\alpha = 30^{\circ}$ are attained in the low speed (Price) runs.

Since actual motions of full-scale missiles are invariably in the turbulent flow regime, the results of the present study of primary practical importance are those pertaining to the high speed (BuWeps) trajectories. Although emphasis apparently was about evenly divided between high and low speed trajectories in the phase of the Basic Finner program devoted to vertical planar trajectory measurements, the relative unimportance of the low speed motions appears to have been considered in the planning of the hydrodynamic force and moment measurements. These essentially were restricted to Reynolds number in the range $0.4 \times 10^{6} \leq R_e \leq 8.5 \times 10.^{6}$ This is similar to the ranges attained in the high speed trajectories, but ignores the range $0 \leq R_e \leq 0.4 \times 10,^{6}$ included in each of

the low speed trajectories. Similarly, the range of attack angles covered in the force and moment measurements, $-13^{\circ} \leq \alpha \leq 20^{\circ}$, encompasses those attained in the high speed trajectories but not those of the low speed runs.

The reason for differentiating between the one degree of freedom and three degrees of freedom trajectories is that with zero angle of attack (one degree of freedom trajectories), the complexity of the hydrodynamic reactions is very much reduced due to the symmetry of the flow. Since Reynolds number and angle of attack effects are strongly coupled, this distinction is particularly significant for the case of the low speed trajectories, where the ranges of flight angle of attack are greatest and where the available hydrodynamic force and moment data are most limited.

This research was performed under the sponsorship of the Bureau of Naval Weapons under BuWeps Contract NOW 60-0341-d and DL Project LM 2328.

EQUATIONS OF MOTION

The motion equations used in the prediction of the Basic Finner model trajectories were derived from general equations of motion for a submerged body formulated by Strumpf.[12] The general equations were simplified by the following assumptions:

1. The mass and mass distribution of the body do not vary with time.
2. The body possesses both horizontal and vertical planes of symmetry.
3. No thrust or control forces or moments act on the body.
4. The center of gravity lies on the longitudinal centerline of the body.
5. The products of inertia are zero.
6. The moments of inertia about the y and z axes are equal.*
7. The body is constrained to move in a vertical plane, i.e., $v=\dot{v}=r=\dot{r}=\psi=\phi=0$. (1)
8. The hydrodynamic derivatives X'_{ww}, X'_{qq}, $Z'_{\dot{q}}$, $M'_{\dot{w}}$ are equal to zero.
9. Hydrodynamic terms of order three and higher (e.g., terms of the form $Z'_{www}w^3$, $Z'_{qww}qw^2$) are negligible.

Assumptions 1 through 6 are based upon the physical properties of the tested Basic Finner model configurations. Assumption 7 restricts the general equations to the three degrees of freedom (vertical plane) cases considered in the present study. Assumption 8 is customary in analyses of this nature and is consistent with the results of previous research.[12,13]

---

* The coordinate system and definitions of all symbols used in this report are presented in Appendix A.

Assumption 9 was dictated by practical considerations. Provided the hydrodynamic forces and moments are analytic functions of the body velocity and acceleration components, they can be approximated theoretically to any accuracy by Taylor series expansions of sufficiently high order. In practical application, however, the inclusion of Taylor series terms of order higher than the first is discouraged by the limitations of available experimental and theoretical methods for determining the numerical values of nonlinear hydrodynamic derivatives. The usual practice in past trajectory prediction work has been to employ linear equations.[8,9,14] The equations used in the present study, however, represent a compromise. Although most nonlinear hydrodynamic effects are neglected, all inertial and gravity forces and moments are included. The drawbacks of linear equations are reduced, whereas the amount of required hydrodynamic data is kept to a minimum. Like linearized equations, however, the present motion equations should not be expected to apply to cases where the hydrodynamic forces and moments are highly nonlinear and the motions deviate appreciably from the point, u, v, w, ...=u, 0, 0, ... (α=0), about which the Taylor series are expanded.[12]

On the basis of assumptions 1 through 9, the general longitudinal force equation, vertical force equation, and pitching moment equation,[12] respectively, reduce to

$$m(\dot{u}+qw-x_G q^2) = -(W-B)\sin\theta + \frac{\rho}{2} A_x X'_0(u^2+w^2) + \frac{\rho}{2} A_x \ell (X'_{\dot{u}}\dot{u} + X'_{wq} wq), \quad (2)$$

$$m(\dot{w}-qu-x_G\dot{q}) = (W-B)\cos\theta + \frac{\rho}{2} A_x Z'_w uw + \frac{\rho}{2} A_x \ell (Z'_{\dot{w}}\dot{w} + Z'_q uq), \quad (3)$$

$$I_{yy}\dot{q} + mx_G(qu-\dot{w}) = -Wx_G\cos\theta + \frac{\rho}{2} A_x \ell^3 M'_{\dot{q}}\dot{q} + \frac{\rho}{2} A_x \ell^2 M'_q uq + \frac{\rho}{2} A_x \ell M'_w uw^{*} \quad (4)$$

All of the quantities appearing in these equations are defined in the Nomenclature (Appendix A) and thoroughly discussed in ref. 12, which is readily available. Accordingly, no detailed discussion will be presented here. However, the various terms

* The subsidiary relation required for solution of these equations reduces to $q = \dot{\theta}$ (see Appendix C).

will be described in a general way. The terms on the left-hand side of each equation are inertial terms; the familiar "$\frac{d}{dt}(mV)$" and "$\frac{d}{dt}(I\omega)$" terms of Newton's second law. The first terms on the right-hand side of the equations are forces and moments arising due to the influence of gravity. All other terms are forces and moments of hydrodynamic origin. Note that the artifice of introducing the so-called "virtual masses" and "virtual moments of inertia," common in the formulation of motion equations for hydrodynamic bodies, is avoided. No distinction is drawn between the hydrodynamic reactions (e.g., $\frac{\rho}{2}A_x \ell X|_{\dot{u}}\dot{u}$) often accounted for in this way,[13,15] and any other hydrodynamic forces and moments.

Equations 2 through 4 are the equations of vertical planar motion employed in this study. They were used in the predictions for both high speed and low speed vertical planar trajectories. However, their applicability to the two different cases is far from equal. Under the conditions prevailing in the important case of the high speed trajectories, all assumptions made in their derivation are reasonable. In these runs, the flight angles of attack are restricted to a range ($|\alpha| < 6.5^\circ$) in which the available data[5] indicate that the nonlinear angle of attack dependence (or, equivalently, w-dependence) of the hydrodynamic forces and moments is not significant. No Basic Finner force and moment data for non-zero values of pitch angular velocity q are available, but results of previous Davidson Laboratory studies[16,17] indicate that q-w coupling and nonlinear q terms may reasonably be neglected for the ranges of angular velocity ($q' < 0.2$) and angle of attack attained in the high speed runs.

The situation is vastly different for the case of the low speed trajectories. Angles of attack as great as 30° are attained in some of these flights. Under these conditions, higher order Taylor series terms definitely are required to

represent the hydrodynamic reactions accurately. Hence the present mathematical model for the hydrodynamic forces and moments is clearly unrealistic under the conditions prevailing in the low speed vertical planar trajectories.

The extreme attack angles in these runs invariably are attained in conjunction with Reynolds numbers lower than the minimum value (0.4×10^6) covered in the Basic Finner force and moment measurements.[2-6] Hence no experimental data for direct evaluation of the nonlinear hydrodynamic effects is available unless it can be assumed that such effects are not significantly Reynolds number dependent. But such an assumption would be in contradiction to previous experience.[18,19] In any event, no Basic Finner force and moment data are available for $|\alpha| > 20^\circ$, at any Reynolds number. Because of the limited practical importance of such low Reynolds number motions of hydrodynamic missiles, applicable experimental data for other configurations similar to the Basic Finner are not available either. Finally, reliable methods for evaluating the required quantities theoretically have not been developed.

Since the low speed vertical planar trajectories are of little practical interest anyway, it was felt that efforts to obtain additional detailed hydrodynamic force and moment data for the low Reynolds number-high attack angle regime were not warranted. However, since the trajectory measurements had been completed already and the results were available,[7] it was felt that an attempt should be made to predict them using the present motion equations.

For the straight horizontal trajectory prediction, eqs. 2 through 4 are modified by the substitutions

$$w = \dot{w} = q = \dot{q} = \theta = x_g = W - B = 0 \qquad (5)$$

Only the longitudinal force equation remains nontrivial, reducing to

$$m\dot{u} = \frac{\rho}{2} A_x X'_o u^2 + \frac{\rho}{2} A_x \ell X'_{\dot{u}} \dot{u} \tag{6}$$

Similarly, for the straight vertical trajectory predictions, the substitutions

$$w = \dot{w} = q = \dot{q} = 0 \ , \quad \theta = -\frac{\pi}{2} \ , \tag{7}$$

yield, simply,

$$m\dot{u} = \frac{\rho}{2} A_x X'_o u^2 + \frac{\rho}{2} A_x \ell X'_{\dot{u}} \dot{u} + (W-B) \tag{8}$$

Note that the restrictions to one degree of freedom motions yield equations (eqs. 6 and 8, respectively, for horizontal and vertical flight) which, although nonlinear, nevertheless are soluble by exact analytic methods, which the three degrees of freedom equations (eqs. 4 through 6) are not (see Appendix C). This simplification in computation is matched by the reduction in the complexity of the actual physical situation resulting from the absence of angles of attack or angular velocities.

HYDRODYNAMIC COEFFICIENTS

There are two major sources of error in predicting underwater trajectories with motion equations.[12] The first is in the functional representations given to the external forces and moments, particularly those of hydrodynamic origin, acting on the missile during flight (discussed in the preceding section). The second is in the numerical values used for the various quantities appearing in the motion equations. Since such quantities as the density of water, the length of the missile, its cross-sectional area, weight, displacement, moment of inertia, and CG location presumably are known with great accuracy, the crux of this problem lies in the hydrodynamic derivative coefficients. For the Basic Finner, values for these quantities are available from the results of several experiments,[2-6] as well as from calculations based on a number of existing theories.

The important features of each of the experiments whose data were used to obtain values for the hydrodynamic force and moment derivative coefficients are summarized in Table I.

The experimental methods customarily employed for evaluating hydrodynamic force and moment derivative coefficients can be divided into two general classes. The first class consists of "static" methods, in which forces and moments acting on a model are measured directly as functions of the linear and angular velocity and acceleration components (and any other pertinent variables). Then the derivatives are evaluated from the data according to their definitions, e.g., Z'_w is the slope of the curve of Z' vs w', with $u'=u'_o$, $\dot{u}'=v'=\dot{v}'=\dot{w}'=p'=\dot{p}'=\ldots=0$, evaluated at the point $w'=0$. In the second general class of experimental methods, the forces and moments are not measured. Instead, forced oscillatory

motions of the model are induced, and such quantities as displacement response amplitude and phase lag are recorded. The hydrodynamic forces and moments are expressed as linear functions of the velocity and acceleration components of the model relative to the fluid, and combined with similar linear representations for the applied forces and moments of mechanical origin, in a system of linear motion equations whose solutions are used to express the hydrodynamic derivatives in terms of the measured motion parameters. The second column of Table I characterizes each of the Basic Finner experiments as "static" or "oscillatory," depending upon the class to which it belongs.

The derivative coefficients obtained from the data of each experiment are listed in the third column of Table I. The derivation of these quantities from the available data consisted, generally, of three steps: 1) evaluation of derivatives from plotted data; 2) conversion to a standard nondimensionalization basis; and 3) adjustment to the x,y,z, coordinate system with origin at the CB. The fourth column of Table I, outlines these steps in detail for each result.

The values of each of the hydrodynamic derivative coefficients determined as indicated in Table I were plotted versus Reynolds number. Figure 2 shows such a plot for the case of the zeroth order derivative X'_o (the drag coefficient), the derivative for which the Reynolds number data are most extensive. Scatter between the various experiments at a given Reynolds number is as great as the variation with Reynolds number within a given experiment. This was found to be the general case when values for a coefficient were available from more than one source. On this basis, it was assumed that the influence of Reynolds number on the Basic Finner hydrodynamic derivative coefficients is negligible for Reynolds numbers in the range, $0.4 \times 10^6 \leq Re \leq 8.5 \times 10,^6$ the total range of the various experiments. This covers the ranges of

Reynolds number attained in all of the high speed vertical planar trajectories.

Experimentally derived values for the Basic Finner hydrodynamic derivative coefficients are presented in Table II. With the exception of the results obtained from the data of Heald and Adams,[5] these values represent averages estimated from all the data reported in each reference. The Heald and Adams data have been given added weight by considering separately the results of experiments using (four) different models. The emphasis on these data is in accordance with the relative thoroughness and clarity of the results presented in the various references.[2-6]

In general, there are substantial differences in measurements of hydrodynamic force and moment derivative coefficients for a supposedly identical configuration tested by different laboratories.[20,21] The present case is by no means an exception to this rule. The ranges of values determined from the various experiments for $X'_{\dot{w}}$, Z'_{w}, M'_{w}, and M'_{q} (the derivatives for which more than one value are available) are, respectively, 53%, 20%, 31%, and 133% of the average value for each. Perhaps more significantly, the ranges of these values determined from the results of a single laboratory, the National Bureau of Standards (reported by Heald and Adams[5]), are, respectively, 40%, 19%, 8%, and 44% of these same averages.

There are three major factors that generally contribute to the discrepancies between repeated experimental determinations of the hydrodynamic derivative coefficients. All undoubtedly are significant in the case of the Basic Finner results. The first is in the subjective methods used in handling the experimental data. Each of the values listed in Table II was established on the basis of at least one curve-fitting procedure. Some of these curve fits were performed at Davidson Laboratory in the course of the present study

(see Appendix B); others were performed at the facilities where the experiments were made. In some of the latter cases,[2,3,4] it is impossible to assess the importance of this factor directly, because the raw test data and/or descriptions of the curve-fitting techniques used are not available. It is reasonable to assume, however, that the uncertainty in fitting these data is no less than that in fitting the other Basic Finner data. That this uncertainty is significant can be seen clearly from the sample derivations of values for hydrodynamic coefficients from test data[5] presented in Appendix B. In fact, listing ranges of values in Table II might have been more appropriate than showing the discrete values. Thus, -11.9 (Table II, row 1, column 1) would be replaced by $-12.0 \leq Z'_w \leq -11.8$. Similarly, -2.4 (row 1, column 2) would be replaced by $-2.5 < M'_w < -2.2$. However, it was felt that the uncertainty in the tabulated values would be sufficiently apparent without introducing this additional complication.

The second factor contributing to the discrepancies between the repeated determinations of the hydrodynamic coefficients is actual physical differences in the hydrodynamic force and moment components measured under supposedly identical conditions. Such differences can arise from many sources. Perhaps the most obvious is variations between the test vehicles themselves. The sharp, characteristically supersonic lines of the Basic Finner are no doubt impossible to duplicate exactly. Possibly small differences in construction or even in surface roughness could have great enough influences on flow development to affect materially the lift and drag characteristics of the body and/or fins. A second source is errors in setting and/or measuring physical parameters. Even small errors in such quantities as angle of attack or flow velocity, or in the alignment of balances, can produce large discrepancies in reported values of force and moment coefficients. A third source common to all experimental

techniques, is the presence of the strut, i.e., the member which supports the test vehicle. Often, the measurements made include the effects of forces and moments acting on the strut as well as those acting on the test vehicle itself. In other cases, the measurements include only the reactions exerted on the test vehicle. In either event, the acting forces and moments can be different from those which would act if the strut were not present in the flow field. In certain of the Basic Finner experiments,[2,4] attempts were made to remove strut effects from the data by methods assuming linear superposition of hydrodynamic effects of different origin. In the remaining cases, strut interference either was assumed negligible,[3,5] or its influence was noted but not evaluated quantitatively.[6]

The remaining factor contributing to the discrepancies in the hydrodynamic coefficients is the presupposition of functional relationships between the hydrodynamic forces and moments and the various motion parameters. This factor is characteristic of the techniques categorized here as "oscillatory" methods (see Table I). These techniques depend upon the assumption that the hydrodynamic forces and moments acting during the tests are linear functions of the various velocity and acceleration components of the test vehicle relative to the fluid. However, since the test motions generally are extremely complicated oscillatory motions (much more complicated than the trajectories now being studied), it is questionable whether the assumption is well founded and, consequently, whether the oscillator derived values for the hydrodynamic coefficients are reliable.

Table II also includes a row of items labeled, "Values Estimated From Theory." This row lists discrete values for all the required hydrodynamic coefficients except the four static and damping derivative coefficients, Z'_w, M'_w, Z'_q, and M'_q. For these quantities, the table refers

to Fig. 3, which shows theoretically derived ranges for their values and the interrelationships between them.

The derivation of all the results presented in Table II and Fig. 3 is described in detail in Appendix B. However, the more important features of the derivations are pointed out and discussed in the present section.

The static and damping derivatives were estimated using two different theories. It is inherent in both theories that the static moment derivative coefficient, M'_w, and the damping force and moment derivative coefficients, Z'_q and M'_q, respectively, are all strongly dependent upon the static force derivative coefficient, Z'_w. In fact, the only differences in the results derived from the two theories as applied herein stem from differences in the estimates for Z'_w. Each method uses slender body theory to predict the contribution to Z'_w made by the bare hull. One of the methods, due to Flax and Lawrence,[32] uses low aspect ratio wing theory[23] to predict the contribution of the fins, and the results of Low and Stone,[24] Spreiter,[25] and Lennertz[40] to account for the fin-body interference effects. The other method, used in the past by Davidson Laboratory and others in airship and torpedo work, uses high aspect ratio wing theory, in conjunction with a fin aspect ratio augmentation based on geometric considerations, to predict z'_i, the contribution to Z'_w due to the force on the fin plus all fin-body interactions. The low aspect ratio theory predicts a value ($Z'_w = -13.7$) considerably greater in magnitude than that derived from the airship theory ($Z'_w = -11.6$). Reference to Table II, however, reveals that both values are included in the range of the experimental results for Z'_w.

A review was made of previous test results, to compare experimentally determined values for z'_i with values computed on the basis of each theory. The results of the review

were inconclusive, as illustrated by the comparisons presented in Table III for four different hydrodynamic missiles. The airship theory value is in closer agreement with the measurement in three of the four cases. However, the opposite is true in the fourth case, which is one of a number of such cases reported by Flax and Lawrence.[22]

The influence of Z'_w on the other static and damping derivatives is dependent upon the parameter x_1, the longitudinal coordinate of the point of application of z_1 (see Appendix B). No theoretical method for a precise determination of this quantity is known. However, experimental evidence[1] indicates that x'_1 corresponds to a longitudinal coordinate of the fins on the body. Various values have been used for this quantity in previous studies. In particular, values corresponding to the fin mid-chord and fin quarter chord (the aerodynamic center in airfoil theory) both have been utilized.[10,24] In the present study, estimates for M'_w, Z'_q, and M'_q were made on the basis of x'_1 values corresponding to all longitudinal coordinates on the fins, i.e., from $x'_1 = -0.30$, the leading edge, to $x'_1 = -0.40$, the trailing edge. The graphs of Fig. 3 present the results as functions of x'_1. Two curves of values are shown for each coefficient. These correspond to results based on values for z'_1 derived using both the low aspect ratio theory and the airship theory.

The ranges of the theoretically estimated values for the static and damping derivative coefficients are $-13.7 \leq Z'_w \leq -11.6$, $-3.83 \leq M'_w \leq -2.02$, $-5.48 \leq Z'_q \leq -3.68$, and $-2.19 \leq M'_q \leq -1.19$. These ranges are, respectively, 17%, 62%, 39%, and 59% of the mean calculated value for each coefficient. In view of the magnitudes of these ranges, the theoretical estimates appear to be of little help in establishing values for the static and damping derivative coefficients for use in trajectory predictions. It will be shown

later, however, that the theoretical relationships are valuable indeed, because of the fact that they express in mathematical terms a basic physical truth, viz., that the static and damping derivatives are not independent quantities but that there exist definite relationships between them. The significance of this fact and the value of its mathematical expression by eqs. B-1 through B-4 is shown in the following section.

The computed estimates for the remaining hydrodynamic coefficients, X'_o, X'_u, Z'_w, M'_q, and X'_{wq}, were derived with the guidance of theoretical and/or empirical relationships published in the literature. In all these estimates, the effects of the mutual interference between body and fins were assumed negligible. The drag coefficient, X'_o, was estimated on the basis of empirical results due primarily to Hoerner.[41] The longitudinal virtual mass coefficient, X'_u, was estimated on the basis of empirical results presented by Yee-Tak Yu.[26,27] The normal virtual mass coefficient, Z'_w, and the virtual moment of inertia coefficient, M'_q, were estimated using equations derived on the basis of geometric considerations, with the bare hull effects estimated using the Lamb coefficients,[15] and the results of Yee-Tak Yu[27] used again to estimate the contributions of the fins. The second order derivative, X'_{wq}, was assumed to be equal to Z'_w on the basis of potential theory.[15]

There are two additional sets of hydrodynamic coefficient values presented in Table II. Each of the "Average Experimental Values" was obtained by averaging the values in the rows above it, i.e., the experimentally derived values discussed previously. The second set, labeled, "NPG Analysis--see section beginning on p. 10" was derived from previous work by Caster.[11] In that study, all but one of the hydrodynamic terms appearing in a system of nonlinear motion

equations are specified and the remaining term (the damping force derivative term) is varied to find the value giving the best overall agreement between three different pairs of predicted and observed Basic Finner trajectories. The derivative coefficients presented here were evaluated from the hydrodynamic input data corresponding to the best fit.

The data presented in Table II and Fig. 3 represent the total body of available information from which the hydrodynamic input data required for the Basic Finner trajectory predictions could be drawn. With the exception of the values derived from the results of the NPG curve-fitting analysis,[11] this information was obtained without recourse to trajectory measurements. This is a very important distinction, since the practical value of a trajectory prediction technique requiring input data obtained from trajectory measurements surely is limited.

Because of the problems discussed previously, however, the selection of one set of hydrodynamic input data from the results obtained independent of trajectory measurements really could not be made in a logical manner. The available experimental data were incomplete and imprecise. The sources of experimental error were numerous and often impossible to evaluate quantitatively. The values estimated by theoretical calculations also were extremely uncertain. Consequently, the primary hope for achieving successful trajectory predictions was that the computed trajectories would prove insensitive to variations in the values used for the hydrodynamic derivative coefficients.

TRAJECTORY PREDICTIONS

High Speed Vertical Planar Trajectories

The ten trajectory predictions discussed in the present section correspond to experiments in which a model is launched with nonzero horizontal velocity and zero vertical velocity and decelerates throughout a trajectory in the vertical plane. The test vehicles range in density from $\frac{W}{B} = 0.81$ to $\frac{W}{B} = 4.0$. In eight of the trajectories ($\frac{W}{B} > 1$), the model falls under the influence of gravity; in the other two ($\frac{W}{B} < 1$) it rises. For a model with $\frac{W}{B} = 2.0$, the longitudinal position of the CG is varied from .025 model lengths aft of the CB to .025 model length forward of the CB. In each run, the model is launched at high enough velocity so that the flow is turbulent throughout virtually the entire trajectory. Hence the high speed vertical planar trajectories are representative of certain motions executed by full scale torpedoes, submarines, and underwater-launched missiles.

The high speed vertical planar trajectory predictions were made using eqs. 2 through 4.* The equations were solved by the numerical procedure presented in Appendix C. The initial conditions and other input data correspond to model trajectory measurements supplied directly by the Bureau of Naval Weapons. Since the model is launched on a horizontal tangent, all of the initial observed values of velocity and displacement components are zero except for the initial longitudinal velocity, $u(0)$. The value of $u(0)$ is given by the slope of the observed x_o versus t curve, evaluated at $t = 0$. But this slope cannot be evaluated precisely since the curve is not defined for $t < 0$. To circumvent this difficulty, the initial conditions for the trajectory predictions were evaluated not at the actual instants of launching, but at times somewhat after launching where the data curves are more clearly defined. Typically, the initial value of t used in the

* Plus the subsidiary relation, $q = \dot{\theta}$.

TRAJECTORY PREDICTIONS

High Speed Vertical Planar Trajectories

The ten trajectory predictions discussed in the present section correspond to experiments in which a model is launched with nonzero horizontal velocity and zero vertical velocity and decelerates throughout a trajectory in the vertical plane. The test vehicles range in density from $\frac{W}{B} = 0.81$ to $\frac{W}{B} = 4.0$. In eight of the trajectories ($\frac{W}{B} > 1$), the model falls under the influence of gravity; in the other two ($\frac{W}{B} < 1$) it rises. For a model with $\frac{W}{B} = 2.0$, the longitudinal position of the CG is varied from .025 model lengths aft of the CB to .025 model length forward of the CB. In each run, the model is launched at high enough velocity so that the flow is turbulent throughout virtually the entire trajectory. Hence the high speed vertical planar trajectories are representative of certain motions executed by full scale torpedoes, submarines, and underwater-launched missiles.

The high speed vertical planar trajectory predictions were made using eqs. 2 through 4.* The equations were solved by the numerical procedure presented in Appendix C. The initial conditions and other input data correspond to model trajectory measurements supplied directly by the Bureau of Naval Weapons. Since the model is launched on a horizontal tangent, all of the initial observed values of velocity and displacement components are zero except for the initial longitudinal velocity, $u(0)$. The value of $u(0)$ is given by the slope of the observed x_o versus t curve, evaluated at $t = 0$. But this slope cannot be evaluated precisely since the curve is not defined for $t < 0$. To circumvent this difficulty, the initial conditions for the trajectory predictions were evaluated not at the actual instants of launching, but at times somewhat after launching where the data curves are more clearly defined. Typically, the initial value of t used in the

* Plus the subsidiary relation, $q = \dot{\theta}$.

predictions corresponds to a time approximately 0.1 sec after launching. The values of the initial conditions and all other input data for each of the ten high speed vertical planar trajectory predictions are given in Table IV.

The values of the hydrodynamic derivative coefficients used in the final high speed vertical planar trajectory predictions were theoretically estimated values (listed in Table V). In particular, the estimates for the static and damping derivative coefficients, Z'_w, M'_w, Z'_q, and M'_q, are those based on the value of z'_1 ($z'_1 = -9.6$) computed using airship theory, and a value of x'_1 ($x'_1 = -0.31$) corresponding to a point 10% of the chord length aft of the fin leading edge (see Fig. 3). As might be expected, the selection of these values for use in the trajectory predictions was by no means a straightforward matter. It was made only after a series of preliminary calculations had been performed which yielded much important and surprising information regarding the influence of the hydrodynamic derivative coefficients on the predicted trajectories.

The measured trajectory chosen as the model for the first preliminary calculations, CIT Run F-56,* is one of the trajectories to which prediction techniques previously have been applied at NPG by Caster.[11] In that previous work, all but one of the hydrodynamic terms in a system of nonlinear motion equations are specified and the remaining term (the damping force derivative term) is varied to find the value giving the best agreement between computed and observed trajectories. Although the concept of varying this term independently of the other static and damping derivative coefficients is not realistic since it ignores the physical inter-

* The characteristics of the CIT model trajectories are summarized in Table IV.

dependence of these quantities,* the degree of accuracy possible through using this curve-fitting technique appears significant. In the three trajectories considered in the previous study, the agreement between observed and predicted values of longitude, depth, and inclination, respectively, is to within 0.19 model lengths, 0.12 model lengths, and 1.1 degs (during the course of trajectories of from 6.6 model lengths to 8.8 model lengths in total length).

As noted in the previous section, the primary hope for the success of the present trajectory predictions was that the computed trajectories would prove so insensitive to variations in the hydrodynamic derivative coefficients that even the wide ranges in the available values for these quantities would not introduce significant errors in the predictions. This hope was soon dispelled by calculations based on two different sets of values for the hydrodynamic coefficients. One calculation was made using the values evaluated from the NPG data (see Table II). The Davidson Laboratory prediction based on these coefficients was virtually identical to the NPG prediction and hence agreed well with the observed results. The other calculation was made using the "average experimental values" for the coefficients (see Table II). In this case, the predicted trajectory differed markedly from the measured results. In particular, the maximum differences between predicted and observed values for depth and inclination were about 20 times as great and about 40 times as great, respectively, as in the previous calculation.

---

* It is found that the hydrodynamic static and damping derivative coefficients derived from the NPG results do not satisfy eqs. B-1 through B-4 for any reasonable set of values for the quantities appearing therein. For this reason, their physical validity is strongly doubted.

The results of these two calculations demonstrated conclusively that the scatter in the available values for the hydrodynamic derivative coefficients was significant from the point of view of its effect on predicted trajectories. Additional preliminary calculations substantiated this result, and also yielded information on the basis of which further conclusions could be drawn. In all, a great many preliminary calculations were made, and their results, taker individually, have little meaning. Accordingly, these results will not be presented in detail. Instead, the major conclusions to which they led will be discussed, and the particular results leading to these conclusions will be noted.

It was found that the predicted trajectories were extremely sensitive to independent variations of the hydrodynamic static and damping derivative coefficients. For example, a mere 10% change in the value of M'_w -- much less than the range of available values for this coefficient (see Table II) was found to produce changes in predicted values of depth and inclination as great as 0.19 model lengths and 2.9 degs, respectively. These variations are both considerably greater than the maximum differences between observed and computed results obtained in the NPG study.[11] As noted previously, however, independent variations of the static and damping derivative coefficients are not realistic in a physical sense. Accordingly, the effect on the predicted trajectories of restricting the static and damping coefficients to mutually consistent combinations was investigated, by comparing the results of trajectory predictions based on theoretically estimated values for these coefficients (see Fig. 3) with those of predictions based on coefficients obtained from other sources. Since all theoretical values were derived by using eqs. B-1 through B-4, they are necessarily self-consistent. The coefficient values obtained from other sources generally are not. It was found that the sensitivity of the computed tra-

jectories to variations in the values used for the derivatives was reduced drastically by restricting the combinations to satisfy the self-consistency condition. The graphs in the left-hand column of Fig. 4 show the maximum differences between observed and computed values of longitude, depth, and inclination obtained in predictions for CIT Run F-56 made using theoretical estimates for the static and damping derivative coefficients computed on the basis of x_i' values from -0.30 to -0.35 and z_i' values of -9.6 and -11.7 (see Fig. 3). The values for the other hydrodynamic coefficients used in all these calculations are the theoretical estimates given in Table II. It is found that the variations in the plotted values from one calculation to another are generally small, particularly compared with differences attained in many of the calculations in which inconsistent values were used for the static and damping derivative coefficients. An example of the results of this latter type is represented on the graphs by the values obtained on the basis of the average measured coefficients.

It also is seen from the graphs of Fig. 4 that differences between the observed results and the Davidson Laboratory preliminary calculations for CIT Run F-56 are generally of the same order of magnitude as those obtained in the previous NPG curve-fitting analysis. This result gave rise to new optimism regarding the prediction of the high speed vertical planar trajectories, and prompted extending the preliminary calculations to additional model trajectories. The results of these calculations are summarized by the graphs in the right-hand column of Fig. 4, which present data similar to that in the left-hand column graphs discussed previously, but on the basis of average values for three runs, CIT Nos. F-56, F-59, and F-64. The average magnitudes of the differences between observed and predicted values generally are even smaller than the corresponding quantities based on the F-56

prediction alone. In addition, the variations in the average quantities with x_1' and z_1' are smaller. On the basis of these results, it was concluded that reasonably accurate trajectory predictions could be obtained on the basis of theoretically estimated values for the static and damping derivative coefficients computed using any x_1' and z_1' values in the ranges included in Fig. 4. On the average, however, the closest agreement with experiment seemed to be achieved using the z_1' value computed using airship theory ($z_1' = -9.6$) and the value $x_1' = -0.31$.* It is for this reason that these values were selected to be used in the subsequent trajectory predictions.

The selection of the theoretically estimated values for the remaining required coefficients was primarily in the interest of consistency. In any event, in the case of the drag coefficient, X_o', the theoretical value is identical to the average measured value and hence is the only logical choice. In the case of the remaining coefficients (the virtual mass and moment of inertia coefficients), the question is an academic one since the results of the preliminary calculations indicated that any reasonable variations in these values have but negligible effects on the predicted trajectories.**

---

* The selection of this value for x_1' was also influenced by the results of preliminary calculations corresponding to CIT Run F-63 which were not included in Fig. 4, because they did not cover the complete range of x_1' and z_1' values considered there. However, the F-63 results do not differ qualitatively from those for CIT Runs F-56, F-59, and F-64 discussed above.

** This result is consistent with the results of an analytic variation of parameter analysis made later for the case of the straight horizontal trajectory.

Curves of the values computed for x_o, z_o, $\dot{x}_o$, $\dot{z}_o$, and θ in each of the final high speed vertical trajectory predictions are plotted versus t in Figs. 5 through 14, together with the corresponding values observed in the model experiments. Tabulations of the extreme values of the differences between the observed and computed values of each of these quantities are presented in Table VI. The predicted values agree with the observations (during the course of trajectories of from 6.6 to 9.6 model lengths in total length) to within 0.22 model lengths in longitude, 0.07 model lengths in depth, and 1.8 degs in inclination. In terms of percentages of maximum measured values, these figures correspond to less than 3% in longitude, 4% in depth, and 6% in inclination, which indicates that the predictions are successful from an engineering point of view. Relative to the results obtained in the earlier NPG curve-fitting analysis, the present results also are impressive. As can be seen from Table VII, which compares the Davidson Laboratory and NPG results for all three trajectories considered in the earlier work, the extreme values of the differences between observed and computed trajectory parameters in most cases are smaller for the present predictions than for the corresponding NPG results.

A significant feature of the results of the high speed vertical planar trajectory predictions is the relative agreement with experiment achieved by those predictions involved in the preliminary calculations and those which were not. As noted previously, the values of the hydrodynamic static and damping derivative coefficients used in the final predictions were established with the guidance of the results of CIT Runs F-56, F-59, F-63, and F-64 (Davidson Laboratory calculations 2, 5, 9, and 10). The remainder of the high speed vertical planar runs were not involved in this work. As can be seen from Table VI and Figs. 5 through 14, however, the agreement with experiment achieved by a prediction is not

noticeably dependent upon whether or not it was involved in the preliminary calculations. This is regarded as strong verification of the validity of the prediction techniques which were employed.

However, the opposite result was found for predictions made using the hydrodynamic coefficients evaluated from the NPG data. The preliminary calculations included predictions made using these values, for two trajectories (CIT Runs F-59 and F-63) which had not been considered previously in the NPG analysis. In both cases, differences between observed and predicted values of both depth and inclination angle were obtained which were greater (often more than twice as great) than the maximum differences obtained for all three runs considered in the earlier study. This result was not surprising, since the failure of the hydrodynamic static and damping derivative coefficients obtained from the NPG data to satisfy the self-consistency condition implied that they were not physically realistic and, consequently, that predictions based on them should not be expected to be generally successful.

In addition to the numerical solution, which may be regarded as exact, an analytic approximate solution applicable to the high speed vertical planar trajectories was developed. The approximate solution is valid for trajectories in which the transverse motions are not excessive. In particular, it is assumed that the following conditions are satisfied throughout the trajectory:

$$\left|\frac{(W-B)\sin\theta}{\frac{\rho}{2}A_x X'_o u^2}\right| \cong w^2 \cong q^2 \cong wq \cong 0 \qquad (9)$$

$$\cos\theta \cong 1 \qquad (10)$$

The approximate solution obtained on the basis of these assumptions is presented in Appendix C. The results of

the approximate solutions for four typical cases and the corresponding results of the numerical solutions are presented in Fig. 15. The approximate and exact solutions are in good agreement except near the end of each trajectory. Therefore, the approximate solution is of value on two counts. First of all, it enables the engineer to make reasonably good trajectory predictions with relatively little work. Secondly, it lends itself to straightforward interpretation and a direct method of estimating the influence on the motion of the various parameters which appear in the motion equations. In the latter connection, it permits the problem to be treated in a manner which is not possible when only a numerical solution is available. However, since the variation of parameter analysis is extremely complicated, it has not been included in the present study. The general method is illustrated, however, by the analysis performed later for the much simpler case of the straight horizontal trajectory.

Straight Horizontal Trajectory

The trajectory prediction discussed in the present section corresponds to an experiment in which a neutrally buoyant model, whose center of gravity and center of buoyancy coincide, is launched in a horizontal direction and decelerates throughout a one-dimensional trajectory along the line of launching. The trajectory actually is a special case of the high speed vertical planar motions discussed earlier in the section beginning on p. 19. It is considered here separately, however, because restriction to straight horizontal motion permits use of eq. 6, which may be integrated directly to yield the solution

$$u = \frac{u(0)}{bt + 1} \tag{11}$$

where,

$$b = - \frac{\frac{\rho}{2} A_x X'_o u(0)}{m - \frac{\rho}{2} A_x \ell X'_u} \tag{12}$$

Since $\dot{x}_o = u$ for the straight horizontal trajectory,

$$\dot{x}_o = \frac{u(0)}{bt + 1} \tag{13}$$

The solution for the longitudinal position is obtained by integrating eq. 13 and making use of the initial condition to get

$$x_o = \frac{u(0)}{b} \log (bt + 1) + x_o(0) \tag{14}$$

The initial conditions and other input parameters for the straight horizontal trajectory prediction are given in Table IV. Again, the initial value of time used in the calculation does not correspond to the instant of launching, but rather to a time 0.02 sec after the launching (see discussion beginning on p. 19).

Figure 16 shows a comparison of the observed and predicted values of velocity and longitude as functions of time. As is the case for the more general high speed vertical trajectory predictions, the computed values are in substantial agreement with the experimental data. Quantitatively, the agreement in longitude is to within 0.35 model lengths, or less than 3.1% of the total trajectory length.

Since an analytic solution is available, it is possible to make a straightforward analysis to assess the effects on the predicted trajectories of possible errors in the values of the input data. For simplicity, the present

analysis considers the effects of errors in only the most obvious sources, the hydrodynamic coefficients and the initial conditions. On this basis, the total differential of the longitudinal velocity is given by

$$d\dot{x}_o = \frac{\partial \dot{x}_o}{\partial X'_o} dX'_o + \frac{\partial \dot{x}_o}{\partial m_1} dm_1 + \frac{\partial \dot{x}_o}{\partial u(0)} du(0) \quad , \tag{15}$$

where the apparent mass,

$$m_1 = m - \frac{\rho}{2} A_x \ell X'_u \tag{16}$$

has been introduced to add symmetry to the resulting expressions. Substituting eq. 13 into eq. 15 and evaluating the derivatives that appear in the resulting equation gives

$$d\dot{x}_o = - \frac{bt}{bt+1} \frac{\dot{x}_o}{X'_o} dX'_o + \frac{bt}{bt+1} \frac{\dot{x}_o}{m_1} dm_1 + \frac{\dot{x}_o}{u(0)} \left(1 - \frac{bt}{bt+1}\right) du(0) \tag{17}$$

whence, to the first order of approximation,

$$\frac{\Delta \dot{x}_o}{\dot{x}_o} = \left(\frac{\Delta m_1}{m_1} - \frac{\Delta X'_o}{X'_o} - \frac{\Delta u(0)}{u(0)} \right) \frac{bt}{bt+1} + \frac{\Delta u(0)}{u(0)} \tag{18}$$

It may be concluded that inaccuracies in the predicted results due to errors in evaluating $u(0)$ are not significant. The basis for this conclusion is that the time-dependent error term which is proportional to $\Delta u(0)$ never becomes as large as the constant term, $\frac{\Delta u(0)}{u(0)}$, which is known to be insignificant because of the perfect agreement between the observed and predicted values at the beginning of the trajectory.

To evaluate the relative sensitivity to errors in X'_o and X'_u, data from Tables IV and V are substituted into eq. 16 and the result is compared with the value of X'_u, to find

$$m_1 = \frac{.0635}{-.14} X'_u = -0.454 X'_u \tag{19}$$

But, on the basis of the assumptions of the analysis,

$$\Delta m_1 = -\frac{\rho}{2} A_x \ell \Delta X'_u \tag{20}$$

whence, substituting from Table IV,

$$\Delta m_1 = -(.0211)(1.667)\Delta X'_u = -.0352 \Delta X'_u \tag{21}$$

Substituting eqs. 19 and 21 into eq. 18, and assuming on the basis of the preceding argument that the errors proportional to $\Delta u(0)$ are negligible, gives

$$\frac{\Delta \dot{x}_o}{\dot{x}_o} = \left(.0775 \frac{\Delta X'_u}{X'_u} - \frac{\Delta X'_o}{X'_o} \right) \frac{bt}{bt+1} \tag{22}$$

From this result, it is seen that an error of a certain percentage in X'_o has an effect on the predicted value of $\dot{x}_o$ almost thirteen times as great as does an error of the same percentage in X'_u.

Further, it is noted that, for $t > 2$ sec, the approximation

$$\frac{bt}{bt+1} \cong 1 \tag{23}$$

is accurate to within better than 10%. Substituting this result into eq. 22 gives

$$\frac{\Delta \dot{x}_o}{\dot{x}_o} \cong \left(.0775 \frac{\Delta X'_u}{X'_u} - \frac{\Delta X'_o}{X'_o} \right) \tag{24}$$

Interpreting $\Delta \dot{x}_o$ to be the difference between the observed and predicted values of longitudinal velocity, the trajectory data for $t > 2$ sec are used in conjunction with eq. 24 to give, approximately,

$$.0775\,\frac{\Delta X'_u}{X'_u} - \frac{\Delta X'_o}{X'_o} \cong -0.1 \quad , \tag{25}$$

where $X'_o + \Delta X'_o$ and $X'_u + \Delta X'_u$ are identified as values of the drag coefficient and the added mass coefficient, respectively, which would yield predictions in perfect agreement with the observed values.

Obviously, there are an infinite number of combinations of $\frac{\Delta X'_u}{X'_u}$ and $\frac{\Delta X'_o}{X'_o}$ satisfying eq. 25. The most interesting of these are the cases where all of the error is attributed to either one or the other of the coefficients. In particular, it is indicated that either a 10% increase in the magnitude of X'_o or a 130% decrease in the magnitude of X'_u would bring the observed and predicted results into agreement. The second alternative may be rejected as physically unreasonable since it corresponds to a negative value for the added mass. The first alternative, however, is reasonable when considering the available experimental data for X'_o (see Fig. 2).

Low Speed Vertical Planar Trajectories

The eight trajectory predictions discussed in the present section correspond to experiments in which a heavier-than-water model is dropped from rest with an initial value of pitch angle not equal to -90°, and accelerates throughout a trajectory in the vertical plane. The test vehicles vary in density from W/B = 1.1 to W/B = 4.0. For a model with W/B = 2.0, the longitudinal position of the CG is varied from .005 model lengths aft of the CB to .012 model lengths forward of the CB. Since the models are dropped from rest, the motions run in or, at least, through the laminar flow regime. Therefore, since actual motions of full-scale missiles are invariably in the turbulent flow regime, the low speed

vertical planar trajectory predictions are of little practical interest. In fact, their results are reported largely because of their remarkable accuracy even though they were derived on the basis of methods that seemed grossly inapplicable. The first of these was the use of motion equations (eqs. 2 through 4), formulated for conditions which are not satisfied throughout by the low speed vertical planar trajectories. This question has already been discussed at length, in the second section. The second was the use of the same constant values for the hydrodynamic coefficients as were employed in the high speed trajectory predictions (see Table V). This step, which is contrary to accepted theory,[18] was necessitated by the limitations of the available hydrodynamic data (see Table I) and the lack of reliable techniques for theoretical estimation of the behavior of the hydrodynamic derivative coefficients at low Reynolds numbers.

The initial conditions and other input parameters for the low speed vertical trajectory predictions correspond to model trajectory tests reported by Price.[7] The initial values of time used in the calculations correspond to the instants of dropping in the tests. Hence all of the initial values except $\theta(0)$ are equal to zero. All input data for each of the low speed vertical trajectory predictions are given in Table IV. Because of the lack of practical interest in the low speed vertical planar trajectories, detailed results of each one of the calculations are not presented. For illustrative purposes, curves of the values predicted for x_o, z_o, $\dot{x}_o$, $\dot{z}_o$, and θ in three typical calculations are plotted versus t in Figs. 17 through 19, together with the corresponding values observed in the model tests. Extreme values of the differences between the observed and computed values of x_o, z_o and θ for each trajectory are presented in Table VI.

The low speed vertical planar trajectory predictions are considerably less accurate than are the high speed predictions. The average magnitudes of the maximum differences between computed and observed values of longitude, depth, and inclination are, respectively, 0.14 model lengths, 0.14 model lengths, and 2.9 degs (see Table VI). The corresponding figures for the high speed vertical trajectory predictions are 0.09 model lengths, 0.03 model lengths, and 0.9 degs, respectively (the comparison is all the more significant since the high speed trajectories have an average total length, in model lengths of more than twice that of the low speed runs). However, the extreme value of the differences between the predicted and observed values of depth has a magnitude of but 0.35 model lengths. Roughly, this means that the displacement is predicted to within less than 10% of the maximum measured depth. This constitutes an adequate estimate for many engineering applications, and a remarkably accurate one in view of the assumptions made in the analysis.

Straight Vertical Trajectories

The seven trajectory predictions discussed in this section correspond to experiments in which a heavier-than-water model is dropped from rest, with an initial pitch angle equal to -90°, and accelerates throughout a one-dimensional vertical trajectory. The trajectories are special cases of the low speed vertical planar trajectories discussed earlier, in the section beginning on p. 31. They are considered here separately, however, because of their relative simplicity (see discussion in the first and second sections). The predictions were made using eq. 8, which may be written in the form

$$\dot{u} = \zeta^2 - \eta^2 u^2 \qquad (26)$$

where

$$\zeta^2 = \frac{W - B}{m - \frac{\rho}{2} A_x \ell X'_u} \tag{27}$$

$$\eta^2 = - \frac{\frac{\rho}{2} A_x X'_o}{m - \frac{\rho}{2} A_x \ell X'_u} \tag{28}$$

Note that the substitutions are made in such a way that the constants ζ and η are real numbers. Equation 26 is integrated to obtain

$$u = \frac{\zeta}{\eta} \tanh (\zeta \eta t) \tag{29}$$

where the initial condition $u(0) = 0$ is incorporated in the solution. Therefore, using the Table of Direction Cosines (Appendix A):

$$\dot{z}_o = \frac{\zeta}{\eta} \tanh (\zeta \eta t) \tag{30}$$

The solution for the depth is obtained by integrating eq. 30 and using the initial condition, $z_o(0) = 0$, to get

$$z_o = \frac{1}{\eta^2} \log \cosh (\zeta \eta t) \tag{31}$$

The input data for the straight vertical drop trajectories are design values (i.e., they correspond to the standard Basic Finner configuration) rather than actual values measured for the various test vehicles. The reason for this is that the actual values of the input parameters are reported in ref. 7 for only some of the models tested, and it was desired that the predictions be made in a consistent manner. Preliminary calculations showed, however, that the magnitudes of the differences between the design values and those actual values which are known are not great enough to affect the predicted motions appreciably except in cases

where the specific gravity is close to unity. The values used for the two required hydrodynamic coefficients, X'_o and X'_u, are the constant theoretical estimates derived as shown in Appendix B. The values of all of the input parameters for each of the seven straight vertical trajectory predictions are given in Table IV.

Curves of the values computed for z_o and $\dot{z}_o$ in each of the straight vertical trajectory predictions are plotted versus t in Figs. 20 through 22, together with the corresponding values observed in the model tests. It is seen that the predicted and observed values agree well in every case. With the exception of Calculation 20, the extreme value of the difference between the predicted and observed values of depth has a magnitude of 0.13 model lengths, or about 1.6% of the maximum measured depth (see Table VI). The value for Calculation 20 is 0.38 model lengths, or about 4.7% of the total depth. But this calculation corresponds to experiments in which certain modifications, too slight to be reflected in the estimates of the hydrodynamic force and moment coefficients were made to the test vehicles. Moreover, the models in two of these runs were released by hand rather than by the mechanical launcher used in the other tests. Hence the greater discrepancy was expected.

In spite of the excellent agreement with observed motions achieved by the straight vertical trajectory predictions made on the basis of a constant drag coefficient, it was felt that some attempt should be made to reconcile the results with accepted theory, i.e., to show that the inclusion of a realistic Reynolds number dependent component of the drag coefficient does not significantly affect the predicted trajectories. Accordingly, trajectory predictions corresponding to CIT vertical drops F-9 and F-47, 48 (Davidson Laboratory Calculations No. 21 and 26) were

repeated on the basis of Reynolds number dependent drag coefficients. These runs represent the extreme values (least and greatest, respectively) of Reynolds number variation in all the trajectories of this type. Hence, it is reasoned that any significant Reynolds number dependent phenomenon must manifest itself in at least one of these two runs.

Reynolds number dependent drag coefficients were derived by amalgamating available Basic Finner data and empirical and theoretical results for the low Reynolds number range which are presented by Hoerner.[41] Two different expressions were employed, one based on the laminar flow drag characteristics of a sphere and the other on the characteristics of a flat plate. The expressions employed were tailored to approximate the laminar flow data in the low Reynolds number range, and to approach the value used in the constant coefficient predictions as the Reynolds number increases into the turbulent flow regime.

The expression for X'_o based on the characteristics of a sphere is

$$X'_{o_s} = - D_s - \frac{R_s}{u} \tag{32}$$

where $D_s = 0.45$ and $R_s = 24. \frac{\nu}{\ell}$ ft/sec. Figure 23 includes a graph showing the variation of X'_{o_s} with Reynolds number over most of the range covered by the vertical drop trajectories.

When eq. 32 for X'_{o_s} is substituted in the straight vertical trajectory motion equation (eq. 26), the result is written in the form

$$\dot{u} = \zeta^2 - \eta_s^2 u^2 - \xi^2 u \tag{33}$$

where

$$\eta_s^2 = \frac{\frac{\rho}{2} A_x D_s}{m - \frac{\rho}{2} A_x \ell X_u'} \tag{34}$$

$$\xi^2 = \frac{\frac{\rho}{2} A_x R_s}{m - \frac{\rho}{2} A_x \ell X_u'} \tag{35}$$

and ζ^2 is as defined by eq. 27. Note that the substitutions are made in such a way that the constants are real numbers. Equation 33 is integrated to obtain

$$\dot{z}_o = \left[\frac{\left(\frac{\chi+\Omega^2}{\chi-\Omega^2}\right) e^{2\chi\eta_s^2 t} - 1}{\left(\frac{\chi+\Omega^2}{\chi-\Omega^2}\right) e^{2\chi\eta_s^2 t} + 1} \right] \chi - \Omega^2 \tag{36}$$

where

$$\chi^2 = \left(\frac{\zeta}{\eta_s}\right)^2 + \frac{1}{4}\left(\frac{\xi}{\eta_s}\right)^4 \tag{37}$$

$$\Omega^2 = \frac{1}{2}\left(\frac{\xi}{\eta_s}\right)^2 \tag{38}$$

and where the initial condition $u(0) = 0$ is incorporated in the solution and eq. C-9 is used with $\theta = -\frac{\pi}{2}$. The solution for the depth is obtained by integrating eq. 36 and using the initial condition $z_o(0) = 0$, to get

$$z_o = (\chi - \Omega^2)t + \frac{1}{\eta_s^2} \log \left[\frac{1 + \left(\frac{\chi-\Omega^2}{\chi+\Omega^2}\right) e^{-2\chi\eta_s^2 t}}{1 + \left(\frac{\chi-\Omega^2}{\chi+\Omega^2}\right)} \right] \tag{39}$$

The expression for X_o' based on the characteristics of a flat plate is

$$X_{o_p}' = -D_p - \frac{R_p}{\sqrt{u}} \tag{40}$$

Here, $R_p = 59.5 \left[\frac{\nu}{\ell} \text{ ft/sec}\right]^{1/2}$, but D_p is given different values for the two different trajectory predictions. In the prediction corresponding to CIT Run No. F-9, $D_p = 0.35$. As seen from Fig. 23, this value is such that X'_{o_p} approaches the constant coefficient value of -0.45 as the Reynolds number approaches the maximum value attained in the observed trajectory (approximately 0.4×10^6).

In the prediction corresponding to CIT Runs F-47, 48, $D_p = 0.45$. As seen from Fig. 23, this value is such that X'_{o_p} is considerably greater in magnitude than the constant coefficient value of -0.45 throughout the Reynolds number range attained in the observed trajectory. Nevertheless, it is sufficient to show that including a term of this type is unimportant, since it overestimates rather than underestimates the effect.

No analytical solution was obtained for the straight vertical trajectory motion equation with $X'_o = X'_{o_p}$. It was solved by a numerical procedure similar to that used in the solution of the vertical planar trajectory motion equations.

The straight vertical trajectory predictions obtained on the basis of the Reynolds number dependent drag coefficients substantiate the predictions obtained assuming that the coefficient is constant. In none of the four repeat predictions were the results appreciably different from the original computations. This result indicates that terms proportional to accelerations (primarily inertial terms) are so dominant in the low velocity portions of the trajectories that even large errors in the hydrodynamic coefficients are unimportant.

CONCLUSIONS

Observed trajectories could not be predicted using hydrodynamic coefficients determined from available experimental data alone. However, coefficients obtained on the basis of existing theory yielded predictions that agreed well with the observed motions (see Table VI).

Computed trajectories were particularly sensitive to independent changes in the values used for the hydrodynamic static and damping derivative coefficients, Z'_w, M'_w, Z'_q, and M'_q. However, when the values were kept consistent with relations expressing the physical interdependence of the coefficients (eqs. B-1 through B-4), they could be varied over fairly wide ranges without appreciably affecting the predictions. This result is particularly significant, and efforts should be made to generalize it. In particular, its validity for the case of a more representative hydrodynamic missile (e.g., a standard torpedo or submarine type configuration) should be investigated. Such an investigation could be in the form of calculations similar to those performed in the present study. The problem also could be approached analytically, however, through the use of approximate methods which make analytic solution of the motion equations possible (e.g., the approximate solution developed herein).

It is felt that the present results demonstrate clearly the potential value of simple analytic methods for predicting hydrodynamic derivative coefficients, and it is urged that greater emphasis be placed on their use in the future.

From a practical standpoint, the important results of the present study are those pertaining to high speed trajectories. The low speed trajectory predictions also are interesting, however, because of their surprising accuracy. Predictions of straight (zero attack angle) vertical drops

from rest agreed well with observed trajectories, even though a constant drag coefficient corresponding to turbulent flow was used in the calculations. Low speed vertical planar trajectory predictions, although markedly less accurate than the high speed predictions, nevertheless yielded results considered adequate for many engineering applications, in spite of the fact that the calculations took into account neither nonlinear hydrodynamic normal forces and pitching moments (although angles of attack as great as 30° were attained) nor variations of hydrodynamic coefficients with Reynolds number. The reason for the unrealistic simplicity of the mathematical model used in the low speed planar predictions was the lack of any reliable experimental or theoretical basis for estimating the extensive hydrodynamic input data required for a more sophisticated formulation. The surprising accuracy of the predictions is attributed to the dominance of terms proportional to acceleration (i.e., inertial terms) in the low velocity portions of the trajectories. It is felt that any improvement in the accuracy of the low speed vertical planar trajectory predictions requires the performance of experiments to obtain detailed hydrodynamic force and moment data for the Basic Finner in the low Reynolds number high attack angle regime.

All available Basic Finner trajectory test results have not been considered in the present study. In particular, several heretofore unpublished six degs of freedom trajectories also are available.[28] It is recommended that attempts be made to predict these more general motions. To do this, it will be necessary to make extensive measurements of hydrodynamic roll moment as a function of roll angle, attack angle, roll angular velocity, and other motion parameters. It is recommended that these measurements be made using a rotating arm facility, which has been shown to be effective for such tests.[29,30,31] At the same time, the hydrodynamic static and

damping derivative coefficients should be measured. This will permit the values used for these coefficients in the present study to be compared with a set of values derived uniformly from the results of a single static experiment.

ACKNOWLEDGMENT

The author wishes to thank Mr. Thomas McLeo for his assistance in performing the trajectory predictions.

REFERENCES

1. Strumpf, A.: "A Study of Optimum Turning Ability and Dynamic Stability of Submarine-Like Vessels," DL Report No. 765, March 1960.

2. Kermeen, R. W.: "Static Force Coefficients of the Basic Finner Missile in Fully Wetted Flow," CIT Report No. E-73.2, September 1957.

3. Kiceniuk, T.: "An Experimental Determination of Dynamic Coefficients for the Basic Finner Missile by Means of the Angular Dynamic Balance," CIT Report No. E-73.3, June 1957.

4. Kiceniuk, T.: "An Experimental Determination of Dynamic Coefficients for the Basic Finner Missile by Means of the Translational Dynamic Balance," CIT Report No. E-73.9, May 1958.

5. Heald, R. H. and Adams, G. H.: "Aerodynamic Characteristics of Five Models of the Basic Finner Missile," Bureau of Standards Report 5721, January 1958.

6. Savitsky, D. and Prowse, R. E.: "Added Mass and Drag Coefficients of Basic Finner Missile," DL Report R-824, December 1960.

7. Price, D. A., Jr.: "Free Body Modeling of the Dynamics of a Fin Stabilized Ballistics Missile in Non-Spinning Vertical Trajectories," CIT Report No. E-73.1, April 1957.

8. Stubstad, G. W.: "Pure Pitching Motion of the Basic Finner," NOTS TP 2115, NAVORD Report 6417, October 1958.

9. Parrish, G. B.: "Planar Motion of a Configurationally Asymmetrical Body With Varying Speed," Bureau of Ordnance Ballistic Technical Note No. 31, November 1956.

10. Stubstad, G. W. and Waugh, J. G.: "Drag Coefficient of Fully Wetted Basic Finner Missile," NOTS 1483, NAVORD Report 5269, June 1956.

11. Caster, H. P.: "Hydrodynamic Trajectory Computations and Analyses for Horizontally Launched Rounds of the Basic Finner Missile," NPG Report No. 1668, 15 August 1959.

12. Strumpf, A.: "Equations of Motion of a Submerged Body With Varying Mass," DL Report No. 771, May 1960.

13. Lopes, L. A.: "Motion Equations for Torpedoes," NAVORD Report 2090, NOTS 827, February 1954.

14. White, J. A.: "A Re-Evaluation of the Hydrodynamic Characteristics of the Polaris Missile," DL Letter Report No. 835, March 1961. CONFIDENTIAL

15. Lamb, H.: Hydrodynamics, Sixth Edition, Dover Publications, 1945.

16. Colombo, C. A.: "Hydrodynamic Characteristics of Subroc Missile," DL Report No. 860, February 1962. CONFIDENTIAL

17. Suarez, A.: "Hydrodynamic Coefficients of Subroc-Bird Configurations," DL Letter Report No. 822, November 1960. CONFIDENTIAL

18. Von Mises, R.: Theory of Flight, McGraw-Hill, 1945.

19. Eskigian, N. M.: "Model Studies of a Systematic Series of Streamline Bodies of Revolution of Varying Fineness Ratio at High Angles of Attack and Angular Velocities," DL Report No. 585, November 1955. CONFIDENTIAL

20. Strumpf, A.: "Rotating-Arm Data: Comparison of Static Rates With Results From Other Laboratories," DL Note No. 530, March 1960. CONFIDENTIAL

21. Jacobs, W. R.: "Correlation of Fluid Dynamic Experimental Data for the Mark 13 Torpedo," DL Report No. 424, January 1952. CONFIDENTIAL

22. Flax, A. and Lawrence, H.: "The Aerodynamics of Low-Aspect-Ratio Wings and Wing-Body Combinations," Cornell Aerodynamical Laboratory, Inc., Report CAL-37, September 1951.

23. Lawrence, H. R.: "The Lift Distribution on Low-Aspect-Ratio Wings at Subsonic Speeds," IAS Preprint No. 313, January 1951.

24. Low, L. and Stone, H.: "The Subsonic Aerodynamic Characteristics of Wings in Combination with Slender Bodies of Revolution," Cornell Aeronautical Laboratory, Inc., Report CAL/CM-679, July 1951.

25. Spreiter, J.: "Aerodynamic Properties of Slender Wing-Body Combinations at Subsonic, Transonic, and Supersonic Speeds," NACA TN 1423, 1947.

26. Yee-Tak Yu: "Virtual Masses and Moments of Inertia of Disks and Cylinders in Various Liquids," Journal of Applied Physics, Volume 13, January 1942.

27. Yee-Tak Yu: "Virtual Masses of Rectangular Plates and Parallelepipeds in Water," Journal of Applied Physics, Volume 16, November 1945.

28. Document transmittal, NWL to DL, 1 December 1960.

29. White, J. A.: "Model Study of the Hydrodynamic Characteristics of the Marlin Missile," DL Letter Report No. 730, Nobember 1958. CONFIDENTIAL

30. Strumpf, A.: "A Rotating-Arm Technique for Measuring the Roll-Damping Rates of Torpedo-Like Missiles," ETT Report No. 693, May 1958. CONFIDENTIAL

31. Strumpf, A.: "The Influence of Induced Roll Moment on Torpedo Roll Stability," ETT Note No. 439, August 1957.

32. Dugoff, H.: "Adjustment of the Hydrodynamic Static and Damping Derivatives to Any Longitudinal Position of the Origin of Coordinates," DL Note No. 621, May 1961.

33. Munk, M. M.: "The Aerodynamic Forces on Airship Hulls," NACA Report 184, 1924.

34. Allen, H. J. and Perkins, E. W.: "Characteristics of Flow Over Inclined Bodies of Revolution," NACA RMA 50L07, March 1951.

35. Kelly, H. R.: "The Estimation of Normal-Force, Drag, and Pitching Moment Coefficients for Blunt-Based Bodies of Revolution at Large Angle of Attack," Journal of Aeronautic Sciences, Volume 21, No. 8, August 1954.

36. Martin, M.: "Preliminary Study of Free Surface Effects On the Water to Air Exit of a Slender Body," DL Technical Memorandum 125, February 1960.

37. IBM 1620 Fortran Bulletin, Form No. J28-4200, International Business Machine Corporation.

38. Dugoff, H.: "Model Tests of a Dynamically Stable, Highly Maneuverable Prototype Submarine-Like Vehicle," DL Note No. 652, to be published.

39. DTMB Report No. C-1043, March 1959.

40. Lennertz, J.: "Influence of the Airplane Body on the Wings," Aerodynamic Theory, W. F. Durand, Editor, Durand Reprinting Committee, pp. 152-158, Volume IV, 1943.

41. Hoerner, S. F.: Fluid Dynamic Drag, published by the author, 1958.

APPENDIX A

Technical and Research Bulletin No. 1-5

Nomenclature for Treating the Motion of a Submerged Body Through a Fluid

Report of the American Towing Tank Conference
prepared by the Hydromechanics Subcommittee
of the Technical and Research Committee
of The Society of Naval Architects and
Marine Engineers

Published in April, 1950, by
The Society of Naval Architects and Marine Engineers
29 West 39th Street, New York 18, N. Y.

Table of Contents

INTRODUCTION A-3
BODY CHARACTERISTICS A-3
Specific Points of Body A-3
Body Axes A-3
Coordinates and Distances A-3
Areas and Volume A-4
Inertia Characteristics A-4
FIXED AXES—ORIENTATION AND MOTION OF BODY A-5
Fixed Axes A-5
Orientation of Body Axes A-5
Space Orientation θ, ψ, ϕ and Corresponding Angular Velocities of Body A-5
Velocity of Origin of Body Axes—Angles of Attack α, and Drift β A-6
Motion Orientation α, β, γ and Corresponding Angular Velocities of Body A-6
Control Surfaces A-7
FORCES AND MOMENTS A-7
DIMENSIONLESS FORMS A-7
Body Shape Parameters A-7
Velocities and Accelerations A-8
Force and Moment Coefficients A-8
Coefficients of Static Force Derivatives A-8
Coefficients of Rotary Force Derivatives A-8
Virtual Inertia Coefficients A-8
Coefficients of Static Moment Derivatives A-9
Virtual Moment of Inertia Coefficients A-9
Coefficients of Rotary Moment Derivatives A-9
LINEARIZED EXPANSION OF FORCE AND MOMENT COEFFICIENTS A-9
EQUATIONS OF MOTION FOR A FREE BODY A-9
EQUILIBRIUM EQUATIONS FOR A TOWED BODY A-10
PHYSICAL AND OTHER TERMS A-10
DEFINITIONS OF STABILITY A-10
Metacentric Stability A-10
Translational Stability A-10
Static (or Weathercock) Stability A-10
Dynamic Stability on Course A-11
SUMMARY A-11
OTHER SYMBOLS A-14

Nomenclature for Treating the Motion of a Submerged Body Through a Fluid

Introduction

The study of the motion of a rigid body through a fluid is considered as a general problem in the motion of rigid bodies under the action of gravity and hydrodynamic forces. Thus a choice of nomenclature for this field must borrow from both rigid dynamics and fluid mechanics.

Like most problems in hydrodynamics, an exact theoretical solution of the equations of motion is available only for an ideal fluid. However, as is well known, for small deviations from uniform linear motion, the equations of motion in a real fluid can be linearized and solved in terms of a set of coefficients, which are determined either by theory or by experiment.

Frequently, rather than to determine the trajectory of a body, it suffices to obtain a measure of its stability. A body in a state of equilibrium is said to be stable if, when slightly disturbed from this state, it returns to it, with perhaps a slight change in position of path. Since there are various possible states of equilibrium, there are, correspondingly, various possible kinds of stability; these are defined in a subsequent section of this Bulletin.

Although the motion can be described adequately only with reference to some fixed coordinate system, it is shown in texts on dynamics that the equations of motion of a rigid body are expressed most conveniently in terms of a rectangular coordinate system moving with the body, the so-called body axes. Consequently, it has been necessary to introduce nomenclature for describing the orientation of the body axes relative to the fixed axes.

Body Characteristics

It is supposed that the body is elongated and has well-defined forward and after ends, such as nose and tail, or bow and stern. It is assumed also that the body has a "principal plane of symmetry," as shown in Fig. 1, and that there is a normal attitude of the body, with the principal plane of symmetry vertical, so that the top (deck) and bottom of the body can be defined. The body may be equipped with wings, stabilizing and control surfaces, and it may be self-propelled or towed.

Specific Points of Body

CB.... center of buoyancy of the body
CG.....center of mass of the body
CM.... metacenter of the body
CP.....center of pressure of the body
CS.... static center; center of resultant of weight and buoyancy
O.....origin of body axes (to be defined)
TP.... towing point or towed point

Body Axes

The origin *O* of a right-handed, rectangular, coordinate system fixed in the body is chosen either to coincide with *CG*, when *CG* is in the principal plane of symmetry, or at any convenient point in the principal plane of symmetry when *CG* does not lie in this plane. Body axes *x*, *y*, *z*, coincident with the principal axes of inertia at *O*, are then defined as follows:

x.... the longitudinal axis, directed from the after to the forward end of the body
y.... the transverse axis, directed to starboard
z.... the normal axis, directed from top to bottom (deck to keel)

The *xz*-plane is the principal plane of symmetry.

Coordinates and Distances

x_B, y_B, z_B coordinates of *CB* relative to body axes
x_G, y_G, z_G..coordinates of *CG* relative to body axes

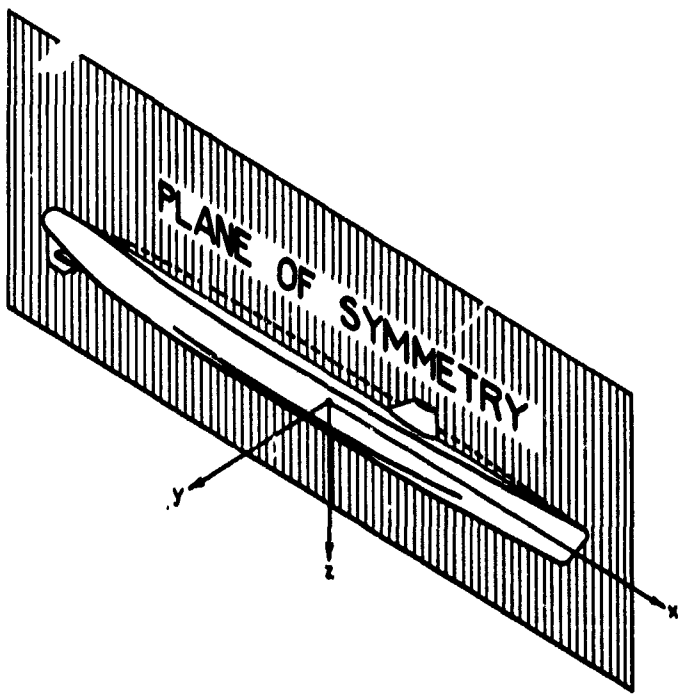

FIG. 1.—SKETCH OF AN UNDERWATER BODY SHOWING PLANE OF SYMMETRY AND BODY AXES

x_B, y_B, z_B . . coordinates of CS relative to body axes
x_T, y_T, z_T . . coordinates of TP relative to body axes
b or B . . . . the beam of the body; a breadth, width, or span
d or D . . . . diameter of a body of revolution
c . . . . . chord length of a wing, rudder, elevator, or diving plane
m or GM . . the metacentric height; the distance from CG to CM, positive upward
H . . . . . the draft of a floating body
h . . . . . the depth of submergence of a submerged body
h . . . . . the hull height of a submerged body, measured from the bottom to the top of the hull (pronounced height)
k . . . . . radius of gyration
l or L . . . . . length of the body
R . . . . . radius of turning circle, or radius of curvature of path
t . . . . . thickness
δ . . . . . thickness of boundary layer

AREAS AND VOLUME

A . . . . . an area, projected or a given plane or on the median plane of a hydrofoil, such as:
A_b . . . . . projected area of bow planes
A_s . . . . . projected area of stern planes
A_r . . . . . projected rudder area
A_x, A_y, A_z . . area of the projection of the submerged part of the body on the ys, xs, and xy planes, respectively
S . . . . . wetted surface area of the body
V . . . . . volume of the body (pronounced vol)

INERTIA CHARACTERISTICS

m . . . . . mass of body
I_x, I_y, I_z . . . moments of inertia of the body about x, y, z axes, respectively
k_x, k_y, k_z . . radii of gyration of the body about x, y, z axes, respectively

Fixed Axes—Orientation and Motion of Body

Fixed Axes

It will be assumed that the accelerations of a point on the surface of the earth can be neglected so that a set of axes fixed relative to the earth may be considered as fixed axes. Choose a right-handed, orthogonal set of "fixed axes," x_0, y_0, z_0, fixed relative to the earth, so that the x_0 and y_0 axes are in a horizontal plane, and the z_0-axis is vertical and directed downwards.

x_0. . . . the fixed longitudinal axis, in a fixed direction in a horizontal plane, considered as the forward direction

y_0. . . the fixed transverse axis, perpendicular to x_0 in a horizontal plane, directed to starboard

z_0. . . . the vertical axis, directed downwards

Orientation of Body Axes

All angular displacements will be taken as positive in the sense of rotation of a right-hand screw advancing in the positive direction of the axis of rotation (right-hand screw rule).

The orientation of the body axes relative to the fixed axes can be described in various ways. In aerodynamics the orientation of a body in space is usually described in terms of an angle of pitch or trim θ, an angle of yaw ψ, and an angle of roll or heel ϕ. In addition it is necessary to introduce a second set of angles α, β, γ, which describes the orientation of the body relative to its direction of motion.

Space Orientation θ, ψ, ϕ and Corresponding Angular Velocities of Body

The space orientation of the body axes x, y, z relative to the fixed axes x_0, y_0, z_0 may be described by the following procedure (see Fig. 2). First suppose the axes x, y, z, to coincide with the axes x_0, y_0, z_0. Rotate the body about z_0 through an angle of yaw ψ so that the axes x_0, y_0 assume the intermediate positions x_1, y_1; then rotate the body about the new position of the y-axis through an angle of trim θ, so that z_0 moves to z_1 and x_1 moves to x; finally rotate the body about the new position of the x-axis through an angle of roll ϕ so that the axes y_1, z_1 assume their final positions y, z. In accordance with this procedure we have the following definitions:

θ. . . . the angle of trim (or pitch); the angle of elevation of the x-axis; i.e., the angle between Ox and the horizontal plane x_0y_0, positive in the sense of rotation from the z_0 to the x-axis

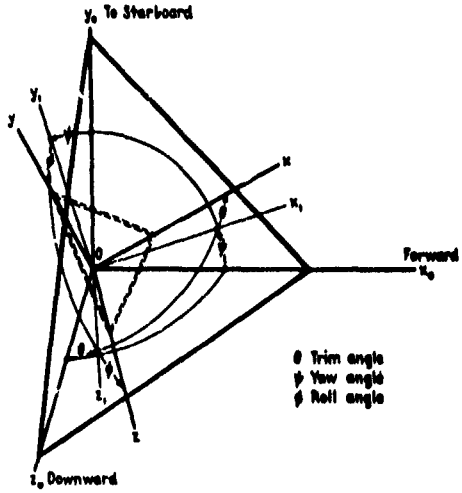

Fig. 2.—Orientation of Body Axes Relative to Fixed Axes in Terms of θ, ψ, ϕ. Viewed from Below xy Plane

ψ. . . . the angle of yaw; the angle from the vertical plane z_0x_0 to the vertical plane z_0x, positive in the positive sense of rotation about the z_0-axis

ϕ. . . . an angle of roll; the angle from the vertical xz_0-plane to the principal plane of symmetry xz, positive in the positive sense of rotation about the x-axis

The direction cosines of x, y, z relative to x_0, y_0, z_0 may be tabulated as in Table 1.

Table 1.—Direction Cosines of Body Axes Relative to Fixed Axes in Terms of θ, ψ, ϕ

	x	y	z
x_0	$\cos\theta\cos\psi$	$-\cos\phi\sin\psi+\sin\theta\sin\phi\cos\psi$	$\sin\phi\sin\psi+\sin\theta\cos\phi\cos\psi$
y_0	$\cos\theta\sin\psi$	$\cos\phi\cos\psi+\sin\theta\sin\phi\sin\psi$	$-\sin\phi\cos\psi+\sin\theta\cos\phi\sin\psi$
z_0	$-\sin\theta$	$\cos\theta\sin\phi$	$\cos\theta\cos\phi$

Also, for the direction cosines of z_0 relative to the body axes, put $n_x = -\sin\theta$, $n_y = \cos\theta \sin\phi$, $n_z = \cos\theta \cos\phi$.

Let p, q, r be the components of the angular velocity vector relative to the body axes x, y, z. Denote the time derivatives of θ, ψ, ϕ by $\dot{\theta}$, $\dot{\psi}$, $\dot{\phi}$. We have the following relations:

$$p = \dot{\phi} - \dot{\psi}\sin\theta$$
$$q = \dot{\psi}\cos\theta\sin\phi + \dot{\theta}\cos\phi$$
$$r = \dot{\psi}\cos\theta\cos\phi - \dot{\theta}\sin\phi$$

p, q, r . . . angular velocity components relative to body axes x, y, z; angular velocities of roll, pitch, and yaw

Velocity of Origin of Body Axes—Angles of Attack α, and Drift β

It should be recalled that the origin of body axes O is taken to coincide with the center of mass CG, when the CG lies in the principal plane of symmetry.

Let u, v, w be the components in the x, y, z coordinate system of the linear velocity of O relative to the fluid.

u, v, w . . components along body axes of velocity of origin of body axes relative to fluid

U or V . . velocity of origin of body axes relative to fluid. In general, the symbol U is used in this Bulletin

Some of the hydrodynamic forces which act on a body, the so-called static forces, depend on the orientation of the body with respect to the relative

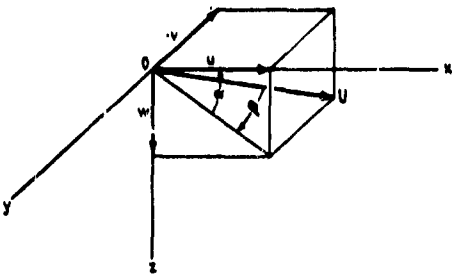

Fig. 3.—Orientation of Body Axes Relative to Velocity of Origin

fluid velocity. This orientation is specified by the velocity components u, v, w but is more usually given in terms of angles α and β which may be defined as follows (see Fig. 3):

α . . . the angle of attack; the angle to the longitudinal body axis from the projection into the principal plane of symmetry of the velocity of the origin of the body axes relative to the fluid, positive in the positive sense of rotation about the y-axis

β . . . the drift or sideslip angle; the angle to the principal plane of symmetry from the velocity of the origin of the body axes relative to the fluid, positive in the positive sense of rotation about the z-axis

We have the following relations between the velocity vector and these angles (see Fig. 3):

$$\tan\alpha = +w/u$$
$$\sin\beta = -v/U$$

where U is the velocity of the origin of the body axes relative to the fluid.

$$U^2 = u^2 + v^2 + w^2$$

Conversely, we have

$$u = U\cos\alpha\cos\beta$$
$$v = -U\sin\beta$$
$$w = U\sin\alpha\cos\beta$$

Motion Orientation α, β, γ and Corresponding Angular Velocities of Body

For bodies towed in a horizontal straight line, the fixed x_0-axis may be chosen to coincide with the direction of motion. The orientation of the body axes x, y, z relative to the fixed axes x_0, y_0, z_0 may then be expressed in terms of angles α, β, and γ, defined as follows:

α . . . . the angle of attack, defined in the previous section

β . . . . the drift or sideslip angle, defined in the previous section

γ . . . . an angle of roll; the angular displacement about the x_0-axis of the principal plane of symmetry from the vertical, positive in the positive sense of rotation about the x_0-axis

When the orientation is specified in terms of α, β, γ, the angles of attack and drift are independent of the angle of roll. This is not the case for the θ, ψ, ϕ system. Indeed $\theta = \alpha$ and $\psi = \beta$ only when $\phi = 0$. For this reason it is preferable to use the angles α, β, γ in cases where some point in the principal plane of symmetry moves in a fixed direction.

The direction cosines of x, y, z relative to x_0, y_0, z_0 may be tabulated as in Table 2.

Denote the time derivatives of α, β, γ by $\dot{\alpha}$, $\dot{\beta}$, $\dot{\gamma}$. We have the following relation between p, q, r and $\dot{\alpha}$, $\dot{\beta}$, $\dot{\gamma}$:

$$p = \dot{\beta}\sin\alpha + \gamma\cos\alpha\cos\beta$$

TABLE 2.—DIRECTION COSINES OF BODY AXES RELATIVE TO FIXED AXES IN TERMS OF α, β, γ

	x	y	z
x_0	$\cos\alpha\cos\beta$	$-\sin\beta$	$\sin\alpha\cos\beta$
y_0	$\sin\alpha\sin\gamma+\cos\alpha\sin\beta\cos\gamma$	$\cos\beta\cos\gamma$	$-\cos\alpha\sin\gamma+\sin\alpha\sin\beta\cos\gamma$
z_0	$-\sin\alpha\cos\gamma+\cos\alpha\sin\beta\sin\gamma$	$\cos\beta\sin\gamma$	$\cos\alpha\cos\gamma+\sin\alpha\sin\beta\sin\gamma$

$$q = \dot{\alpha} - \dot{\gamma}\sin\beta$$
$$r = \dot{\beta}\cos\alpha + \dot{\gamma}\sin\alpha\cos\beta$$

CONTROL SURFACES

δ.....angular displacement of a control surface

δ_r....rudder angle, positive in the sense of positive rotation about the z-axis

δ_b....angular displacement of the bow plane, positive in the sense of positive rotation about the y-axis

δ_s....angular displacement of the stern plane, positive in the sense of positive rotation about the y-axis

Forces and Moments

It is convenient to distinguish between the hydrodynamic forces, which include the propeller thrust when the body is self-propelled, and other external forces such as those due to gravity (weight and buoyancy) and towlines.

As is the case for angular displacements, moments are taken as positive in accordance with the right-hand screw rule.

X, Y, Z....hydrodynamic force components relative to body axes, referred to as longitudinal, lateral, and normal forces, respectively

D or $\bar{R}$.....drag component of hydrodynamic force in direction of relative flow; may be qualified by an appropriate subscript to indicate a component of the drag; resistance

C.....cross force; component of hydrodynamic force normal to lift and drag, positive to starboard

L.....lift; component of hydrodynamic force in the principal plane of symmetry normal to relative flow, positive when directed from bottom to top of body (keel to deck)

K, M, N. .hydrodynamic moment components relative to body axes, referred to as rolling, pitching, and yawing moments, respectively

Q.....torque about the axis of a control surface, with appropriate subscript

$\bar{T}$.....towline tension (pronounced toll)

$\bar{T}_x$, $\bar{T}_y$, $\bar{T}_z$..components of towline tension relative to body axes

W or Δ....weight of the body; $W = mg$

B.....buoyancy force

$W - B$....resultant of weight and buoyancy

Dimensionless Forms

A given physical quantity will be non-dimensionalized by considering its dimensions in terms of mass, length, and time as fundamental units, and dividing the mass by $(\frac{1}{2})\rho l^3$, the length by l, and the time by l/U. For example, the dimensions of $\partial M/\partial q$ are mass $\times$ (length)^2 $\times$ (time)$^{-1}$. Hence

$$\frac{\partial M}{\partial q}\frac{1}{(\frac{1}{2})\rho l^3}\frac{1}{l^2}\frac{l}{U} = \frac{\partial M/\partial q}{(\frac{1}{2})\rho l^4 U}$$

is the corresponding dimensionless expression.

The non-dimensionalized form of a given physical quantity will be indicated by the prime of that quantity, unless explicitly defined otherwise. Thus

$$m' = \frac{m}{(\frac{1}{2})\rho l^3},\quad t' = \frac{tU}{l},\quad I_x' = \frac{I_x}{(\frac{1}{2})\rho l^5},\quad x_0' = \frac{x_0}{l}$$

When a stability analysis has been completely expressed in non-dimensional form, the primes may be omitted, provided that a statement to that effect is made.

BODY SHAPE PARAMETERS

The shape of a body may be described conveniently in terms of the ratios of some of its principal dimensions, such as:

$b' = b/l$..... beam-length ratio

$d' = d/l$ . . . . . diameter-length ratio of a body of revolution

l/d . . . . . fineness ratio

$H' = H/l$ . . . . . draft-length ratio

b/H . . . . . beam-draft ratio

$C_x = A_x/bH$ . . . . maximum section coefficient

$S' = S/l^2$ . . . . . a wetted-surface coefficient

$S/\sqrt{Vl}$ . . . . a wetted-surface coefficient

$V' = V/l^3$ . . . . volumetric coefficient

$C_p = V/lA_x$ . . . . prismatic coefficient

$C_b = V/bHl$ . . . . block coefficient

$a = b^2/A_r$ . . . . . aspect ratio of a wing

Velocities and Accelerations

$u' = u/U, v' = v/U,$
$w' = w/U$ . . . . . dimensionless velocity components

$\dot{u}' = \dot{u}l/U^2, \dot{v}' = \dot{v}l/U^2,$
$\dot{w}' = \dot{w}l/U^2$ . . . . . dimensionless acceleration components

$p' = pl/U, q' = ql/U,$
$r' = rl/U$ . . . . . dimensionless angular velocity components

$\dot{p}' = \dot{p}l^2/U^2, \dot{q}' = \dot{q}l^2/U^2,$
$\dot{r}' = \dot{r}l^2/U^2$ . . . . dimensionless angular acceleration components

Force and Moment Coefficients

Since forces and moments are frequently nondimensionalized in terms of S, A, or V, alternate forms will be presented.

$X' = X/(\frac{1}{2})\rho l^2U^2$ . . . longitudinal force coefficient

$Y' = Y/(\frac{1}{2})\rho l^2U^2$ . . . lateral force coefficient

$Z' = Z/(\frac{1}{2})\rho l^2U^2$ . . . normal force coefficient

$D' = D/(\frac{1}{2})\rho l^2U^2$ . . . . drag or resistance coefficient

$C_D = D/(\frac{1}{2})\rho AU^2$ . . drag or resistance coefficient, alternate form

$c_D = D/(\frac{1}{2})\rho V^{2/3}U^2$. drag or resistance coefficient, alternate form

$C_t = D/(\frac{1}{2})\rho SU^2$ . . . . drag or resistance coefficient, alternate form

$C_f = D_f/(\frac{1}{2})\rho SU^2$. friction drag or resistance coefficient

$C_r = D_r/(\frac{1}{2})\rho SU^2$. residuary drag coefficient; $C_r = C_t - C_f$

$C' = C/(\frac{1}{2})\rho l^2U^2$ . . . cross force coefficient

$C_c = C/(\frac{1}{2})\rho AU^2$. cross force coefficient, alternate form

$L' = L/(\frac{1}{2})\rho l^2U^2$. lift coefficient

$C_L = L/(\frac{1}{2})\rho AU^2$. lift coefficient, alternate form

$K' = K/(\frac{1}{2})\rho l^3U^2$ . . rolling moment coefficient

$C_K = K/(\frac{1}{2})\rho AlU^2$ rolling moment coefficient, alternate form

$M' = M/(\frac{1}{2})\rho l^3U^2$ pitching moment coefficient

$C_M = M/(\frac{1}{2})\rho AlU^2$ . . pitching moment coefficient, alternate form

$N' = N/(\frac{1}{2})\rho l^3U^2$ . . . yawing moment coefficient

$C_N = N/(\frac{1}{2})\rho AlU^2$ . . . yawing moment coefficient, alternate form

Coefficients of Static Force Derivatives

The partial derivative of a force or moment component X, Y, Z, K, M, or N with respect to a linear or angular velocity or acceleration u, v, w, p, q, r, $\dot{u}$, $\dot{v}$, $\dot{w}$, $\dot{p}$, $\dot{q}$, $\dot{r}$ will be designated by the force or moment with the velocity or acceleration as a subscript; e.g., $\partial Y/\partial p = Y_p$.

$$X_u' = \frac{X_u}{(\frac{1}{2})\rho l^2U}, X_v' = \frac{X_v}{(\frac{1}{2})\rho l^2U}, X_w' = \frac{X_w}{(\frac{1}{2})\rho l^2U}$$

$$Y_u' = \frac{Y_u}{(\frac{1}{2})\rho l^2U}, Y_v' = \frac{Y_v}{(\frac{1}{2})\rho l^2U}, Y_w' = \frac{Y_w}{(\frac{1}{2})\rho l^2U}$$

$$Z_u' = \frac{Z_u}{(\frac{1}{2})\rho l^2U}, Z_v' = \frac{Z_v}{(\frac{1}{2})\rho l^2U}, Z_w' = \frac{Z_w}{(\frac{1}{2})\rho l^2U}$$

Note that also $X_u' = \partial X'/\partial u'$, $X_v' = \partial X'/\partial v'$, etc.

Coefficients of Rotary Force Derivatives

$$X_p' = \frac{X_p}{(\frac{1}{2})\rho l^3U}, X_q' = \frac{X_q}{(\frac{1}{2})\rho l^3U}, X_r' = \frac{X_r}{(\frac{1}{2})\rho l^3U}$$

$$Y_p' = \frac{Y_p}{(\frac{1}{2})\rho l^3U}, Y_q' = \frac{Y_q}{(\frac{1}{2})\rho l^3U}, Y_r' = \frac{Y_r}{(\frac{1}{2})\rho l^3U}$$

$$Z_p' = \frac{Z_p}{(\frac{1}{2})\rho l^3U}, Z_q' = \frac{Z_q}{(\frac{1}{2})\rho l^3U}, Z_r' = \frac{Z_r}{(\frac{1}{2})\rho l^3U}$$

Note that also $X_p' = \partial X'/\partial p'$, $X_q' = \partial X'/\partial q'$, etc.

Virtual Inertia Coefficients

$$X_{\dot{u}}' = \frac{X_{\dot{u}}}{(\frac{1}{2})\rho l^3}, X_{\dot{v}}' = \frac{X_{\dot{v}}}{(\frac{1}{2})\rho l^3}, X_{\dot{w}}' = \frac{X_{\dot{w}}}{(\frac{1}{2})\rho l^3}$$

$$Y_{\dot{u}}' = \frac{Y_{\dot{u}}}{(\frac{1}{2})\rho l^3}, Y_{\dot{v}}' = \frac{Y_{\dot{v}}}{(\frac{1}{2})\rho l^3}, Y_{\dot{w}}' = \frac{Y_{\dot{w}}}{(\frac{1}{2})\rho l^3}$$

$$Z_{\dot{u}}' = \frac{Z_{\dot{u}}}{(\frac{1}{2})\rho l^3}, Z_{\dot{v}}' = \frac{Z_{\dot{v}}}{(\frac{1}{2})\rho l^3}, Z_{\dot{w}}' = \frac{Z_{\dot{w}}}{(\frac{1}{2})\rho l^3}$$

$$X_{\dot{p}}' = \frac{X_{\dot{p}}}{(\frac{1}{2})\rho l^4}, X_{\dot{q}}' = \frac{X_{\dot{q}}}{(\frac{1}{2})\rho l^4}, X_{\dot{r}}' = \frac{X_{\dot{r}}}{(\frac{1}{2})\rho l^4}$$

$$Y_{\dot{p}}' = \frac{Y_{\dot{p}}}{(\frac{1}{2})\rho l^4}, Y_{\dot{q}}' = \frac{Y_{\dot{q}}}{(\frac{1}{2})\rho l^4}, Y_{\dot{r}}' = \frac{Y_{\dot{r}}}{(\frac{1}{2})\rho l^4}$$

$$Z_{\dot{p}}' = \frac{Z_{\dot{p}}}{(\frac{1}{2})\rho l^4}, Z_{\dot{q}}' = \frac{Z_{\dot{q}}}{(\frac{1}{2})\rho l^4}, Z_{\dot{r}}' = \frac{Z_{\dot{r}}}{(\frac{1}{2})\rho l^4}$$

Note that also $X_{\dot{u}}' = \partial X'/\partial \dot{u}'$, $X_{\dot{p}}' = \partial X'/\partial \dot{p}'$, etc.

Coefficients of Static Moment Derivatives

$$K_u' = \frac{K_u}{(\frac{1}{2})\rho l^3 U}, K_v' = \frac{K_v}{(\frac{1}{2})\rho l^3 U}, K_w' = \frac{K_w}{(\frac{1}{2})\rho l^3 U}$$

$$M_u' = \frac{M_u}{(\frac{1}{2})\rho l^3 U}, M_v' = \frac{M_v}{(\frac{1}{2})\rho l^3 U}$$

$$M_w' = \frac{M_w}{(\frac{1}{2})\rho l^3 U}$$

$$N_u' = \frac{N_u}{(\frac{1}{2})\rho l^3 U}, N_v' = \frac{N_v}{(\frac{1}{2})\rho l^3 U}, N_w' = \frac{N_w}{(\frac{1}{2})\rho l^3 U}$$

Note that also $K_u' = \partial K'/\partial u'$, $K_v' = \partial K'/\partial v'$, etc.

Virtual Moment of Inertia Coefficients

$$K_{\dot u}' = \frac{K_{\dot u}}{(\frac{1}{2})\rho l^4}, K_{\dot v}' = \frac{K_{\dot v}}{(\frac{1}{2})\rho l^4}, K_{\dot w}' = \frac{K_{\dot w}}{(\frac{1}{2})\rho l^4}$$

$$M_{\dot u}' = \frac{M_{\dot u}}{(\frac{1}{2})\rho l^4}, M_{\dot v}' = \frac{M_{\dot v}}{(\frac{1}{2})\rho l^4}, M_{\dot w}' = \frac{M_{\dot w}}{(\frac{1}{2})\rho l^4}$$

$$N_{\dot u}' = \frac{N_{\dot u}}{(\frac{1}{2})\rho l^4}, N_{\dot v}' = \frac{N_{\dot v}}{(\frac{1}{2})\rho l^4}, N_{\dot w}' = \frac{N_{\dot w}}{(\frac{1}{2})\rho l^4}$$

$$K_p' = \frac{K_p}{(\frac{1}{2})\rho l^5}, K_q' = \frac{K_q}{(\frac{1}{2})\rho l^5}, K_r' = \frac{K_r}{(\frac{1}{2})\rho l^5}$$

$$M_p' = \frac{M_p}{(\frac{1}{2})\rho l^5}, M_q' = \frac{M_q}{(\frac{1}{2})\rho l^5}, M_r' = \frac{M_r}{(\frac{1}{2})\rho l^5}$$

$$N_p' = \frac{N_p}{(\frac{1}{2})\rho l^5}, N_q' = \frac{N_q}{(\frac{1}{2})\rho l^5}, N_r' = \frac{N_r}{(\frac{1}{2})\rho l^5}$$

Note that also $K_p' = \partial K'/\partial p'$, $K_q' = \partial K'/\partial p'$, etc.

Coefficients of Rotary Moment Derivatives

$$K_p' = \frac{K_p}{(\frac{1}{2})\rho l^4 U}, K_q' = \frac{K_q}{(\frac{1}{2})\rho l^4 U}, K_r' = \frac{K_r}{(\frac{1}{2})\rho l^4 U}$$

$$M_p' = \frac{M_p}{(\frac{1}{2})\rho l^4 U}, M_q' = \frac{M_q}{(\frac{1}{2})\rho l^4 U}$$

$$M_r' = \frac{M_r}{(\frac{1}{2})\rho l^4 U}$$

$$N_p' = \frac{N_p}{(\frac{1}{2})\rho l^4 U}, N_q' = \frac{N_q}{(\frac{1}{2})\rho l^4 U}, N_r' = \frac{N_r}{(\frac{1}{2})\rho l^4 U}$$

Note that also $K_p' = \partial K'/\partial p'$, $K_q' = \partial K'/\partial q'$, etc.

Linearized Expansion of Force and Moment Coefficients

In the following analysis, all quantities are non-dimensionalized, so that primes may be omitted.

It will be assumed that the hydrodynamic force and moment coefficients depend only upon the non-dimensionalized linear and angular velocity and acceleration components; i.e., $X = X(u, v, w, p, q, r, \dot u, \dot v, \dot w, \dot p, \dot q, \dot r)$, with similar forms for Y, Z, K, M, and N.

Let $u_o, v_o, w_o, p_o, q_o, r_o, \dot u_o, \dot v_o, \dot w_o, \dot p_o, \dot q_o, \dot r_o$ describe the state of motion of the body at a time t_o. Then, for small changes from this initial state we have the linearized Taylor expansion

$$\begin{aligned} X = X_o &+ X_u(u - u_o) + X_v(v - v_o) + \\ &X_w(w - w_o) \\ &+ X_p(p - p_o) + X_q(q - q_o) + \\ &X_r(r - r_o) \\ &+ X_{\dot u}(\dot u - \dot u_o) + X_{\dot v}(\dot v - \dot v_o) + \\ &X_{\dot w}(\dot w - \dot w_o) \\ &+ X_{\dot p}(\dot p - \dot p_o) + X_{\dot q}(\dot q - \dot q_o) + \\ &X_{\dot r}(\dot r - \dot r_o) \end{aligned}$$

with similar expressions for Y, Z, K, M, and N.

Equations of Motion for a Free Body

The simplest form of the equations of motion is obtained with body axes coincident with the principal axes of inertia, and the origin at the center of mass CG. For this case the equations are, in dimensionless form,

$$\begin{aligned} X &= m[\dot u + qw - rv] \\ Y &= m[\dot v + ru - pw] \\ Z &= m[\dot w + pv - qu] \\ K &= I_x\dot p + (I_z - I_y)qr \\ M &= I_y\dot q + (I_x - I_z)rp \\ N &= I_z\dot r + (I_y - I_x)pq \end{aligned}$$

When the origin of the body axes is not at CG, as has been proposed when CG does not lie in the plane of symmetry, the equations of motion assume the more complex form

$$\begin{aligned} X = m[&\dot u + qw - rv - x_o(q^2 + r^2) + \\ &y_o(pq - \dot r) + z_o(pr + \dot q)] \end{aligned}$$

with similar expressions for Y and Z.

$$\begin{aligned} K = I_x\dot p + (I_z - I_y)qr + \\ m[y_o(\dot w + pv - qu) - z_o(\dot v + ru - pw)] \end{aligned}$$

with similar expressions for M and N.

The linearization of these equations in a particular problem introduces considerable simplification.

Equilibrium Equations for a Towed Body

The application of the proposed nomenclature to the case of a stable kite or paravane will be considered as an example. Equations for determining the attitude of the body when the hydrodynamic characteristics of the body are known will be presented.

It will be supposed that the body is towed at a uniform speed in a fixed direction in the horizontal plane. Let the x_0-axis be in the direction of tow.

Since equilibrium is assumed, the hydrodynamic forces and moments are functions of u, v, and w, or α, β, U only; e.g., $X = X(u, v, w)$.

The resultant of weight and buoyancy is the force $W - B$ in the z_0 direction, acting at CS. The direction cosines of the z_0-axis relative to the body axis, n_x, n_y, n_z, in terms of α, β, γ, may be read from Table 2.

The towline tension acts at a point TP whose coordinates (x_T, y_T, z_T) are functions of α, β, γ which depend upon the type of bridle used for attaching the towline to the body. In the simplest case, when the towline is attached directly to the body (single point of attachment), we may take the origin of body axes, O, at TP, so that $x_T = y_T = z_T = 0$.

The equations may be written as follows:

$$X(\alpha, \beta, U) + F_x + n_x(W - B) = 0$$
$$Y(\alpha, \beta, U) + F_y + n_y(W - B) = 0$$
$$Z(\alpha, \beta, U) + F_z + n_z(W - B) = 0$$

$$K(\alpha, \beta, U) + y_T F_z - z_T F_y + (W - B)(y_B n_z - z_B n_y) = 0$$
$$M(\alpha, \beta, U) + z_T F_x - x_T F_z + (W - B)(z_B n_x - x_B n_z) = 0$$
$$N(\alpha, \beta, U) + x_T F_y - y_T F_x + (W - B)(x_B n_y - y_B n_x) = 0$$

Since n_x, n_y, n_z are functions of α, β, γ from Table 2, and x_T, y_T, z_T are also assumed to be known functions of α, β, γ from the bridle geometry, these are six equations in the unknowns α, β, γ, F_x, F_y, F_z.

Physical and Other Terms

ρ ..... mass density
g ..... acceleration due to gravity
$F = U/\sqrt{gl}$, $V/\sqrt{gl}$ ..... Froude number
μ ..... coefficient of viscosity
ν ..... kinematic viscosity, μ/ρ

$R_l = Ul/\nu$, Vl/ν
$R_d = Ud/\nu$, Vd/ν
$R_x = Ux/\nu$, Vx/ν
$R_\delta = U\delta/\nu$, $V\delta/\nu$
} Reynolds numbers corresponding to various linear dimensions

λ ..... linear ratio of full size body to model
t ..... time
n ..... a frequency
$S_l = nl/U$, $S_d = nd/U$ ..... Strouhal numbers corresponding to various linear dimensions
σ ..... cavitation number
σ_i ..... roots of the stability equation, $i = 1, 2, \ldots$

Definitions of Stability

Metacentric Stability

A body, floating in equilibrium either completely submerged or on the surface of a fluid, is said to have *metacentric stability* if, when disturbed from the equilibrium position in either trim or heel, it returns to the original position. If it is stable against a disturbance in heel, it is said to have *transverse metacentric stability*. If it is stable against a disturbance in trim, it is said to have *longitudinal metacentric stability*. A body may have metacentric stability about a position other than the upright position; in this case, the position of equilibrium must be stated. Metacentric stability implies that the metacentric height m is positive; that is, CM is above CG.

Translational Stability

In discussing the directional stability of a body it is convenient to distinguish between the stability of the body when restrained to move only like a weathercock, and the stability of the unrestrained motion.

(*a*) *Static (or Weathercock) Stability.* Suppose the body to be moving in a constant direction and restrained so that its only freedom of motion is that of rotation about an axis perpendicular to

the direction of motion. The body is said to be statically stable about the given axis in some equilibrium orientation about it, if it returns to this orientation after a slight disturbance. If the body is stable about the transverse axis, it is said to have *static pitching stability;* in this case, the slope of the pitching moment curve M_θ is negative. If stable about the normal axis, it is said to have *static yawing stability;* in this case, the slope of the yawing moment curve N_ψ is negative. Static stability requires that the center of pressure be aft of the axis of rotation. The negative magnitudes of the derivatives M_θ and N_ψ for some orientation of a body are a measure of the static stability of the body.

(*b*) *Dynamic Stability on Course.* A body is said to be *dynamically stable on course* if, after its steady state motion has been slightly disturbed from a straight course with fixed control surfaces, it resumes its motion on another straight course.

A ship is said to be *dynamically stable in a turn* if, after its motion has been slightly disturbed from a given circular turn with fixed control surfaces, it resumes a motion in a turn of the same diameter, with a slight displacement of the path.

Dynamic stability can be further classified as *longitudinal stability*, for motion in the plane of symmetry; or *lateral stability*, for motions involving rolling, yawing, and sideslipping.

Summary

Operations	Example	Definitions
(dot) over a symbol	$\dot{u} = du/dt$	Derivative with respect to time
′ (prime) of a symbol	$m' = m/(\frac{1}{2})\rho l^3$	Non-dimensional form of a symbol
subscript $u, v, w, p, q, r, \dot{u}, \dot{v}, \dot{w}, \dot{p}, \dot{q}$, or $\dot{r}$ applied to X, Y, Z, K, M, or N	$Y_p = \partial Y/\partial p$	Partial derivative with respect to subscript
′ (prime) of result of previous operation	$Y_p' = (\partial Y/\partial p)'$ $= \partial Y''/\partial p'$	Non-dimensional form of the partial derivative with respect to the subscript

Symbol	Typical non-dimensional formula	Definition of symbol
$a = b^2/A_s$	.....	Aspect ratio
A	$A' = A/l^2$	A projected area, qualified by an appropriate subscript
A_b, A_r, A_s	$A_b' = A_b/l^2$	Projected area of bow plane, rudder and stern plane, respectively
A_x, A_y, A_z	$A_x' = A_x/l^2$ $C_x = A_x/bll$	Area of projection of submerged part of body on ys, zx, and xy-planes, respectively
b	$b' = b/l$	Beam of body
B	$B' = B/(\frac{1}{2})\rho l^2 U^2$	Buoyancy force
c	$c' = c/l$	Chord length
C	$C' = C/(\frac{1}{2})\rho l^2 U^2$ $C_a = C/(\frac{1}{2})\rho A U^2$	Cross force
CB	.....	Center of buoyancy
CG	.....	Center of mass of body
CM	.....	Metacenter of body
CP	.....	Center of pressure
CS	.....	Static center; center of resultant of weight and buoyancy
d or D	$d' = d/l = D/l$	Diameter of a body of revolution
D or R	$D' = D/(\frac{1}{2})\rho l^2 U^2$ $C_D = D/(\frac{1}{2})\rho A U^2$ $c_D = D/(\frac{1}{2})\rho V^{2/3} U^2$ $C_l = D/(\frac{1}{2})\rho S U^2$	Drag force; resistance
D_f	$C_f = D_f/(\frac{1}{2})\rho S U^2$	Friction drag
D_r	$C_r = D_r/(\frac{1}{2})\rho S U^2$	Residuary drag, $C_r = C_l - C_f$
F	.....	Froude number, $U/\sqrt{gl}$, $V/\sqrt{gl}$

Symbol	Typical non-dimensional formula	Definition of symbol
g	.....	Acceleration of gravity
m or GM	.....	Metacentric height
H	$H' = H/l$	Draft of a body
h	.....	The depth of submergence of a submerged body
h	.....	The hull height of a submerged body, measured from the bottom to the top of the hull (pronounced height)
I_x, I_y, I_z	$I_x' = I_x/(\frac{1}{2})\rho l^5$	Moments of inertia about x, y, z axes, respectively
k	$k' = k/l$	Radius of gyration
k_x, k_y, k_z	$k_x' = k_x/l$	Radii of gyration about x, y, z axes, respectively
K, M, N	$K' = K/(\frac{1}{2})\rho l^3 U^2$ $C_K = K/(\frac{1}{2})\rho A l U^2$	Rolling, pitching, and yawing moments, respectively
K_u	$K_u' = K_u/(\frac{1}{2})\rho l^3 U = \partial K'/\partial u'$	Typical static moment derivative; derivative of a moment component with respect to a velocity component, $\partial K/\partial u$
$K_{\dot{u}}$	$K_{\dot{u}}' = K_{\dot{u}}/(\frac{1}{2})\rho l^4 = \partial K'/\partial \dot{u}'$	Typical moment of inertia coefficient; derivative of a moment component with respect to an acceleration component, $\partial K/\partial \dot{u}$
K_p	$K_p' = K_p/(\frac{1}{2})\rho l^4 U = \partial K'/\partial p'$	Typical rotary moment derivative of a moment component with respect to an angular velocity component, $\partial K/\partial p$
$K_{\dot{p}}$	$K_{\dot{p}}' = K_{\dot{p}}/(\frac{1}{2})\rho l^5 = \partial K'/\partial \dot{p}'$	Typical moment of inertia coefficient; derivative of a moment component with respect to an angular acceleration component, $\partial K/\partial \dot{p}$
l or L	$l' = 1$	A characteristic length of body
L	$L' = L/(\frac{1}{2})\rho l^2 U^2$ $C_L = L/(\frac{1}{2})\rho A U^2$	Lift force
m or GM	.....	Metacentric height
m	$m' = m/(\frac{1}{2})\rho l^3$	Mass of body
n	$n' = nl/U$	Frequency
n_x, n_y, n_z	.....	Direction cosines of vertical relative to body axes
O	.....	Origin of body axes
p, q, r	$p' = pl/U$	Angular velocities of roll, pitch, and yaw, respectively
Q	$Q' = Q/(\frac{1}{2})\rho l^3 U^2$	Torque about axis of a control surface
R or D	.....	Resistance or drag force
R_c	.....	Radius of turning path, or radius of curvature
R_l, R_d, R_x, R_δ	.....	Reynolds number, Ul/ν, Ud/ν, Ux/ν, $U\delta/\nu$
S	$S' = S/l^2$	Wetted surface area
S_l, S_d	.....	Strouhal number, nl/U, nd/U
t	$t' = t/l$	Thickness
t	$t' = tU/l$	Time
$\mathcal{T}$	$\mathcal{T}' = \mathcal{T}/(\frac{1}{2})\rho l^2 U^2$	Towline tension (pronounced toll)
$\mathcal{T}_x$, $\mathcal{T}_y$, $\mathcal{T}_z$	.....	Components of towline tension relative to body axes
TP	.....	Towpoint at body
u, v, w	$u' = u/U$	Longitudinal, transverse, and normal components, respectively, of the velocity of the origin of body axes relative to the fluid
U or V	$U' = 1$	Velocity of origin of body axes relative to fluid
$\mathcal{V}$	$\mathcal{V}' = \mathcal{V}/l^3$ $C_B = \mathcal{V}/lbH$ $C_P = \mathcal{V}/lA_x$	Volume of body (pronounced vol) Block coefficient Prismatic coefficient
W or Δ	$W' = W/(\frac{1}{2})\rho l^3 U^2$	Weight of body
x, y, z	$x' = x/l$	Body axes, or coordinates of a point relative to body axes

Symbol	Typical non-dimensional formula	Definition of symbol
x_p, y_p, z_p	. . . . .	Coordinates of center of buoyancy relative to body axes
x_g, y_g, z_g	$x_g' = x_g/l$	Coordinates of center of mass relative to body axes
x_0, y_0, z_0	. . . . .	Fixed axes, or coordinates of a point relative to fixed axes
x_s, y_s, z_s	. . . . .	Coordinates of static center relative to body axes
x_T, y_T, z_T	. . . . .	Coordinates of towpoint (at body) relative to body axes
X, Y, Z	$X' = X/(\frac{1}{2})\rho l^2 U^2$	Longitudinal, lateral, and normal components, respectively, of hydrodynamic force on body
X_u	$X_u' = X_u/(\frac{1}{2})\rho l^2 U = \partial X'/\partial u'$	Typical static force derivative; derivative of a force component with respect to a velocity component, $\partial X/\partial u$
$X_{\dot{u}}$	$X_{\dot{u}}' = X_{\dot{u}}/(\frac{1}{2})\rho l^3 = \partial X'/\partial \dot{u}'$	Typical inertia coefficient; derivative of a force component with respect to an acceleration component, $\partial X/\partial \dot{u}$
X_p	$X_p' = X_p/(\frac{1}{2})\rho l^3 U = \partial X'/\partial p'$	Typical rotary force derivative; derivative of a force component with respect to an angular velocity component, $\partial X/\partial p$
$X_{\dot{p}}$	$X_{\dot{p}}' = X_{\dot{p}}/(\frac{1}{2})\rho l^4 = \partial X'/\partial \dot{p}'$	Typical inertia coefficient; derivative of a force component with respect to an angular acceleration component, $\partial X/\partial \dot{p}$
α, β, γ	. . . . .	Angles of attack, drift, and roll, respectively
δ	. . . . .	Thickness of boundary layer
δ	. . . . .	Angular displacement of a control surface
$\delta_r, \delta_b, \delta_s$	. . . . .	Rudder angle, bow plane angle, stern plane angle
Δ	. . . . .	Weight of body
θ, ψ, ϕ	. . . . .	Angles of pitch, yaw, and roll, respectively
λ	. . . . .	Linear ratio, full-scale size to model size
μ	. . . . .	Coefficient of viscosity
ν	. . . . .	Kinematic viscosity, μ/ρ
ρ	. . . . .	Mass density
σ	. . . . .	Cavitation number
σ_i	. . . . .	Roots of stability equation, $i = 1, 2, \ldots$

OTHER SYMBOLS

Other symbols used in this report not included in the SNAME Technical and Research Bulletin 1-5 (pp. A-1 through A-13) follow:

Dimensionless Forms. The characteristic area used in forming dimensionless quantities is A_x, the maximum cross-sectional area of the bare hull. The length ℓ is the overall length of the missile.

Origin of Body Axes. The origin of the body axes is considered to be the center of buoyancy, CB, of the hull.

A,B,C,D,A*,B*,C*	constants appearing in approximate form of high speed vertical planar motion equations
$(A_p)_F$	projected area of (2) fins
AR'	aspect ratio of fins - augmented to account for fin-body interference effects when used in Prandtl formula for z_i'.
b	constant appearing in solutions of motion equations
b_t	tip-to-tip fin span
$C_{z_{Bi}}$	body interference vertical force coefficient
C_{z_w}	fin normal force coefficient
C_{z_α}	fin normal force derivative coefficient based on $(A_p)_F$
D_p, R_p	constants appearing in representation for X_o' based on the drag characteristics of a flat plate
D_s, R_s	constants appearing in representation for X_o' based on the drag characteristics of a sphere

I_{y_o}	moment of inertia of displaced fluid
K_1, K_2, K_3, K_4	constants appearing in approximate solution of motion equations for high speed vertical planar trajectories
m_v	added mass of parallelepiped - used to estimate virtual masses and moments of inertia of fins
m_1	apparent mass
q_H, q_P	homogeneous and particular components, respectively, of solution for q obtained from approximate form of high speed vertical planar motion equations
s_1, s_2, t_1	dimensions of parallelepiped, in cm - used in calculation of added mass
t_o	initial value of time in trajectory predictions
X'_{o_b}	base drag coefficient
X'_{o_f}	friction drag coefficient
X'_{o_p}	drag coefficient function based on drag characteristics of a flat plate
X'_{o_s}	drag coefficient function based on drag characteristics of a sphere
$(X'_o)_{BH}$, $(Z'_w)_{BH}$, $(M'_q)_{BH}$, etc.	hydrodynamic coefficients of bare hull
$(X'_o)_F$, $(Z'_w)_F$, $(M'_q)_F$, etc.	hydrodynamic coefficients of fins
x_b	x-coordinate of base of hull
x_F	x-coordinate of point of application of $(Z'_w)_F$

x_1	x-coordinate of point of application of z_1
z_1	increase in normal force derivative due to the addition of fins to the bare hull
Δm_1, $\Delta X'_o$,	
$\Delta u(0)$, etc.	errors in values of input parameters
Δt	iteration period in numerical solution of motion equations
$\Delta \dot{x}_o$, $\Delta \dot{z}_o$, etc.	errors in solutions of motion equations
ζ, η	constants appearing in straight vertical trajectory motion equation with constant drag coefficient
ζ_s, η_s, ξ	constants appearing in straight vertical trajectory motion equation with drag coefficient function based on drag characteristics of a sphere
χ, Ω	constants appearing in solution of straight vertical trajectory motion equation with drag coefficient function based on drag characteristics of a sphere
$\lambda, \mu, \lambda^*, \mu^*$	constants appearing in approximate solution of motion equations for high speed vertical planar trajectories
σ_1 σ_2	roots of indicial equation in approximate solution of motion equations for high speed vertical planar trajectories
τ	function appearing in approximate solution of motion equations for high speed vertical planar trajectories

APPENDIX B
EVALUATION OF HYDRODYNAMIC DERIVATIVE COEFFICIENTS

1. Evaluation From Experimental Data

a. Fairing of Curves

Certain data were presented in the form of graphs of hydrodynamic force and moment coefficients plotted versus angle of attack. To evaluate derivative coefficients from these data, curves were faired and the values of their slopes or intercepts were estimated. Since the curves were faired by "eye," the process was repeated several times, by two different people. The reported values for the derivatives are averages of the repeated evaluations.

b. Conversion of Coefficients from Aerodynamic Reference Frame to x, y, z System

Forces and moments measured with respect to a standard aerodynamic reference frame (see sketch) may be converted into hydrodynamic coefficients with respect to the x, y, z frame with coincident origin by applying the following three equations:

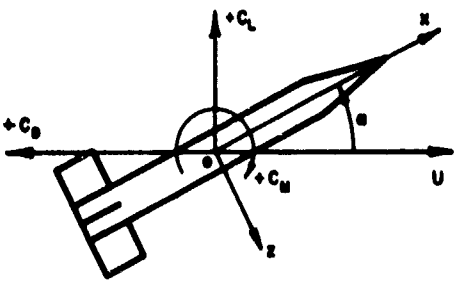

$$X' = -C_D \cos\alpha + C_L \sin\alpha,$$

$$Z' = -C_D \sin\alpha - C_L \cos\alpha,$$

$$M' = -C_M$$

In the present case, however, it was more convenient to transform the derivative coefficients themselves. Using the preceding equations, taking the required derivatives and evaluating them at $\alpha = 0$, gives the necessary relationships:

$$X'_o = -C_{D_o}$$

$$Z'_\alpha = -C_{D_o} - C_{L_\alpha}$$

$$M'_\alpha = -C_{M_\alpha}$$

c. Conversion of Derivatives with respect to α into Derivatives with respect to w'

From Fig. 3 of Appendix A,

$$w' = \frac{w}{U} = \sin \alpha$$

Therefore, by the chain rule for differentiation,

$$\frac{\partial}{\partial \alpha} = \frac{dw'}{d\alpha} \frac{\partial}{\partial w'} = (\cos \alpha) \frac{\partial}{\partial w'}$$

Thus, for $\alpha = 0$,

$$Z'_w = Z'_\alpha$$

$$M'_w = M'_\alpha$$

etc.

d. Conversion of Yaw Plane Derivative into Pitch Plane Derivative

Because the xy plane and the xz plane are similar planes of symmetry for the Basic Finner, the yaw plane and pitch plane hydrodynamic derivatives are directly related by the following formulas, easily derived by geometric considerations.

$$Z'_w = Y'_v \qquad M'_w = -N'_v$$

$$Z'_w = Y'_v \qquad M'_q = N'_r$$

$$Z'_q = -Y'_r \qquad M'_q = N'_r$$

$$X'_{wq} = -X'_{vr}$$

e. Conversion of Derivatives to x, y, z System with Origin at CB

Let quantities measured with respect to the x,y,z frame whose origin is at the CB be identified by the subscript "g." Consider another x,y,z coordinate system whose origin

has coordinates $(x_{ts},0,0)$ in the "s" frame. Let quantities measured with respect to this frame be identified by the subscript "t." The hydrodynamic derivative coefficients measured with respect to the "t" frame are converted to the "s" frame by application of the following equations.[32]

$$(Z'_w)_s = (Z'_w)_t$$

$$(Z'_{\dot{w}})_s = (Z'_{\dot{w}})_t$$

$$(Z'_q)_s = (Z'_q)_t - x'_{ts}\,(Z'_w)_t$$

$$(M'_w)_s = (M'_w)_t - x'_{ts}\,(Z'_w)_t$$

$$(M'_q)_s = (M'_q)_t - x'_{ts}\left[(Z'_q)_t + (M'_w)_t\right] + x'^{2}_{ts}\,(Z'_w)_t$$

$$(M'_{\dot{q}})_s = (M'_{\dot{q}})_t - x'_{ts}\left[(Z'_{\dot{q}})_t + (M'_{\dot{w}})_t\right] + x'^{2}_{ts}\,(Z'_{\dot{w}})_t$$

f. Conversion of Derivative Coefficients to Standard Nondimensionalization Basis

The characteristic area used herein in forming dimensionless quantities is A_x, the maximum cross-sectional area of the bare hull. The length ℓ is the overall length of the missile. Derivative coefficients based on different nondimensionalizing parameters are converted to this basis, by multiplying them by appropriate ratios. For example, if $(M'_q)_{A_x,d}$ denotes the coefficients of damping moment derivative based on maximum cross-sectional area and maximum diameter, i.e., $M_q = \frac{1}{2}\rho A_x d^2 (M'_q)_{A_x,d}$ the conversion is made by applying

$$M'_q = \left(\frac{d}{\ell}\right)^2 (M'_q)_{A_x,d}$$

where M'_q denotes the coefficient based on A_x and ℓ.

2. Sample Calculation

Several of the procedures described in the preceding section now will be illustrated in determining one of the derivative coefficient values. The example shows the derivation of the value of M'_w based on data for a 4"D wood model reported by Heald and Adams.[5]

The relevant test data are presented in a graph of $\left[(M')_{A_x,d}\right]_t$ vs α, where the interior subscripts indicate the nondimensionalizing parameters, A_x and d, and the exterior subscript t indicates that the origin of coordinates of the x,y,z system is not at the CB, but at the base of the missile.*

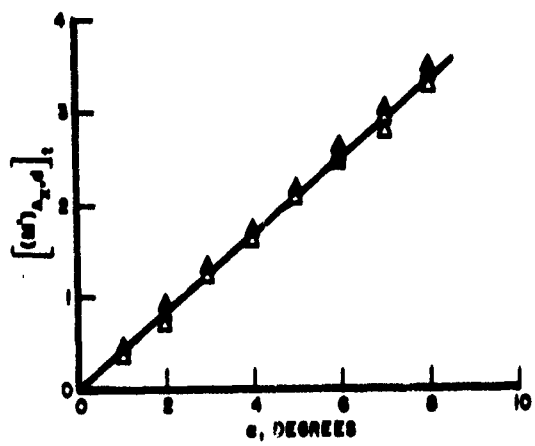

Repeated fairings of these data by two different people yielded estimates of slopes in the range, $23.0 \leq \left[(M'_\alpha)_{A_x,d}\right]_t \leq 25.1$ (α in radians). The value used in the

* This is not the notation of ref. 5. It has been introduced here for consistency with the preceding sections.

subsequent calculations is $\left[(M'_\alpha)_{A_x,d}\right]_t = 24.0$. This value corresponds to the line shown on the graph above.

To convert to the nondimensional form based on A_x and ℓ, the rules on p. B-3 are used to give

$$\left[M'_\alpha\right]_t = \left(\frac{d}{\ell}\right)\left[(M'_\alpha)_{A_x,d}\right]_t = \left(\frac{4}{40}\right)\ (24.0) = 2.40$$

Then, using the results on p. B-2,

$$\left[M'_w\right]_t = \left[M'_\alpha\right]_t = 2.40$$

To adjust this value to the x,y,z coordinate system with origin at the CB by the methods on p. B-2, it is necessary to know the corresponding value for the coefficient of static force derivative, Z'_w. Repeated fairings of the Z' vs α curve and application of the results on p. B-2 yielded the range $-12.0 \leq Z'_w \leq -11.8$. Using the value $Z'_w = -11.9$ together with $x'_{ts} = -0.40$, the dimensionless longitudinal coordinate of the base relative to the CB yields the final result

$$\left[M'_w\right]_s = \left[M'_w\right]_t - x'_{ts}\left[Z'_w\right]_t = 2.40 - (-.4)(-11.9) = -2.4$$

3. Theoretical Estimates

The hydrodynamic static and damping derivative coefficients were estimated by means of relationships based on geometric arguments. These equations, similar to many geometrically founded relationships commonly used in theoretical aerodynamics,[18] were formulated in the form below by Strumpf.[1]

$$Z'_w = (Z'_w)_{BH} + z'_1 \qquad \text{(B-1)}$$

$$Z'_q = (Z'_q)_{BH} - x'_1 z'_1 \qquad \text{(B-2)}$$

$$M'_w = (M'_w)_{BH} - x'_1 z'_1 \qquad \text{(B-3)}$$

$$M'_q = (M'_q)_{BH} + x'^2_1 z'_1 \qquad \text{(B-4)}$$

where the coefficients with subscripts "BH" represent bare hull values, z_1' is the increase in the static force derivative coefficient due to the addition of fins to the bare hull, and x_1' is the dimensionless longitudinal coordinate of the point of application of z_1'. The bare hull coefficients were estimated using slender body theory as developed by Munk,[33] and modified by Allen and Perkins,[34] Kelly,[35] and Martin.[36] On the basis of these results,

$$(Z_w')_{BH} = -2.0$$

$$(M_w')_{BH} = 2(C_p + x_b')$$

$$(Z_q')_{BH} = 2x_b'$$

$$(M_q')_{BH} = -2x_b'^2$$

where C_p is the prismatic coefficient and x_b' is the non-dimensionalised x coordinate of the base of the hull.

The value of z_1' was estimated using two different theories. The first of these, due to Flax and Lawrence,[32] uses low aspect ratio wing theory[37] to predict the contribution of the fins, and the results of Low and Stone,[34] Spreiter,[38] and Lennertz[40] to account for the fin body interference effects. z_1' is determined from

$$z_1' = C_{z_\alpha} \left(1 + \frac{d}{b_t}\right) \left(1 + \frac{C_{z_{Bi}}}{C_{z_w}}\right) \frac{(A_p)_F}{A_x} \qquad \text{(B-5)}$$

where C_{z_α} is the fin normal force derivative coefficient based on wing area, d is the body diameter, b_t is the tip-to-tip fin span, $C_{z_{Bi}}$ is the body interference normal force coefficient, C_{z_w} is the fin normal force coefficient, $(A_p)_F$ is the projected area of the (2) fins and A_x is the body cross-sectional area. The values of both C_{z_α} and the ratio $C_{z_{Bi}}/C_{z_w}$

are obtained from curves presented by Flax and Lawrence. The values obtained are $C_{z_\alpha} = -2.5$, $C_{z_{Bl}}/C_{z_w} = 0.38$, on the basis of which, eq. B-5 yields $z_i' = -11.7$.

The second method of predicting z_i', used previously by Davidson Laboratory and others in airship and torpedo work, uses the Prandtl formula for elliptically loaded high aspect ratio wings,[18]

$$z' = -\frac{2\pi}{1+2/AR'}\frac{(A_p)_F}{A_x} \tag{B-6}$$

where the augmented aspect ratio, AR', is defined by

$$AR' = \frac{b_t}{c} \tag{B-7}$$

where c is the chord of the fins. This definition of the aspect ratio of the fin system accounts for the effects of all fin-body interactions. On the basis of eqs. B-6 and B-7, $Z_i' = -9.6$.

No theoretical or empirical method for determining x_i' precisely is known. Experimental evidence indicates, however, that x_i' corresponds to a longitudinal coordinate of the fin on the body. Accordingly, estimates for M_w', Z_q', and M_q' were made on the basis of all x_i' values corresponding to fin coordinates, and for z_i' values derived using both the low aspect ratio theory and the airship theory. The results are presented in graphical form in Fig. 3. The values ultimately selected for use in the trajectory predictions, corresponding to $z_i' = -9.6$ and $x_i' = -0.31$, also are listed in Table I.

The drag coefficient X_o', was estimated with the guidance of empirical results published in the literature. The effect on the drag coefficient of the mutual interference between the body and the fins was assumed negligible. Thus,

$$X_o' = (X_o')_{BH} + (X_o')_F \tag{B-8}$$

where $(X'_o)_{BH}$ and $(X'_o)_F$ are, respectively, the coefficients for the bare hull and for the fins, each evaluated as though the other component were not present. A value of $(X'_o)_F = -0.24$ was estimated on the basis of experimental data for two-dimensional wedges presented by Hoerner.[41] The friction drag coefficient for the bare hull, $(X'_{o_f})_{BH}$, was estimated to be -0.13, a value which approximates the Schoenherr friction line for Reynolds numbers near 2×10^8. The base drag coefficient for the bare hull, $(X'_{o_b})_{BH}$, was estimated using an empirical formula presented by Hoerner,[41]

$$(X'_{o_b})_{BH} = -\frac{0.029}{\sqrt{-(X'_{o_f})_{BH}}}$$

which gives $(X'_{o_b})_{BH} = -0.08$. It was assumed that the bare hull coefficient, $(X'_o)_{BH}$, is equal to the sum of $(X'_{o_f})_{BH}$ and $(X'_{o_b})_{BH}$. On this basis, eq. B-8 yields $X'_o = -0.45$.

The longitudinal virtual mass coefficient, X'_u, also was estimated on the basis of published empirical results. Again, mutual interference effects were neglected, so that

$$X'_u = (X'_u)_{BH} + (X'_u)_F \qquad \text{(B-9)}$$

where the subscripts have the same connotation as in the representation for X'_o. Yee-Tak Yu[26] reports experiments indicating that the virtual mass of two cylindrical cups placed base to base is equal to the virtual mass of a disk having a radius the same as that of the cylinder plus the mass of the water contained in the cylinder. On the basis of these results, it was assumed that the virtual mass for the Basic Finner bare hull may be approximated by the value obtained for the corresponding disk. According to the experimental results,[26] this is given by

$$(X'_u)_{BH} = -\frac{3.41\, r^3 \rho}{\frac{\rho}{2} A_x \ell}$$

whence, $(X'_u)_{BH} = -0.11$

It was assumed that the longitudinal virtual mass of one of the Basic Finner's wedge-shaped fins is equal to that of a flat plate fin with thickness equal to the maximum thickness of the wedge. This value was estimated by means of an empirical formula for the virtual mass of a rectangular parallelepiped also developed by Yee-Tak Yu,[27]

$$m_v = \rho \frac{6.3\, s_1^2\, s_2^2}{(s_1^2 + s_2^2)^{1/2}} + 3.5\, s_1 s_2 t_1^{1/2} \qquad \text{(B-10)}$$

where m_v is the virtual mass, in grams, ρ is the fluid density in grams/cm^3, and $2\,s_1$, $2\,s_2$, and $2t_1$ are the dimensions of the parallelepiped, in cm, $2t_1$ being the dimension in the direction of the acceleration. Since this formula is not dimensionally homogeneous, it cannot be written in terms of nondimensional quantities. Consequently, the calculation must be made relative to a particular sized configuration. For this purpose, $s_1 = t_1$ 2 cm; $s_2 = 0.16$ cm was chosen.* This corresponds to a configuration 4 cm in diameter (see Fig. 1), intermediate in size relative to the configurations employed in the Basic Finner trajectory experiments. On this basis, $m_v = 1.91$ grams, whence $(X'_u)_F = -0.03$. Substitution into eq. B-9 gives $X'_u = -0.14$.

To estimate the normal virtual mass coefficient, Z'_w, fin-body interference effects again were assumed to be negligible. Thus,

* The variation in size of the configurations employed in the model tests has very little effect on the results of these calculations.

$$Z'_w = (Z'_w)_{BH} + (Z'_w)_F \qquad \text{(B-11)}$$

The bare hull coefficient, $(Z'_w)_{BH}$, was assumed to be equal to that of a prolate spheroid with the same length-diameter ratio as the Basic Finner hull. According to the results of Lamb,[18] this is given by

$$(Z'_w)_{BH} = \frac{0.96\ \rho(\text{Volume})}{\frac{\rho}{2} A\ell} = -0.96\ \ 2C_p$$

whence, $(Z'_w)_{BH} = -1.6$

It was assumed that the normal virtual mass of one of the Basic Finner's wedge-shaped fins is equal to that of a flat plate with thickness equal to the average thickness of the wedge. This value was estimated by applying eq. B-10, in this instance taking $s_1 = s_2 = 2$ cm, $t_1 = 0.08$ cm.* Thus $m_v = 39.6$ grams, whence $(Z'_w)_F = -0.3$. Substitution into eq. B-11 gives $Z'_w = -1.9$.

The virtual moment of inertia coefficient, M'_q, was estimated by means of the equation

$$M'_q = (M'_q)_{BH} + x'^2_F (Z'_w)_F \qquad \text{(B-12)}$$

This equation was derived by analogy with eq. B-1. Interference effects, however, were neglected. Hence x'_F is the dimensionless longitudinal coordinate of the point of application of $(Z'_w)_F$, taken to be the longitudinal midpoint of the fin, i.e., $x'_F = -0.35$. The bare hull coefficient, $(M'_q)_{BH}$, was assumed to be equal to that of a prolate spheroid with the same length-diameter ratio as the Basic Finner hull.

* See note on preceding page.

From Lamb,[18]

$$(M'_q)_{BH} = -\frac{0.87\, I_{y_o}}{\frac{\rho}{2} A_x \ell^3}$$

where I_{y_o} is the moment of inertia of the displaced fluid. Thus $(M'_q)_{BH} = -0.08$. Substitution into eq. B-12 gives $M'_q = -0.12$.

The second order derivative X'_{wq} was estimated on the basis of the results of potential theory, which indicate[18]

$$X'_{wq} = Z'_w$$

whence,

$$X'_{wq} = -1.9$$

The values of each of the hydrodynamic coefficients derived herein are reproduced in Table V.

APPENDIX C
SOLUTION OF VERTICAL PLANAR MOTION EQUATIONS

Numerical (Exact) Solution

Let t_o denote the initial value of the independent variable t (time). The initial values $u(t_o)$, $w(t_o)$, $q(t_o)$, and $\theta(t_o)$ are given. Equations 2 through 4 are solved for the three unknown quantities, $\dot{u}(t_o)$, $\dot{w}(t_o)$, $\dot{q}(t_o)$, to obtain

$$\dot{u}(t_o) = \frac{-(W-B)\sin\left[\theta(t_o)\right] + \frac{\rho}{2}A_x X'_{\dot{0}}\left\{\left[u(t_o)\right]^2 + \left[w(t_o)\right]^2\right\} - \left[m - \frac{\rho}{2}A_x \ell X'_{\dot{w}q}\right] w(t_o) q(t_o) + mx_G \left[q(t_o)\right]^2}{m - \frac{\rho}{2}A_x \ell X'_{\dot{u}}} \quad (C\text{-}1)$$

$$\dot{w}(t_o) = -\frac{\left\{(W-B)\cos\left[\theta(t_o)\right] + \frac{\rho}{2}A_x Z'_{\dot{w}} u(t_o) w(t_o) + \left[m + \frac{\rho}{2}A_x \ell Z'_{\dot{q}}\right] u(t_o) q(t_o)\right\}\left\{I_{yy} - \frac{\rho}{2}A_x \ell^3 M'_{\dot{q}}\right\}}{\left[m - \frac{\rho}{2}A_x \ell Z'_{\dot{w}}\right]\left[I_{yy} - \frac{\rho}{2}A_x \ell^3 M'_{\dot{q}}\right] - m^2 x_G^2}$$

$$+ \frac{mx_G\left\{\frac{\rho}{2}A_x \ell M'_{\dot{w}} u(t_o) w(t_o) - \left[mx_G + \frac{\rho}{2}A_x \ell^3 M'_{\dot{q}}\right] u(t_o)\, q(t_o) - Wx_G \cos\left[\theta(t_o)\right]\right\}}{\left[m - \frac{\rho}{2}A_x \ell Z'_{\dot{w}}\right]\left[I_{yy} - \frac{\rho}{2}A_x \ell^3 M'_{\dot{q}}\right] - m^2 x_G^2} \quad (C\text{-}2)$$

$$\dot{q}(t_o) = \frac{\frac{\rho}{2}A_x \ell M'_{\dot{w}} u(t_o) w(t_o) - \left[mx_G - \frac{\rho}{2}A_x \ell^3 M'_{\dot{q}}\right] u(t_o) q(t_o) - Wx_G \cos\left[\theta(t_o)\right] + mx_G \dot{w}(t_o)}{I_{yy} - \frac{\rho}{2}A_x \ell^3 M'_{\dot{q}}} \quad (C\text{-}3)$$

where the value of $\dot{w}(t_o)$ is first obtained from eq. C-2 and then substituted into eq. C-3 to solve for $\dot{q}(t_o)$. The values of the linear and angular velocities at time $t_o + \Delta t$ are, to the first order of approximation,

$$u(t_o + \Delta t) = u(t_o) + \dot{u}(t_o)\Delta t \quad (C\text{-}4)$$

$$w(t_o + \Delta t) = w(t_o) + \dot{w}(t_o)\Delta t \quad (C\text{-}5)$$

$$q(t_o + \Delta t) = q(t_o) + \dot{q}(t_o)\Delta t \quad (C\text{-}6)$$

Now, since $\phi = 0$, $q = \dot{\theta}$ (see Appendix A). Thus

$$\theta(t_o + \Delta t) = \theta(t_o) + \dot{\theta}(t_o)\Delta t = \theta(t_o) + q(t_o)\Delta t \quad \text{(C-7)}$$

The velocities of the body relative to the fixed (x_o, y_o, z_o) coordinate systems are obtained from the results of eqs. C-4, C-5, C-7 by applying the following transformation equations (see Table of Direction Cosines, Appendix A):

$$\dot{x}_o(t) = u(t) \cos \theta(t) + w(t) \sin \theta(t) \quad \text{(C-8)}$$

$$\dot{z}_o(t) = -u(t) \sin \theta(t) + w(t) \cos \theta(t) \quad \text{(C-9)}$$

The position is then obtained from

$$x_o(t_o + \Delta t) = x_o(t_o) + \dot{x}_o(t_o)\Delta t \quad \text{(C-10)}$$

$$z_o(t_o + \Delta t) = z_o(t_o) + \dot{z}_o(t_o)\Delta t \quad \text{(C-11)}$$

where the initial values $x_o(t_o)$ and $z_o(t_o)$ are given quantities.

The results of eqs. C-4 through C-11 are now regarded as the initial data, and the same procedure is repeated. The process is continued until t attains a value corresponding to the value of time specified as the endpoint of the run.

If the functions involved are well behaved, the sequences of functions obtained by this procedure will converge as the increment Δt is taken smaller and smaller. In the present case, the results obtained on the basis of $\Delta t = 0.005$ sec are indistinguishable from those computed using $\Delta t = 0.0025$ sec. Accordingly, the former value is used in the predictions.

The solution was programmed and coded using the IBM 1620 Fortran programming language.[37] The calculations were performed using the IBM 1620 Computer Stevens Institute of Technology.

Analytic (Approximate) Solution

Upon substitution of eqs. 9 and 10, eqs. 2 through 4 may be written in the form

$$\dot{u} = \frac{\frac{\rho}{2}A_x X'_o}{m - \frac{\rho}{2}A_x \ell X'_u} u^2 \qquad \text{(C-12)}$$

$$\dot{w} = A + (Bw + Cq)u \qquad \text{(C-13)}$$

$$\dot{q} = A^* + (B^*w + C^*q)u \qquad \text{(C-14)}$$

where,

$$A = \frac{(W-B)(I_{yy} - \frac{\rho}{2}A_x \ell^3 M'_q) - Wmx_G^2}{D} \qquad \text{(C-15)}$$

$$B = \frac{\frac{\rho}{2}A_x Z'_w I_{yy} - \frac{\rho}{2}A_x \ell^3 M'_q + \frac{\rho}{2}A_x \ell M'_w mx_G}{D} \qquad \text{(C-16)}$$

$$C = \frac{(m + \frac{\rho}{2}A_x \ell Z'_q)(I_{yy} - \frac{\rho}{2}A_x \ell^3 M'_q) + (\frac{\rho}{2}A_x \ell^2 M'_q - mx_G)mx_G}{D} \qquad \text{(C-17)}$$

$$A^* = \frac{(W-B)mx_G - Wx_G(m - \frac{\rho}{2}A_x \ell Z'_w)}{D} \qquad \text{(C-18)}$$

$$B^* = \frac{\frac{\rho}{2}A_x Z'_w mx_G + \frac{\rho}{2}A_x \ell M'_w(m - \frac{\rho}{2}A_x \ell Z'_w)}{D} \qquad \text{(C-19)}$$

$$C^* = \frac{(m + \frac{\rho}{2}A_x \ell Z'_q)mx_G + (\frac{\rho}{2}A_x \ell^2 M'_q - mx_G)(m - \frac{\rho}{2}A_x \ell Z'_w)}{D} \qquad \text{(C-20)}$$

$$D = (m - \frac{\rho}{2}A_x \ell Z'_w)(I_{yy} - \frac{\rho}{2}A_x \ell^3 M'_q) - m^2 x_G^2 \qquad \text{(C-21)}$$

The longitudinal force equation (eq. C-12) is identical to the equation for the straight horizontal trajectory (eq. 6). Hence the solution is given by eq. 11. This is substituted into eqs. C-13 and C-14. Introduction of a new independent variable,

$$\tau = bt + 1 \tag{C-22}$$

in the resulting equations gives

$$b\frac{dw}{d\tau} = A + \frac{1}{\tau}(\lambda w + \mu q) \tag{C-23}$$

$$b\frac{dq}{d\tau} = A^* + \frac{1}{\tau}(\lambda^* w + \mu^* q) \tag{C-24}$$

where

$$\lambda = Bu(0),\ \mu = Cu(0),\ \lambda^* = B^*u(0),\ \mu^* = C^*u(0) \tag{C-25}$$

Equation C-24 is solved for w and differentiated with respect to τ. The results are substituted into eq. C-23 to obtain

$$b^2\tau^2\frac{d^2q}{d\tau^2} + (b-\mu^*-\lambda)b\tau\frac{dq}{d\tau} + (\mu^*\lambda-\mu\lambda^*)q = (\lambda^*A+bA^*-\lambda A^*)\tau \tag{C-26}$$

The nomogeneous equation, a differential equation of the Euler-Cauchy type, has the solution,

$$q_H = K_1\tau^{\sigma_1} + K_2\tau^{\sigma_2} \tag{C-27}$$

where

$$\sigma_{1,2} = \frac{(\lambda+\mu^*) \pm \sqrt{(\lambda+\mu^*)^2 - 4(\mu^*\lambda - \mu\lambda^*)}}{2b} \tag{C-28}$$

The particular solution is given by

$$q_p = K_3\tau \tag{C-29}$$

where

$$K_3 = \frac{\lambda^*A + (b-\lambda)A^*}{b^2 - b(\lambda+\mu^*) + (\mu^*\lambda - \mu\lambda^*)} \tag{C-30}$$

Hence the complete solution is

$$q = K_1\tau^{\sigma_1} + K_2\tau^{\sigma_2} + K_3\tau \tag{C-31}$$

as can be verified directly by substitution into eq. C-26.

Equation C-31 is substituted into eq. C-24 to obtain the solution for the normal velocity,

$$w = \left[\frac{b^{\sigma_1} - \mu^*}{\lambda^*}\right] K_1 \tau^{\sigma_1} + \left[\frac{b^{\sigma_2} - \mu^*}{\lambda^*}\right] K_2 \tau^{\sigma_2} + \left[\frac{b-\mu^*}{\lambda^*}\right] K_3 \tau - \frac{A^*}{\lambda^*}\tau \tag{C-32}$$

The remaining unknown constants, K_1 and K_2, determined from the initial conditions, are given by

$$K_2 = \left[\frac{1-\sigma_1}{\sigma_1-\sigma_2}\right] K_3 + \left[\frac{b^{\sigma_1}-\mu^*}{b(\sigma_1-\sigma_2)}\right] q(0) - \left[\frac{\lambda^*}{b(\sigma_1-\sigma_2}\right] w(0) \frac{A^*}{b(\sigma_1-\sigma_2)} \tag{C-33}$$

$$K_1 = q(0) - K_2 - K_3 \tag{C-34}$$

Now, since $\phi = 0$, $q = \frac{d\theta}{dt} = b\frac{d\theta}{d\tau}$. Therefore, integrating eq. C-31,

$$\theta = \left[\frac{K_1}{b(\sigma_1+1)}\right]\tau^{\sigma_1+1} + \left[\frac{K_2}{b(\sigma_2+1)}\right]\tau^{\sigma_2+1} + \frac{K_3}{2b}\tau^2 + K_4 \tag{C-35}$$

where the constant of integration, determined from the initial conditions, is given by

$$K_4 = \theta(0) - \frac{1}{b}\left[\frac{K_1}{\sigma_1+1} + \frac{K_2}{\sigma_2+1} + \frac{K_3}{2}\right] \tag{C-36}$$

Solutions for the longitudinal and vertical displacements may be obtained similarly by integrating eqs. 11 and C-32. This is not done in the present work, since it is felt that the solutions already obtained are sufficient for the comparisons for which they are intended. The important results are repeated below in terms of the original independent variable, t.

$$u = \frac{u(0)}{bt + 1} \tag{11}$$

$$w = \frac{1}{\lambda^*}\left[(b\sigma_1-\mu^*)K_1(bt+1)^{\sigma_1-1} + (b\sigma_2-\mu^*)K_2(bt+1)^{\sigma_2-1} + (b-\mu^*)K_3 - A^*(bt+1)\right] \quad \text{(C-37)}$$

$$\theta = \left[\frac{K_1}{b(\sigma_1+1)}\right](bt+1)^{\sigma_1+1} + \left[\frac{K_2}{b(\sigma_2+1)}\right](bt+1)^{\sigma_2+1} + \frac{K_3}{2b}(bt+1)^2 + K_4 \quad \text{(C-38)}$$

The various constants appearing in the equations are evaluated by the successive application of the equations by which they are defined. The velocities of the body relative to the fixed (x_o, y_o, z_o) coordinate system are obtained from the above results by applying eqs. C-8 and C-9.

Table I

Important Features of Basic Finner Force and Moment Experiments

FACILITY AND REFERENCE	TYPE OF EXPERIMENT	OBTAINABLE DERIVATIVE COEFFICIENTS	PROCEDURES USED BY DL IN OBTAINING COEFFICIENTS (see Appendix B)	RANGE OF ATTACK ANGLES COVERED	RANGE OF REYNOLDS NUMBERS COVERED
NBS Wind Tunnel Heald and Adams[5]	Static	X'_o, Z'_w, M'_w	Ia, c, e, f	$0 \leq \alpha \leq 20^\circ$	$0.4\times10^6 \leq Re \leq 2.1\times10^6$
	Oscillatory	M'_q **			
CIT Water Tunnel Kermeen[2]	Static	X'_o, Z'_w, M'_w	Ia, b, c, e, f	$-13^\circ \leq \alpha \leq 14^\circ$	$0.7\times10^6 \leq Re \leq 8.5\times10^6$
CIT Water Tunnel Angular Dynamic Balance Kiceniuk[3]	Oscillatory	Z'_w, Z'_q *, M'_w, M'_q **, $M'_{\dot{q}}$	Id, f	$\alpha = 0$ ***	$1.7\times10^6 \leq Re \leq 4.5\times10^6$
CIT Water Tunnel Translational Dynamic Balance Kiceniuk[4]	Oscillatory	Z'_w	If	$\alpha = 0$ ***	$0.8\times10^6 \leq Re \leq 2.3\times10^6$
		$Z'_{\dot{w}}$			$0 \leq Re \leq 2.3\times10^6$
DL Towing Tank Savitsky and Prowse[6]	Static	X'_o, $X'_{\dot{u}}$	Ib, f	$\alpha = 0$	$0.8\times10^6 \leq Re \leq 5.8\times10^6$

* Necessary to use value of $Z'_{\dot{w}}$ from translational dynamic balance data[4] to modify measured quantity, $Z'_q + Z'_{\dot{w}}$.

** Necessary to use assumed value $M'_{\dot{w}} = 0$ to modify measured quantity $M'_q + M'_{\dot{w}}$.

*** All derivatives evaluated at $\alpha = 0$. Oscillations induce instantaneous nonzero values of α, however.

TABLE II

HYDRODYNAMIC DERIVATIVES FOR BASIC FINNER MISSILE
with respect to coordinate system with origin at the CB

SOURCE		Z'_w	M'_w	Z'_q	M'_q	$Z'_{\dot{w}}$	$M'_{\dot{q}}$	X'_o	X'_u	X'_{wq}
NBS WIND TUNNEL MEASUREMENTS.[5] $M'_q + M'_{\dot{w}}$ MEASURED USING OSCILLATOR EQUIPMENT; ALL OTHER QUANTITIES MEASURED STATICALLY	4'd. Wood Model	-11.9	-2.4		-0.7(a,b)			(d)		
	2'd. Wood Model	-13.5	-2.5		-0.5(a,b)			(d)		
	2'd. Metal Model	-14.0	-2.5		-0.9(a,b)			(d)		
	3/4'd. Metal Model	-11.5	-2.3		-0.9(a,b)			(d)		
CIT WATER TUNNEL MEASUREMENTS.[2,3,4] OSCILLATOR (DYNAMIC BALANCES) AND STATIC TESTS.	Angular Dynamic Balance[3]	-14.1	-3.1	-5.1(c)	-1.7(a)		-0.10			
	Translational Dynamic Balance[4]	-13.5				-1.7				
	Static Tests[2]	-12.7	-3.0					(d)		
DL Towing Tank measurements; nonoscillatory motions[6]								(d)	-0.25	
Average Experimental values		-13.0	-2.6	-5.1	-0.9	-1.7	-0.10	-0.45	-0.25	
NPG Analysis[11] (see section beginning on p. 10)		-14.6	-2.9	-2.5	-1.25	0	0	-0.435	0	0
Values estimated from theory		(see Figure 3)				-1.9	-0.12	-0.45	-0.14	-1.9

(a) Assumed value $M'_{\dot{w}} = 0$ used to modify measured quantity, $M'_q + M'_{\dot{w}}$.

(b) Value of Z'_q from CIT angular dynamic balance data[3] used to refer coefficient to standard origin of coordinates.

(c) Value of $Z'_{\dot{w}}$ from translational dynamic balance data[4] used to modify measured quantity, $Z'_q + Z'_{\dot{w}}$.

(d) See Figure 2.

TABLE III

COMPARISON OF VALUES OF z_1' PREDICTED USING TWO DIFFERENT THEORIES WITH EXPERIMENTALLY DERIVED VALUES

CASE NO.	VEHICLE	REFERENCE	VALUES OBTAINED FOR z_1'		
			EXPERIMENTAL	FLAX AND LAWRENCE THEORY	AIRSHIP THEORY
1	Submarine	38	-2.78	-3.67	-3.15
2	Missile	29	-2.29	-3.24	-2.51
3	Missile	39	-2.51	-2.01	-2.44
4	Missile	22	-14.5	-13.5	-11.8

TABLE IV
INPUT PARAMETERS FOR TRAJECTORY PREDICTIONS

CALCULATION NO.	CIT Run No(s)	W-B, lbs.	$\frac{\rho}{2}A_x$, sl./ft.	s, ft.	m, sl.	W, lb.	x_G, ft.	I_{yy}, sl.-ft.^{2}	t_o, sec.	$u(t_o)$, ft./sec.	$w(t_o)$, ft./sec.	$x_o(t_o)$, ft.	$z_o(t_o)$, ft.	$q(t_o)$, rad./sec.	$\theta(t_o)$, rad.
HIGH SPEED VERTICAL PLANAR TRAJECTORIES															
1	F-55	1.88	.0211	1.667	.117	3.77	0.0	.0107	0.10	31.5	0.20	3.69	0.05	-.243	-.0174
2	F-56	1.88	.0211	1.667	.117	3.77	0.0	.0107	0.10	25.7	0.38	2.97	0.07	-.309	-.0280
3	F-57	1.88	.0211	1.667	.117	3.77	-.0416	.0104	0.20	22.2	0.32	5.47	0.15	-.251	-.0418
4	F-58	1.88	.0211	1.667	.117	3.77	.0416	.0113	0.12	26.0	0.24	3.65	0.09	-.321	-.0332
5	F-59	1.88	.0211	1.667	.117	3.77	-.0416	.0194	0.10	26.1	0.06	3.00	0.07	-.287	-.0244
6	F-60	1.88	.0211	1.667	.117	3.77	0.0	.0197	0.10	26.8	0.20	3.05	0.07	-.227	-.0297
7	F-61	-0.35	.0211	1.667	.0475	1.53	0.0	.0114	0.06	22.5	-0.11	1.65	-0.01	.073	.0052
8	F-62	-0.35	.0211	1.667	.0475	1.53	0.0	.0114	0.10	22.0	-0.01	2.95	-0.03	.087	.0087
9	F-63	0.19	.0211	1.667	.0645	2.07	0.0	.0105	0.08	24.9	0.07	2.46	0.00	-.055	.0050
10	F-64	5.65	.0211	1.667	.234	7.53	0.0	.0173	0.08	37.7	0.46	3.21	0.07	-.332	-.0280
LOW SPEED VERTICAL PLANAR TRAJECTORIES															
11	F-19	1.88	.0211	1.667	.117	3.77	0.0	.0108	0.0	0.0	0.0	0.0	0.0	0.0	-1.193
12	F-25	1 88	.0211	1.667	.117	3.77	0.0	.0200	0.0	0.0	0.0	0.0	0.0	0.0	-1.161
13	F-26	1.88	.0211	1.667	.117	3.77	0.0	.0200	0.0	0.0	0.0	0.0	0.0	0.0	-1.175
14	F-37	0.188	.0211	1.667	.0645	2.07	.0198	.0108	0.0	0.0	0.0	0.0	0.0	0.0	- .882
15	F-38	0 188	.0211	1.667	.0645	2.07	.0115	.0108	0.0	0.0	0.0	0.0	0.0	0.0	- .875
16	F-39	0.188	.0211	1.667	.0645	2.07	0.0	.0108	0.0	0.0	0.0	0.0	0.0	0.0	- .882
17	F-41	0 188	.0211	1 667	.0645	2.07	-.00833	.0108	0.0	0.0	0.0	0.0	0.0	0.0	- .907
18	F-51	5.66	.0211	1.667	.235	7.54	0.0	.0184	0.0	0.0	0.0	0.0	0.0	0.0	-1.215
STRAIGHT HORIZONTAL TRAJECTORY															
19	F-52		.0211	1.667	.0586				0.02	36.6		0.79			
STRAIGHT VERTICAL TRAJECTORIES															
20	F-1,2,6,8	0.283	.0053	0.833	.0161										
21	F-9	0.066	.0053	0.833	.0094										
22	F-10	0.236	.0053	0.833	.0147										
23	F-11	1.097	.0053	0.833	.0414										
24	F-15,36	0.189	.0211	1.667	.0645										
25	F-23,24	1.888	.0211	1.667	.117										
26	F-47,48	5.664	.0211	1.667	.235										

TABLE V

PARTICULARS OF THE BASIC FINNER MISSILE

Diameter of bare hull, d	1.000
Length of bare hull, ℓ	10.00 d
Maximum cross-sectional area of bare hull, A_x	0.785 d^2
Wetted area of bare hull, S_{BH}	27.0 d^2
Base area of fins (4), $(A_b)_F$	0.320 d^2
Wetted area of fins (4), S_F	8.16 d^2
Projected area of fins (2), $(A_p)_F$	2.00 d^2
Total volume, Vol.	6.53 d^3
Moment of inertia of fluid displaced by hull, I_{y_o}	36.8 ρd^5

Hydrodynamic Coefficients: *

X'_o ..... -0.45	$Z'_q = -Y'_{\dot{r}}$... -3.78
$X'_{\dot{u}}$ ..... -0.14	$Z'_{\dot{q}} = -Y'_{\dot{v}}$... 0
$X'_{ww} = X'_{vv}$... 0	$M'_w = -N'_v$... -2.12
$X'_{wq} = -X'_{vr}$.. -1.9	$M'_{\dot{w}} = -N'_{\dot{v}}$... 0
$X'_{qq} = X'_{rr}$... 0	$M'_q = N'_r$.... -1.24
$Z'_w = Y'_v$.... -11.6	$M'_{\dot{q}} = N'_{\dot{r}}$.... -0.12
$Z'_{\dot{w}} = Y'_{\dot{v}}$.... -1.9	

* See sections beginning on pp. 10 and 19.

TABLE VI
COMPARISON OF OBSERVED AND PREDICTED TRAJECTORY PARAMETERS

DL CALCULATION NO.	TOTAL LENGTH OF TRAJECTORY, Model Lengths	EXTREME VALUE OF DIFFERENCE: PREDICTED VALUE - OBSERVED VALUE				
		LONGITUDE, x_o, Model Lengths	DEPTH, z_o, Model Lengths	LONG. VELOCITY, $\dot{x}_o$, Ft./Sec.	VERTICAL VELOCITY, $\dot{z}_o$, Ft./Sec.	INCLINATION, Θ, Degrees
HIGH SPEED VERTICAL PLANAR TRAJECTORIES						
1	9.2	.07	-.02	+.41	-.45	- .5
2	8.3	-.09	+.07	-.20	+.46	-1.8
3	7.4	+.04	-.05	+.28	-.19	-1.0
4	7.9	+.05	+.09	-.23	+.28	-1.1
5	8.7	+.06	-.07	+.25	-.29	+1.1
6	8.5	+.05	+.03	+.67	+.39	-1.0
7	7.0	+.11	-.05	-.84	-.14	+1.4
8	6.6	+.11	-.01	+.28	+.17	[illegible]
9	9.6	+.22	-.02	+.30	-.16	+ .9
10	8.6	+.07	-.01	+.39	+.38	- .4
LOW SPEED VERTICAL PLANAR TRAJECTORIES						
11	3.5	+.12	+.28	N.E.	N.E.	+5.5
12	4.2	+.28	+.05	N.E.	N.E.	+5.0
13	4.2	+.12	-.01	N.E.	N.E.	+3.3
14	3.7	-.22	-.07	N.E.	N.E.	-5.0
15	3.6	-.16	+.35	N.E.	N.E.	-4.4
16	4.2	+.04	+.17	N.E.	N.E.	+3.0
17	3.7	+.13	+.06	N.E.	N.E.	-4.0
18	3.5	+.01	+.16	N.E.	N.E.	-1.0
STRAIGHT HORIZONTAL TRAJECTORY						
19	11.4	+.35		+.36		
STRAIGHT VERTICAL TRAJECTORIES						
20	8.0		-.30		N.E.	
21	7.9		-.13		N.E.	
22	8.1		-.08		N.E.	
23	8.0		-.06		N.E.	
24	4.0		+.05		N.E.	
25	4.2		-.06		N.E.	
26	3.1		-.01		N.E.	

N.E. - Not evaluated

TABLE VII
COMPARISON OF DL AND NPG RESULTS

DL CALCULATION NO.	CIT RUN NO.	MAXIMUM DIFFERENCE BETWEEN OBSERVED AND COMPUTED VALUE					
		LONGITUDE, x_o MODEL LENGTHS		DEPTH, z_o MODEL LENGTHS		INCLINATION, θ DEGREES	
		DL	NPG	DL	NPG	DL	NPG
2	F-56	.09	.11	.07	.12	1.8	0.4
8	F-62	.11	.19	.01	.06	0.4	1.1
10	F-64	.07	.00	.01	.08	0.4	0.8

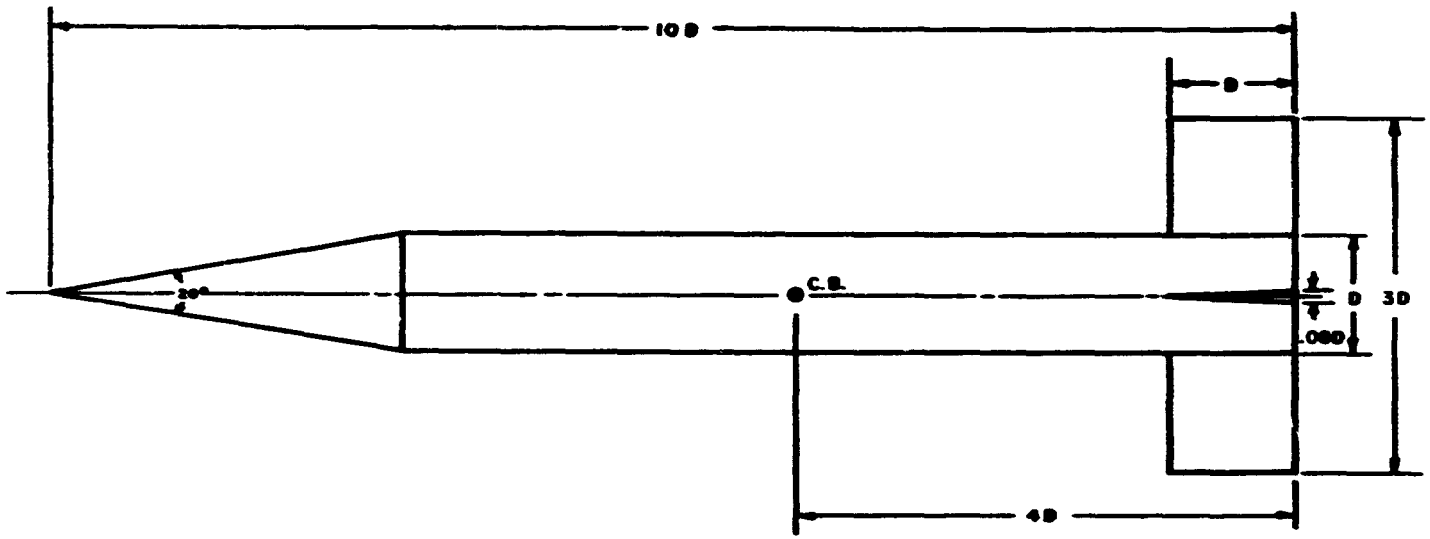

FIGURE 1 BASIC FINNER MISSILE CONFIGURATION

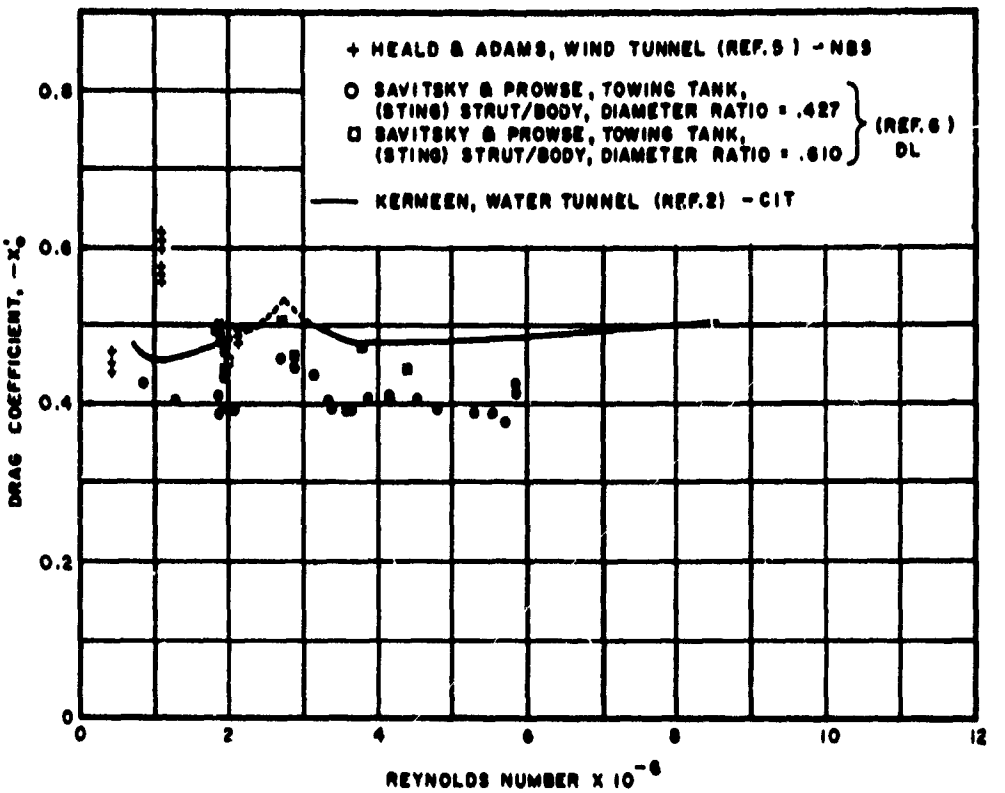

FIGURE 2. EXPERIMENTALLY DETERMINED VALUES OF DRAG COEFFICIENT VERSUS REYNOLDS NUMBER

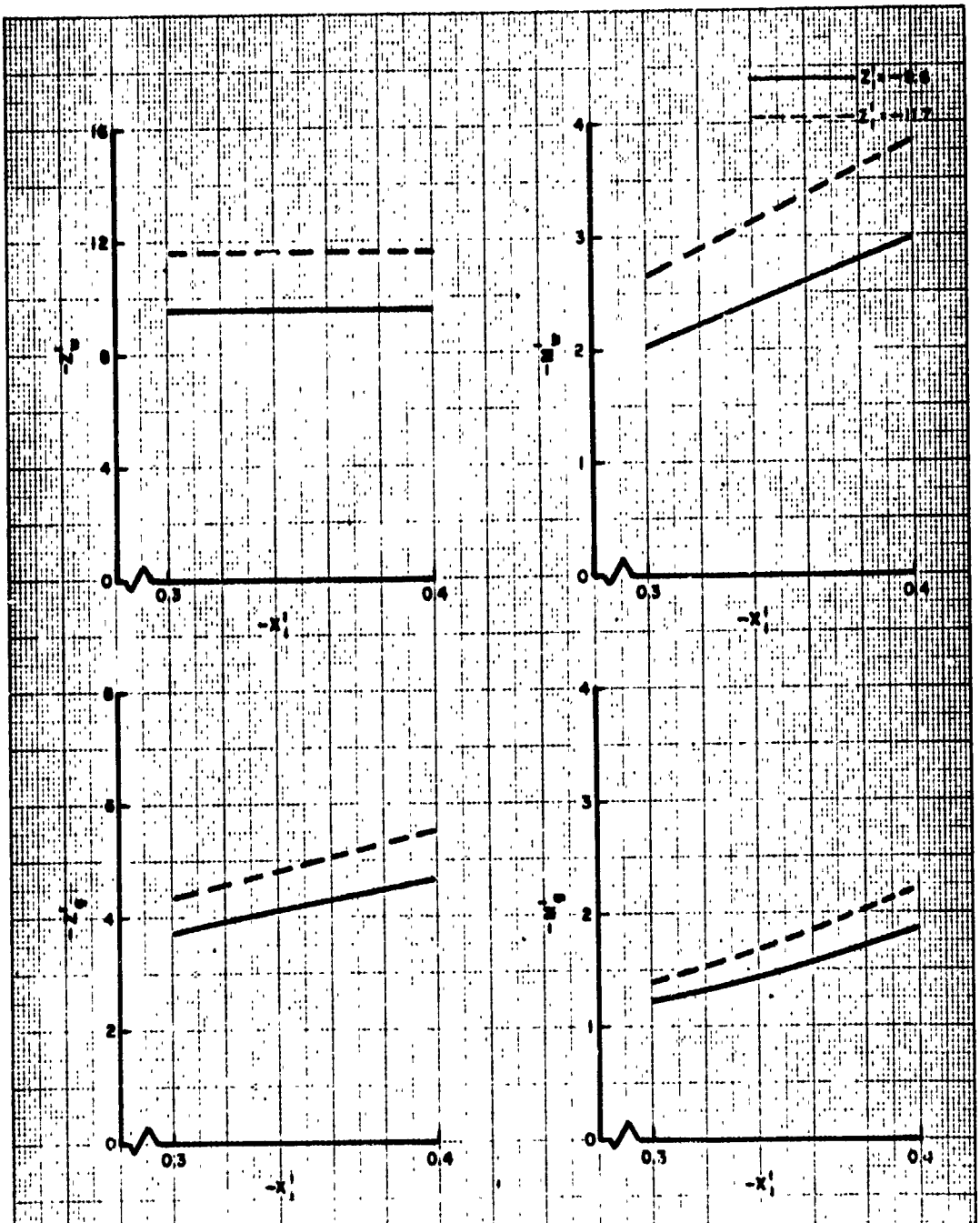

FIGURE 3. THEORETICALLY ESTIMATED VALUES FOR HYDRODYNAMIC STATIC AND DAMPING DERIVATIVE COEFFICIENTS AS FUNCTIONS OF X'_1 AND Z'_1.

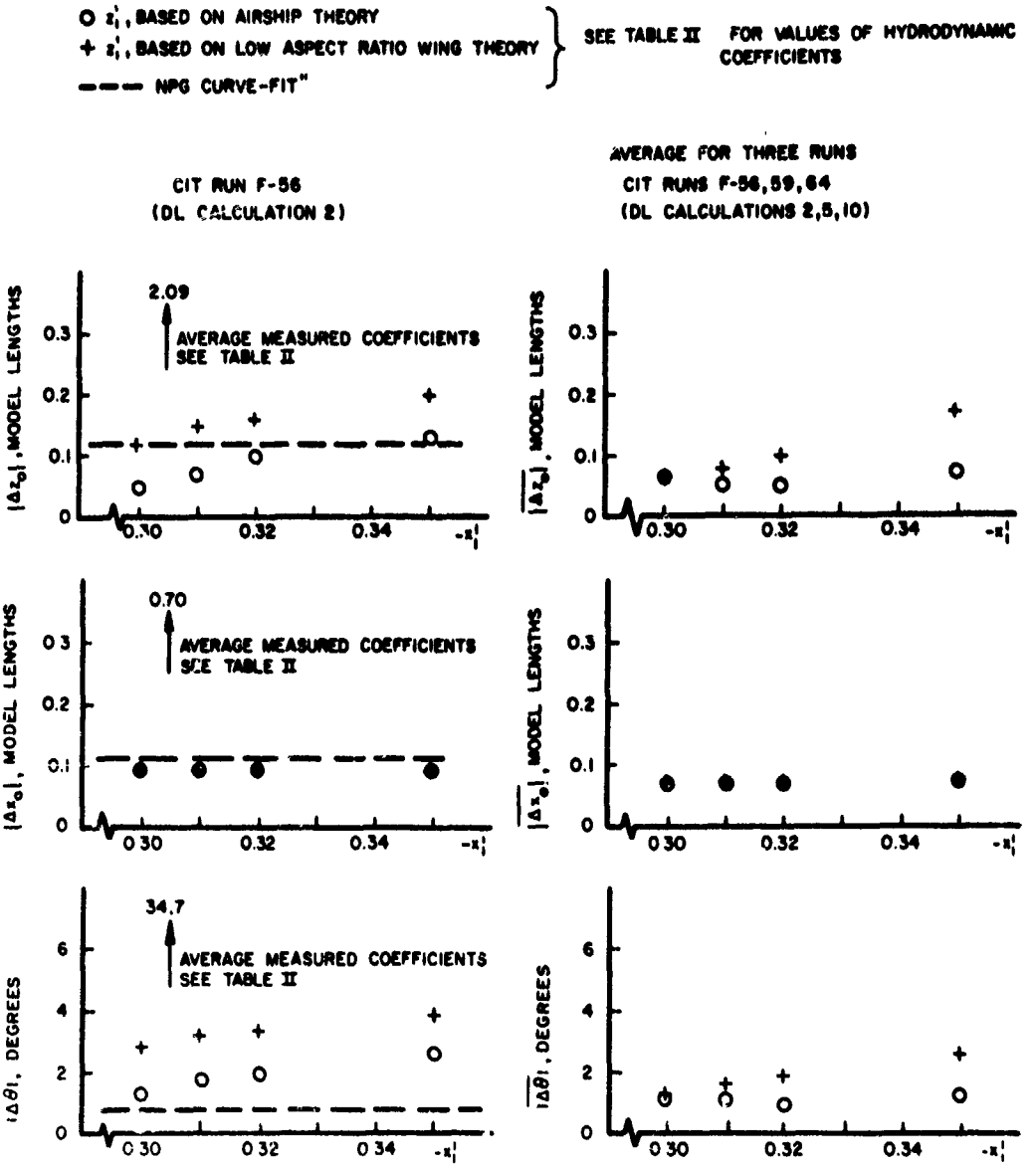

FIGURE 4. MAGNITUDES OF MAXIMUM DIFFERENCES BETWEEN OBSERVED AND COMPUTED VALUES OF TRAJECTORY PARAMETERS WITH VARIOUS SETS OF HYDRODYNAMIC INPUT DATA

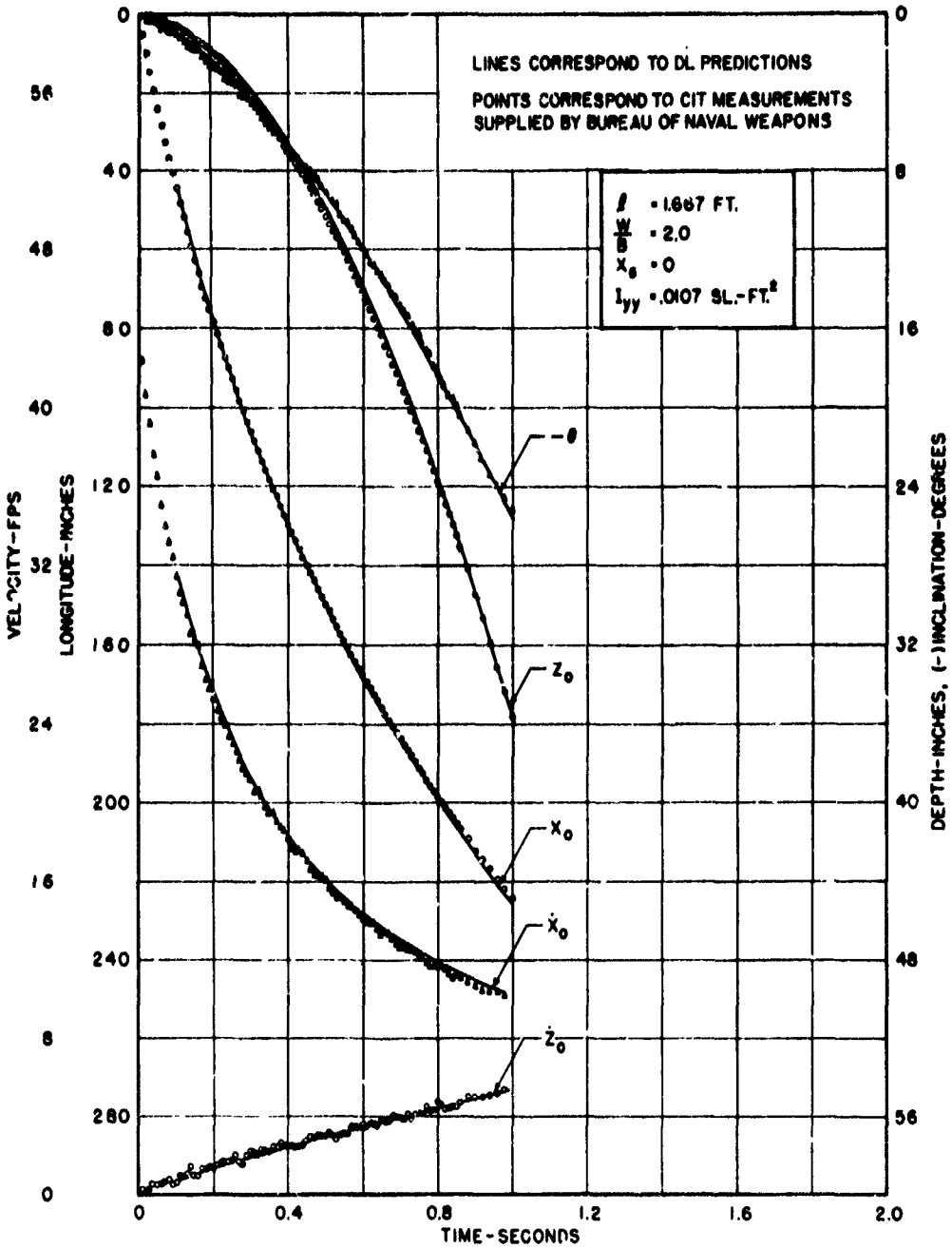

FIGURE 5. COMPARISON OF EXPERIMENTAL AND PREDICTED TRAJECTORIES FOR D.L. CALCULATION NO. 1

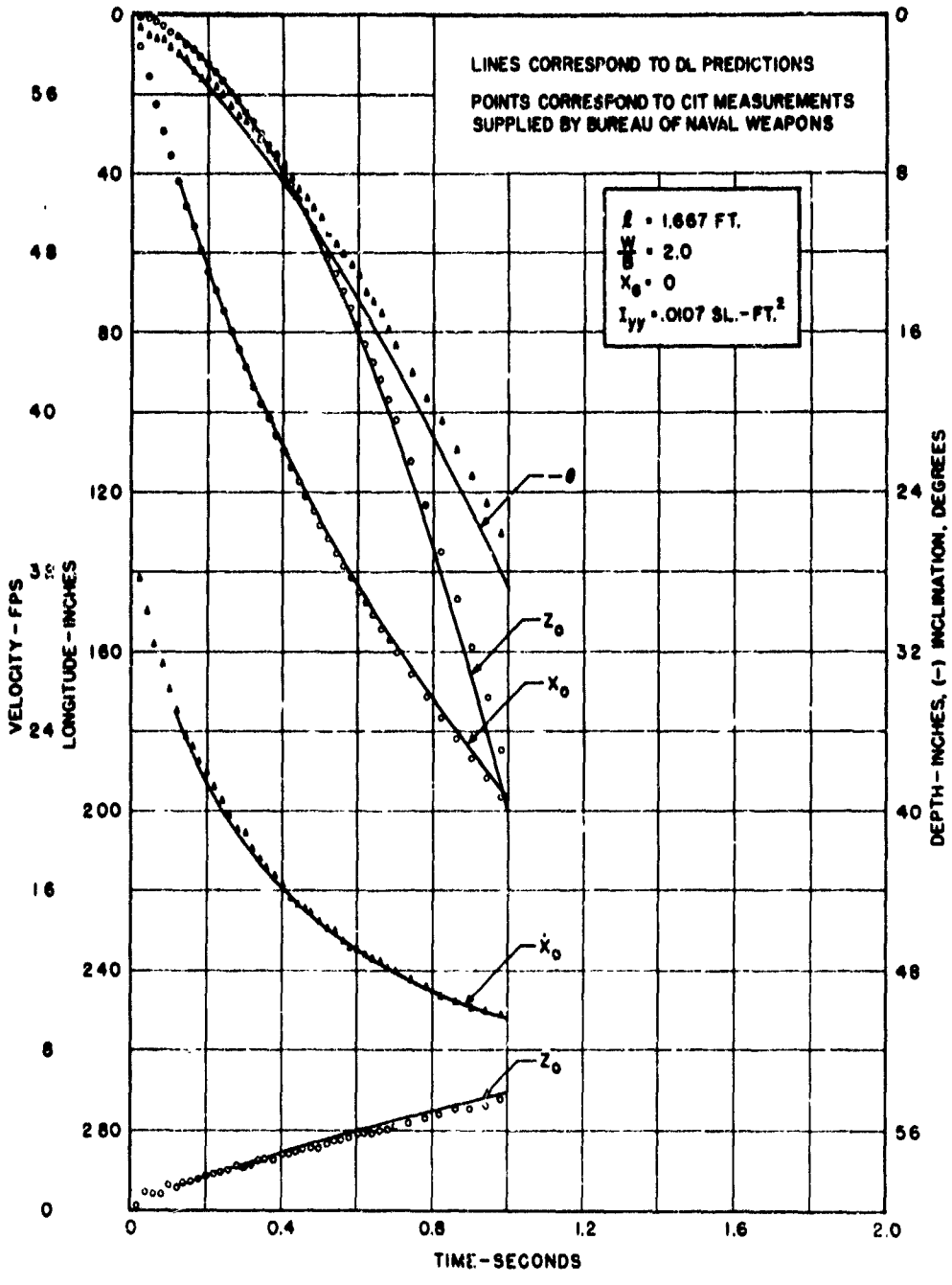

FIGURE 6. COMPARISON OF EXPERIMENTAL AND PREDICTED TRAJECTORIES FOR D.L. CALCULATION NO 2

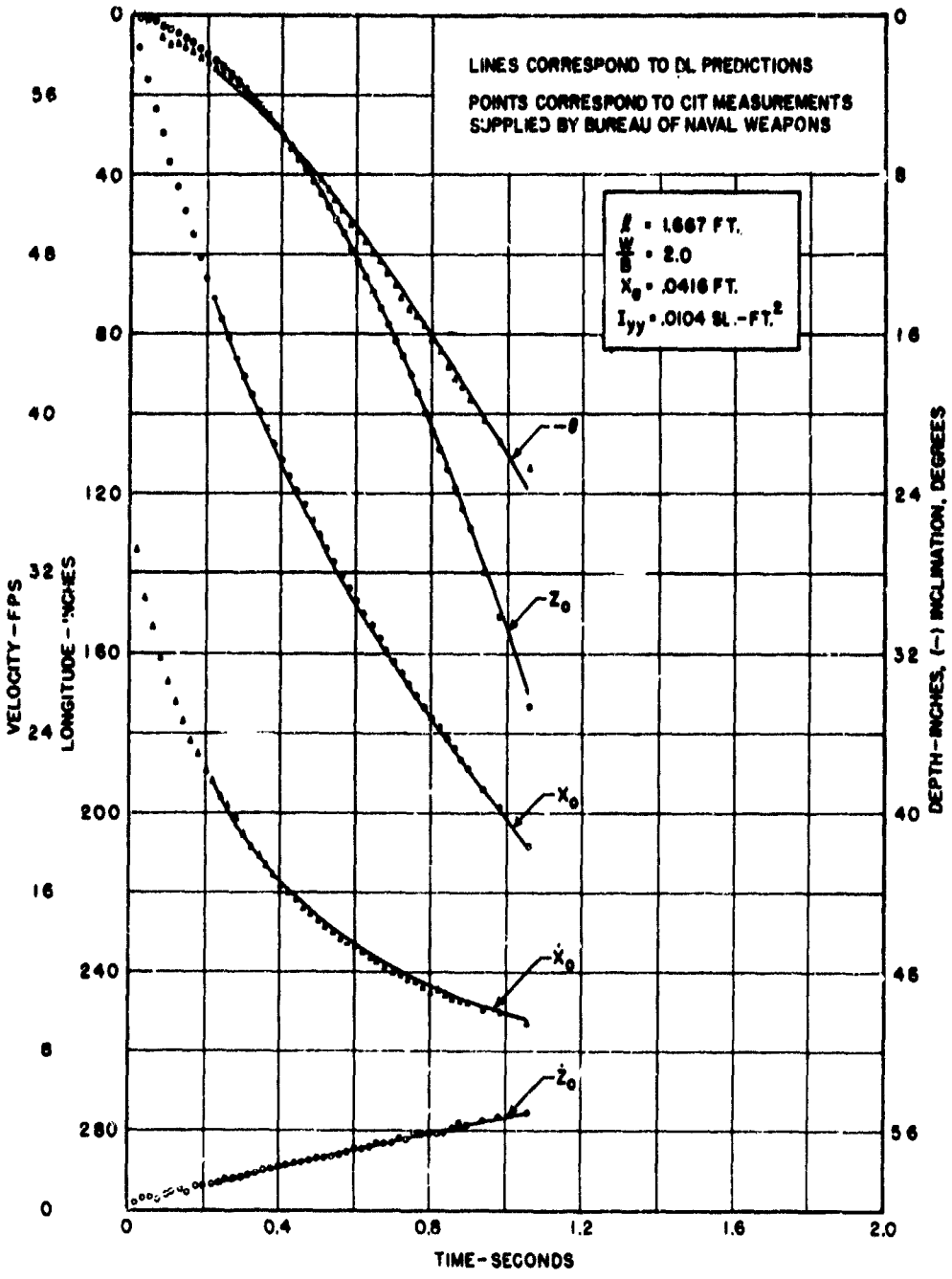

FIGURE 7. COMPARISON OF EXPERIMENTAL AND PREDICTED TRAJECTORIES FOR D.L. CALCULATION NO. 3

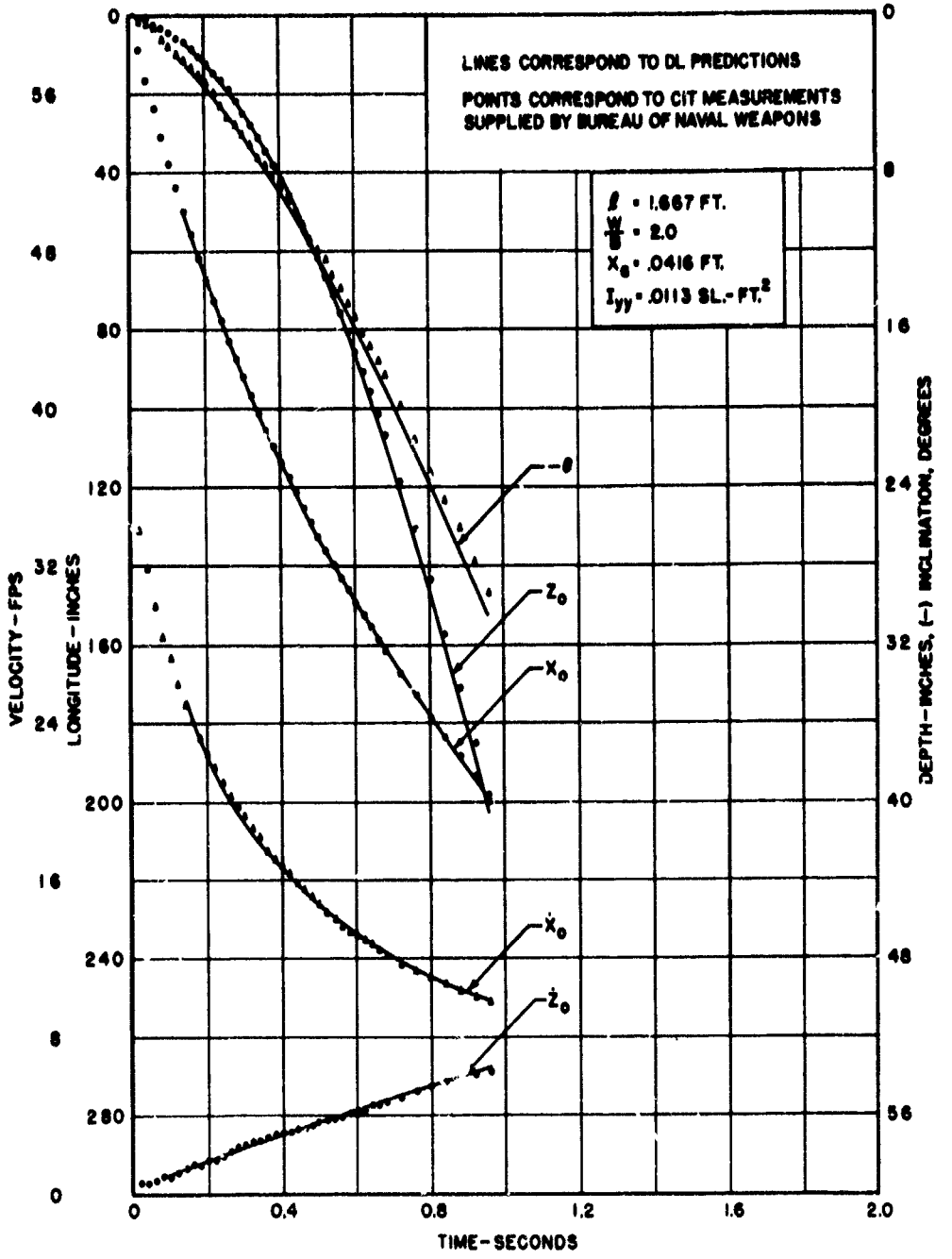

FIGURE 8. COMPARISON OF EXPERIMENTAL AND PREDICTED TRAJECTORIES FOR D.L. CALCULATION NO. 4

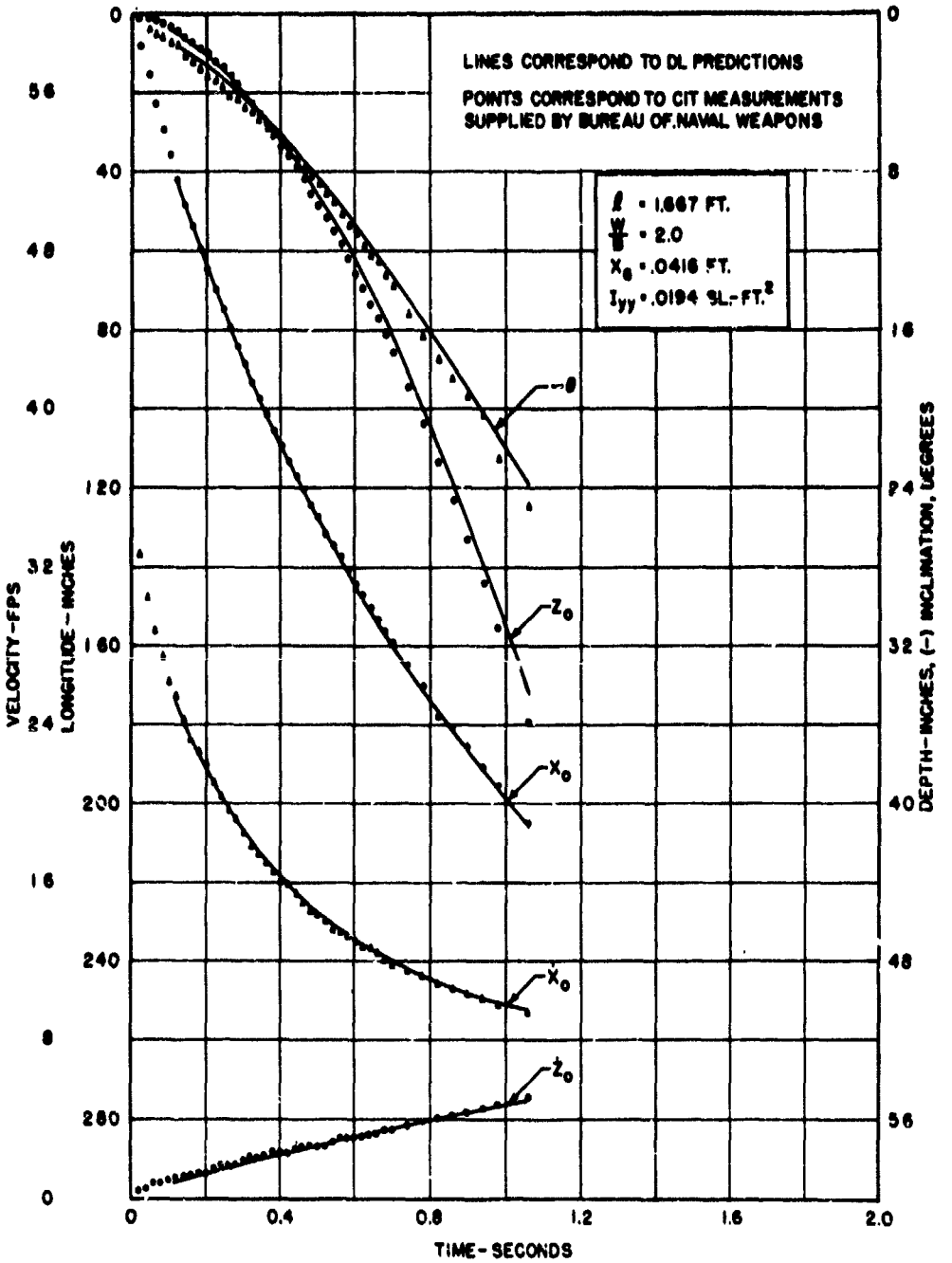

FIGURE 9. COMPARISON OF EXPERIMENTAL AND PREDICTED TRAJECTORIES FOR D.L. CALCULATION NO. 5

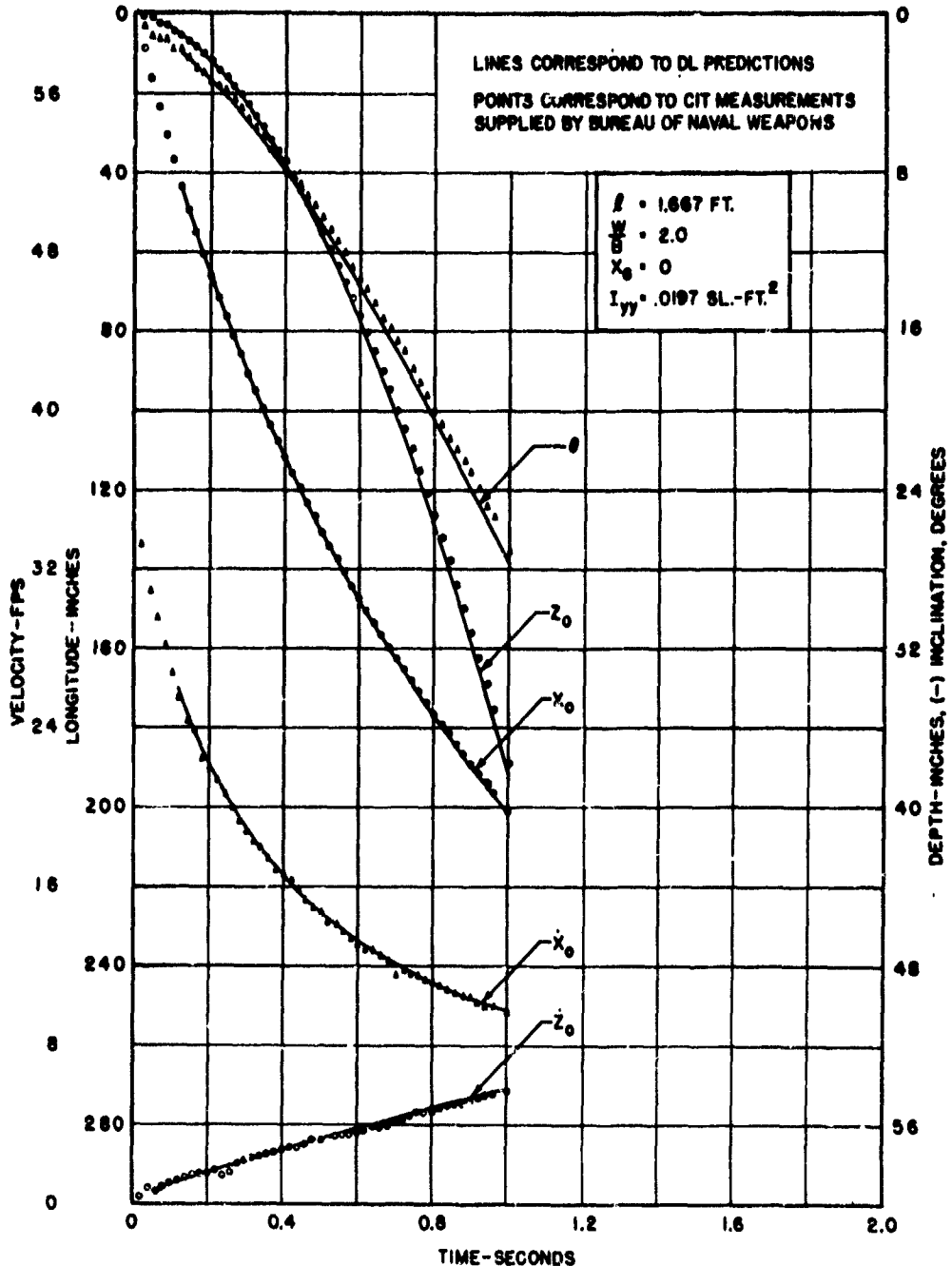

FIGURE 10. COMPARISON OF EXPERIMENTAL AND PREDICTED TRAJECTORIES FOR D.L CALCULATION NO. 6

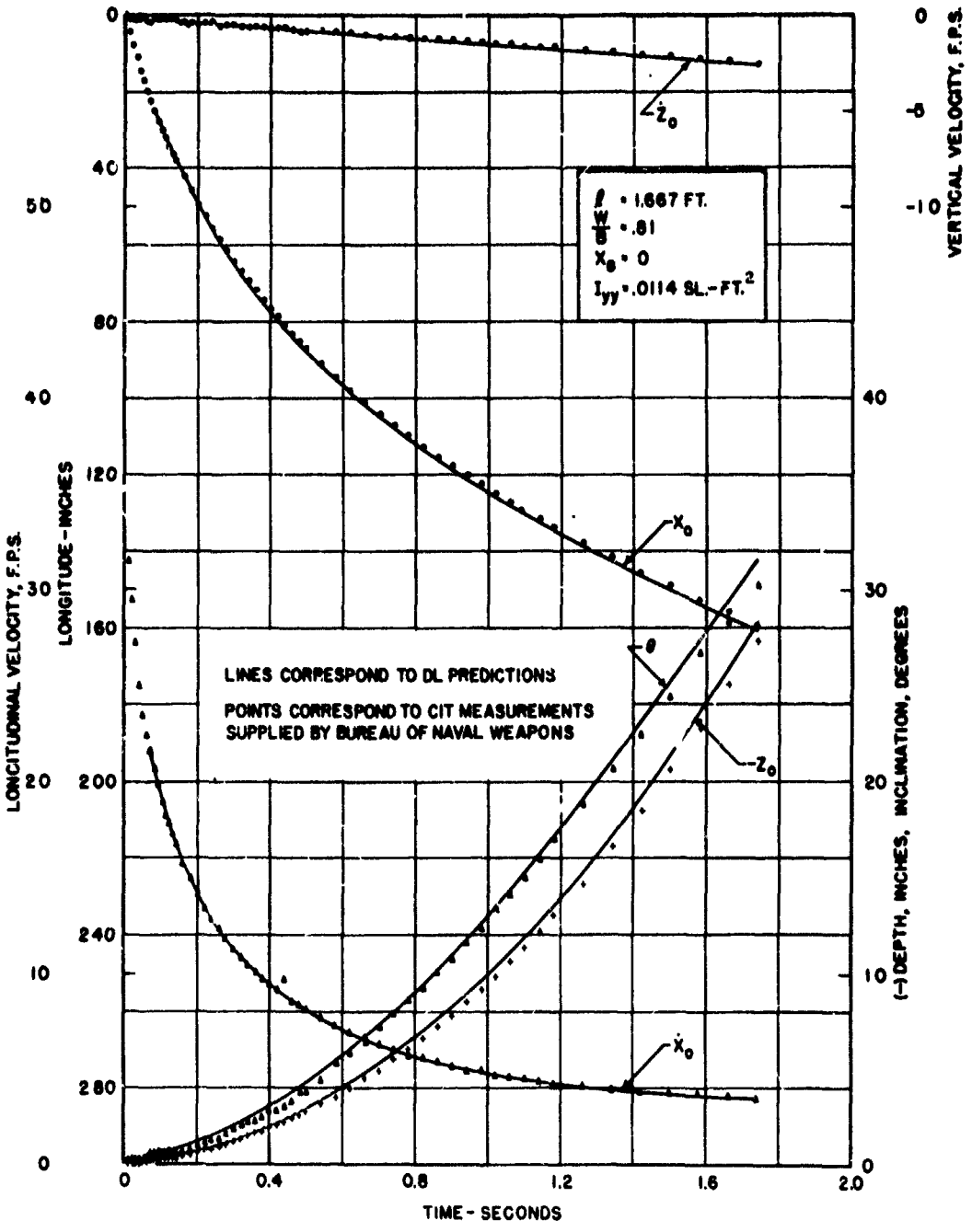

FIGURE II. COMPARISON OF EXPERIMENTAL AND PREDICTED TRAJECTORIES FOR D.L. CALCULATION NO. 7

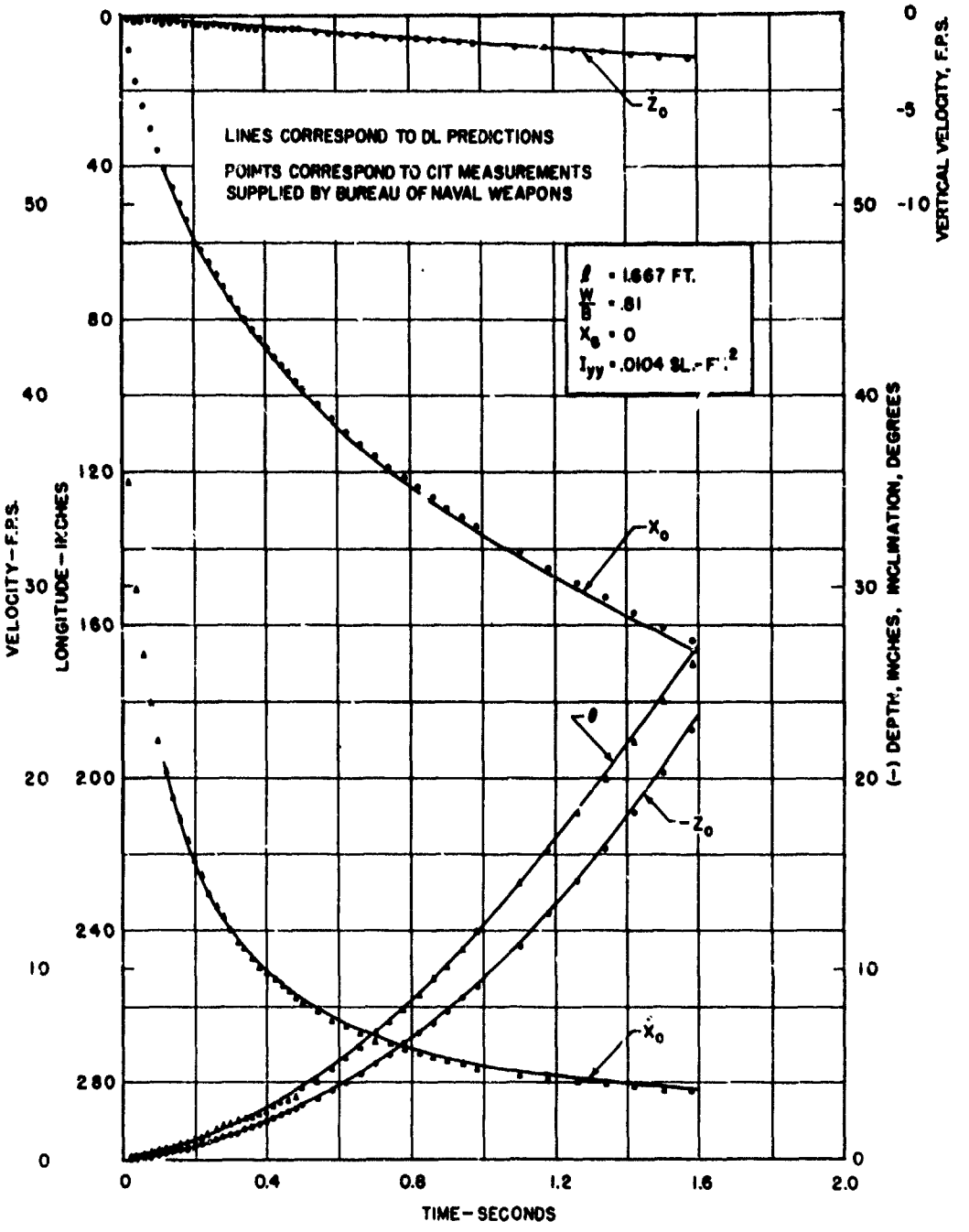

FIGURE 12. COMPARISON OF EXPERIMENTAL AND PREDICTED TRAJECTORIES FOR D.L. CALCULATION NO. 8

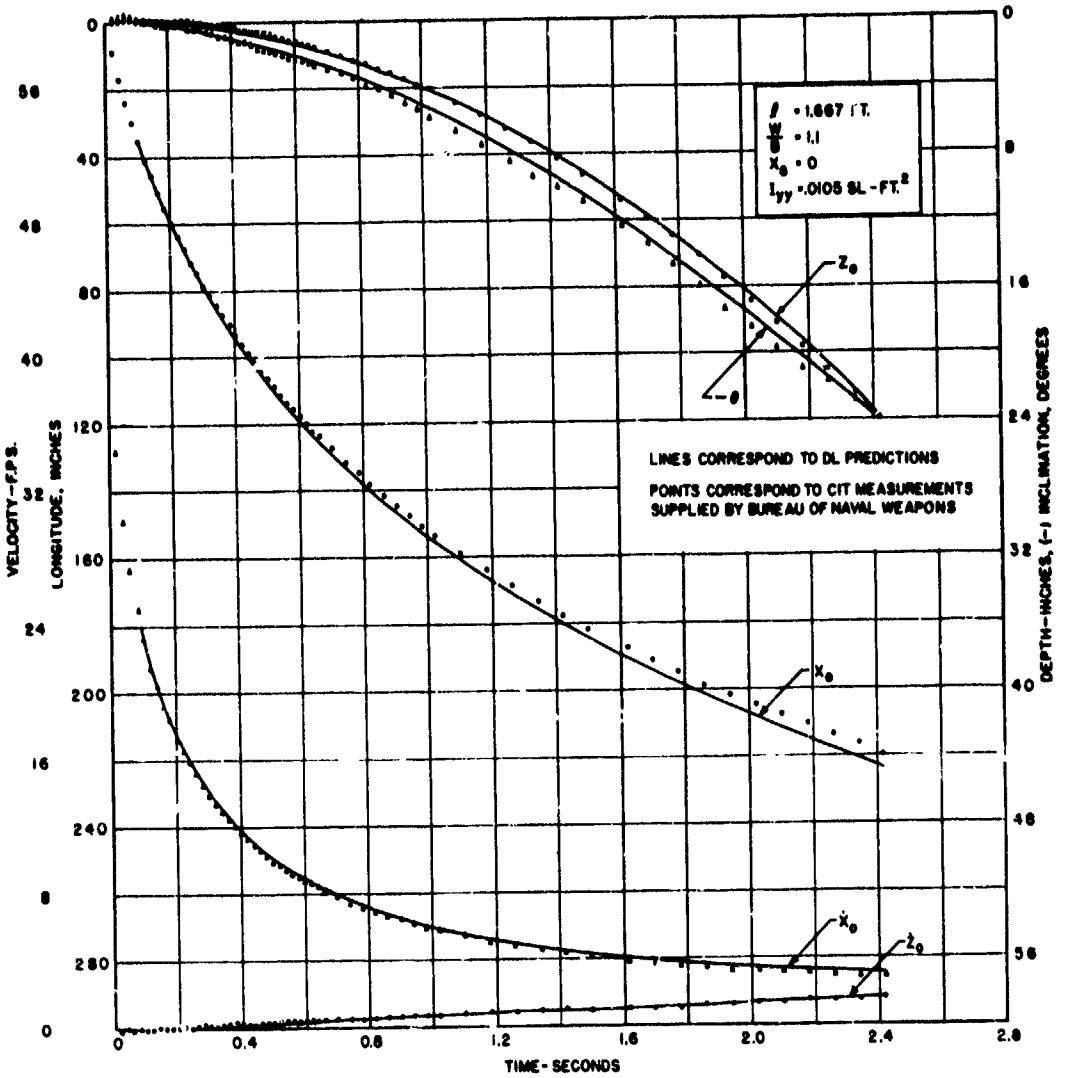

FIGURE 13. COMPARISON OF EXPERIMENTAL AND PREDICTED TRAJECTORIES FOR D.L. CALCULATION NO. 9

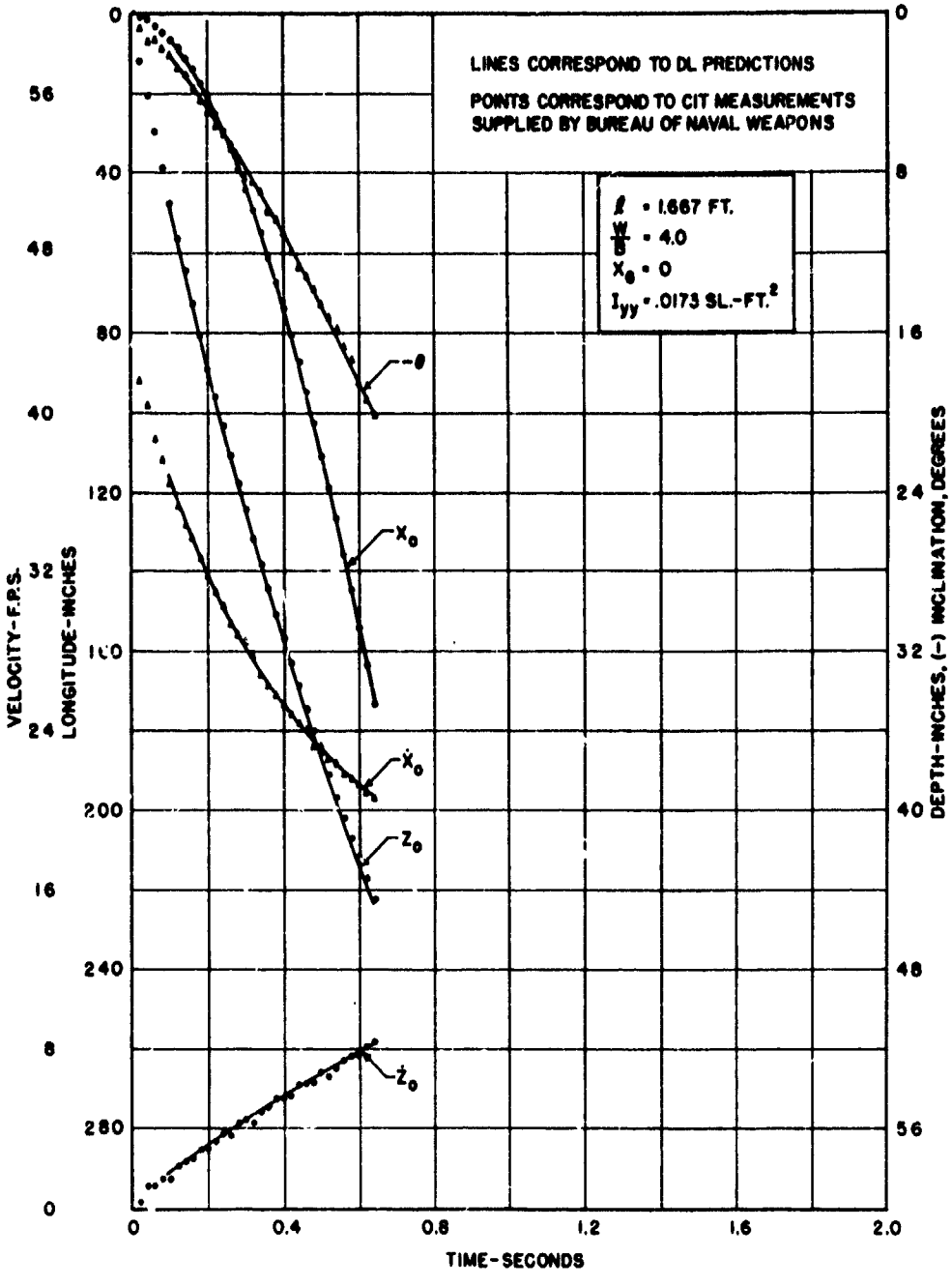

FIGURE 14. COMPARISON OF EXPERIMENTAL AND PREDICTED TRAJECTORIES FOR D.L. CALCULATION NO. 10

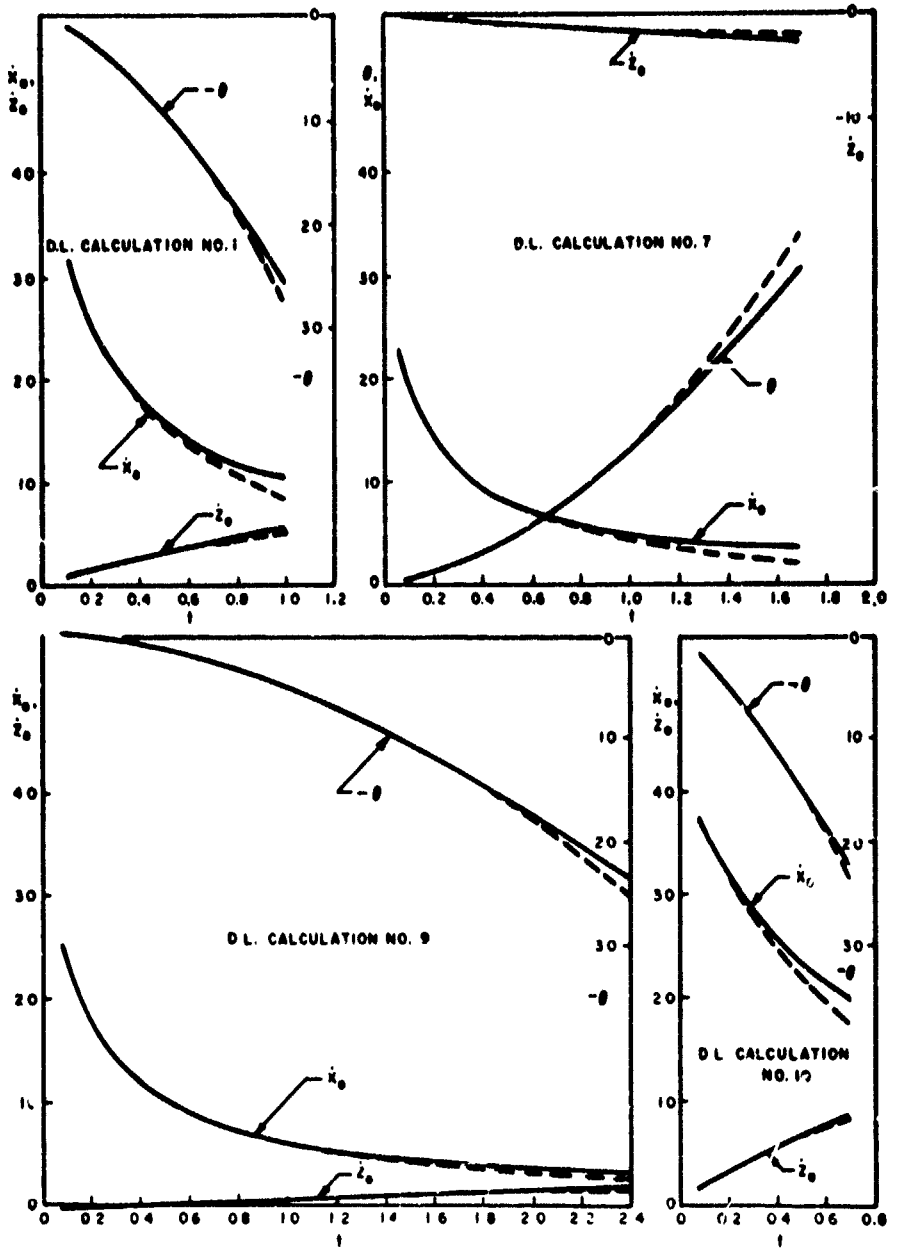

FIGURE 15. COMPARISON OF EXACT (SOLID LINES) AND APPROXIMATE (DASHED LINES) SOLUTIONS FOR FOUR TYPICAL HIGH SPEED VERTICAL TRAJECTORY PREDICTIONS.

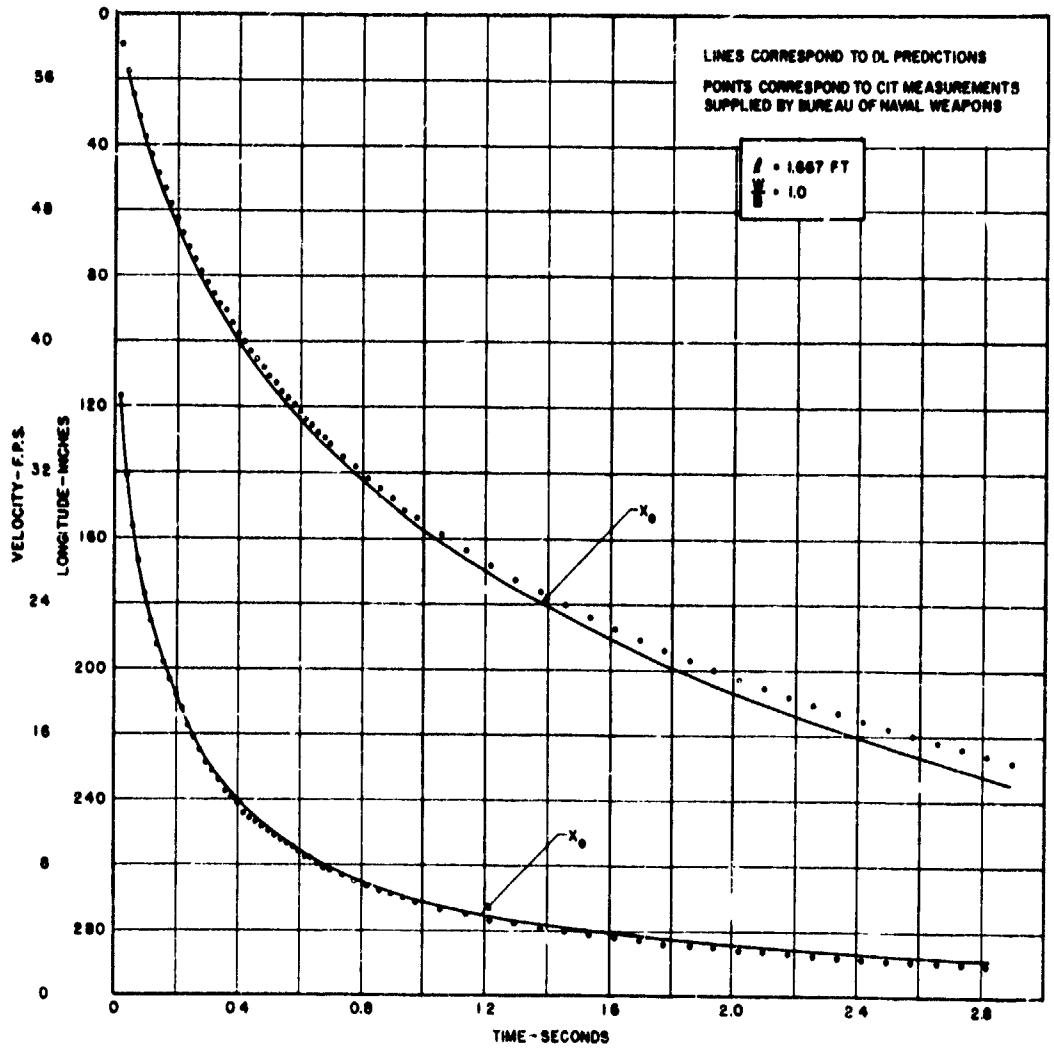

FIGURE 16. COMPARISON OF EXPERIMENTAL AND PREDICTED TRAJECTORIES FOR D.L CALCULATION NO. 19

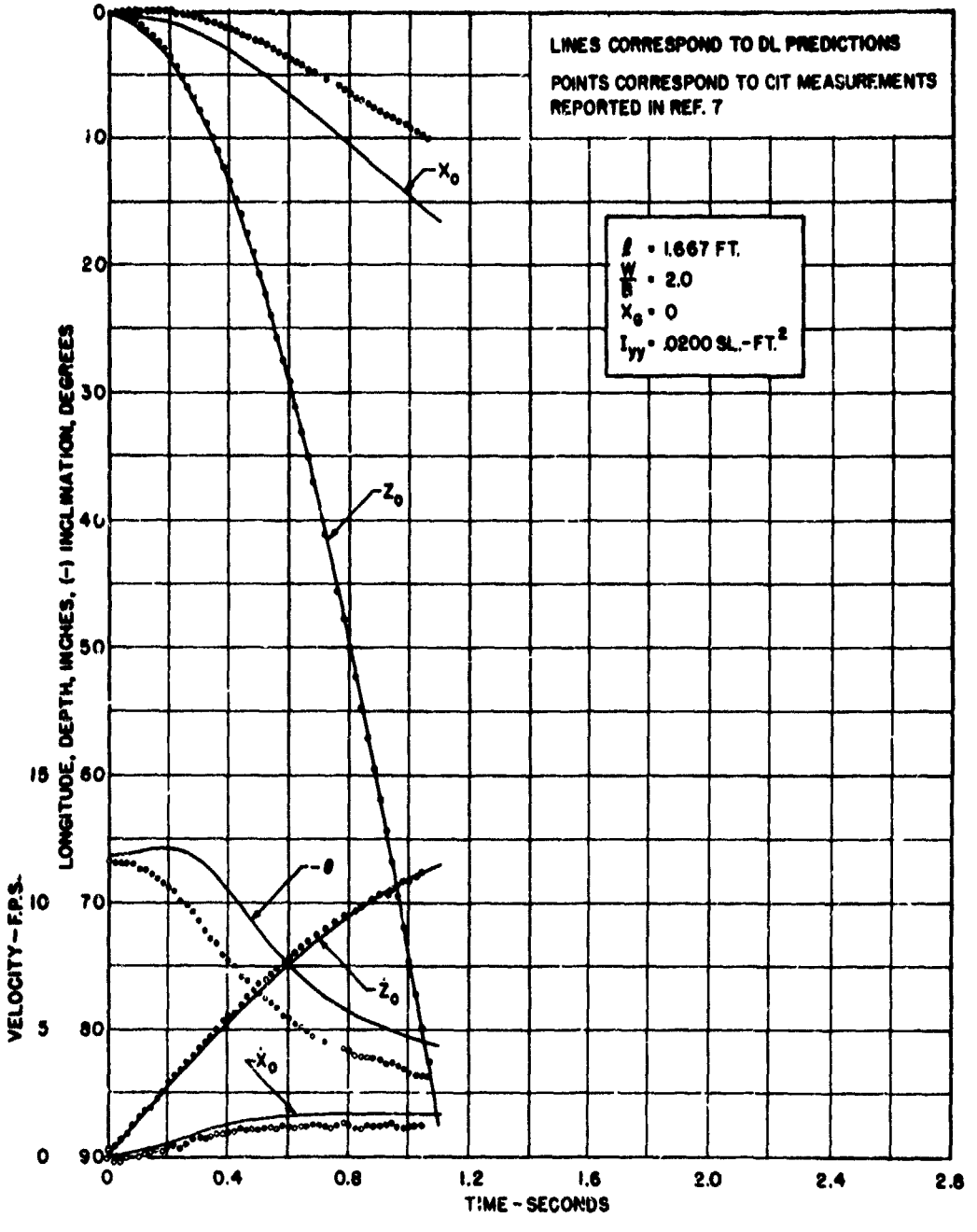

FIGURE 17. COMPARISON OF EXPERIMENTAL AND PREDICTED TRAJECTORIES FOR D.L. CALCULATION NO. 12

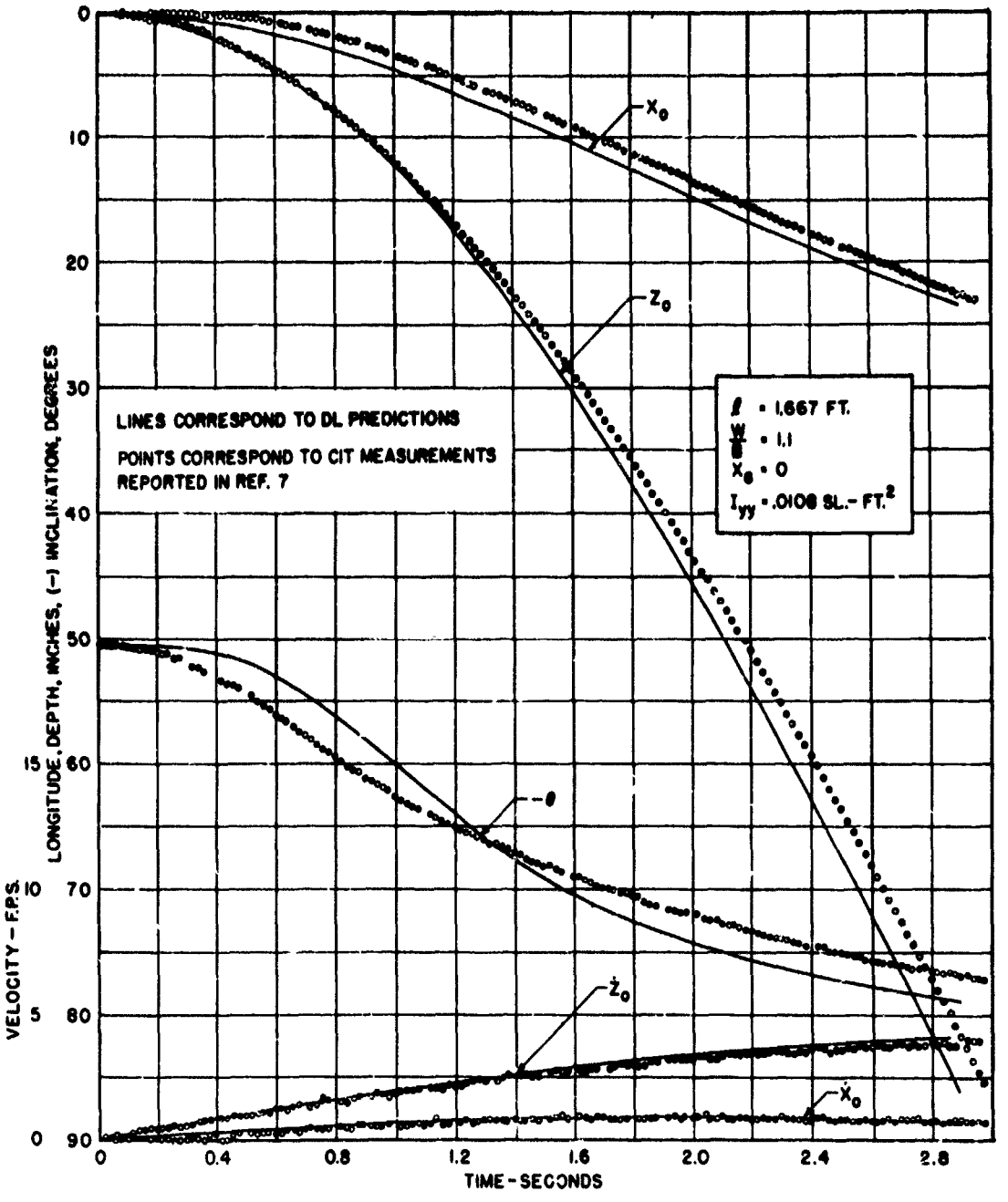

FIGURE 18. COMPARISON OF EXPERIMENTAL AND PREDICTED TRAJECTORIES FOR DL CALCULATION NO. 16

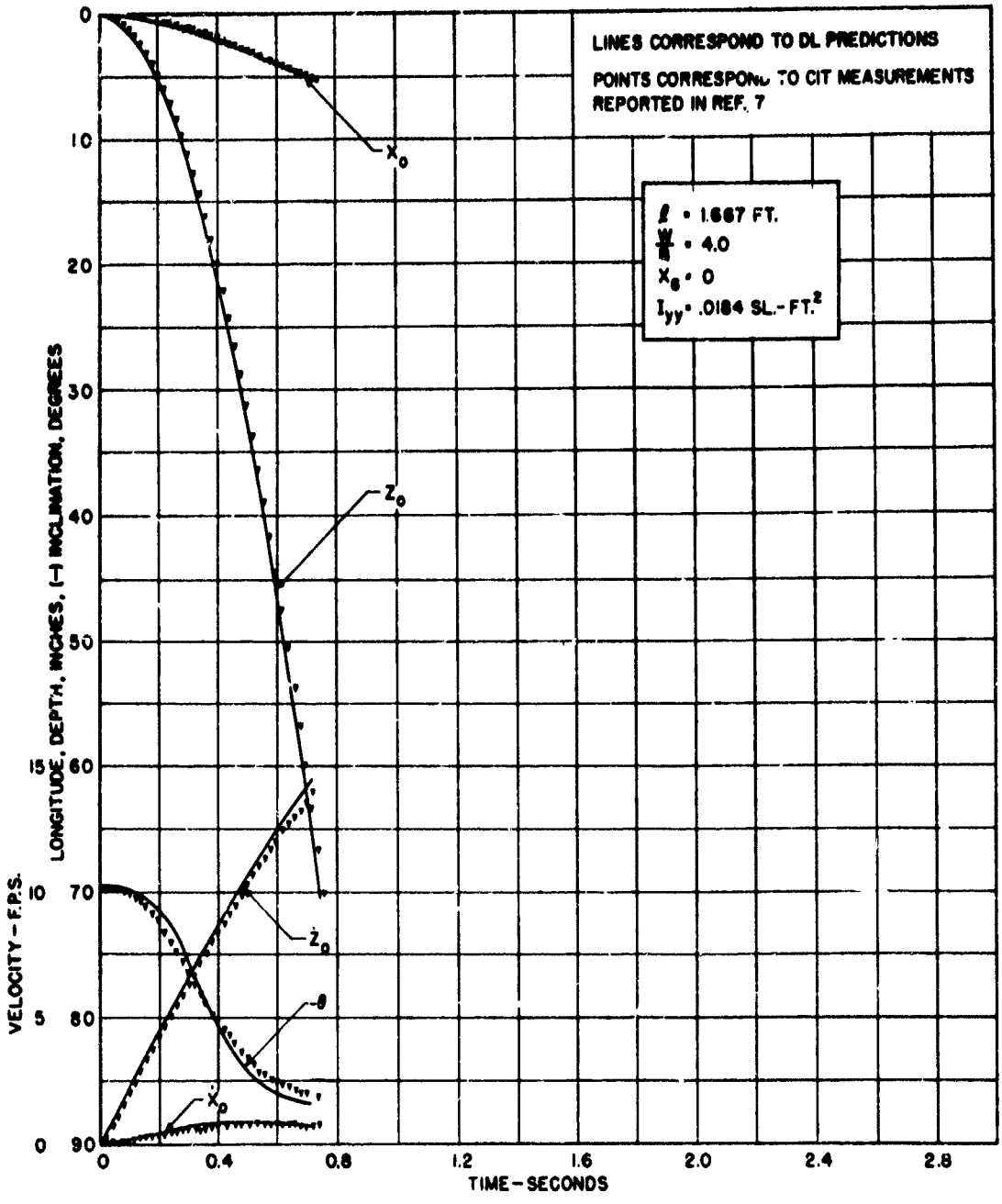

FIGURE 19. COMPARISON OF EXPERIMENTAL AND PREDICTED TRAJECTORIES FOR DL CALCULATION NO. 18

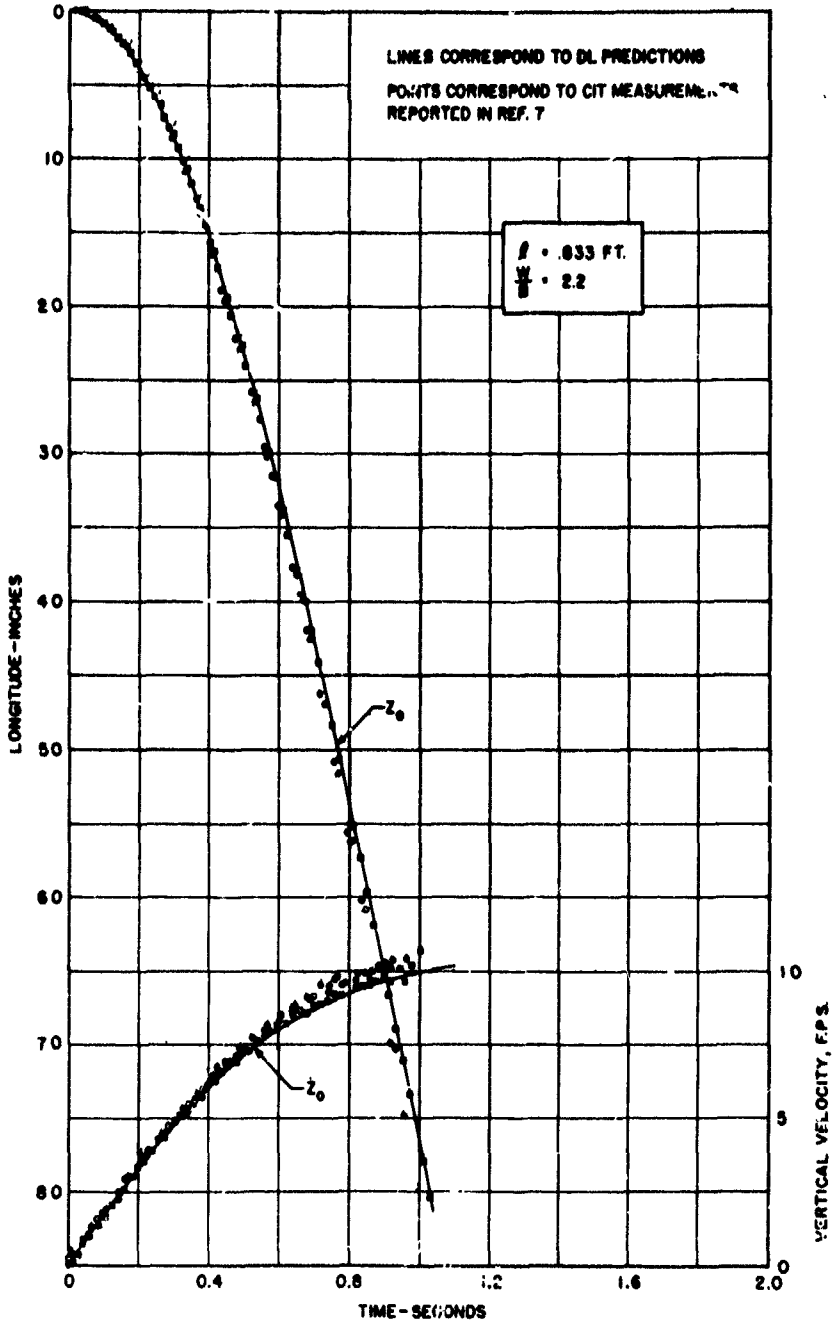

FIGURE 20. COMPARISON OF EXPERIMENTAL AND PREDICTED TRAJECTORIES FOR DL CALCULATION NO 20

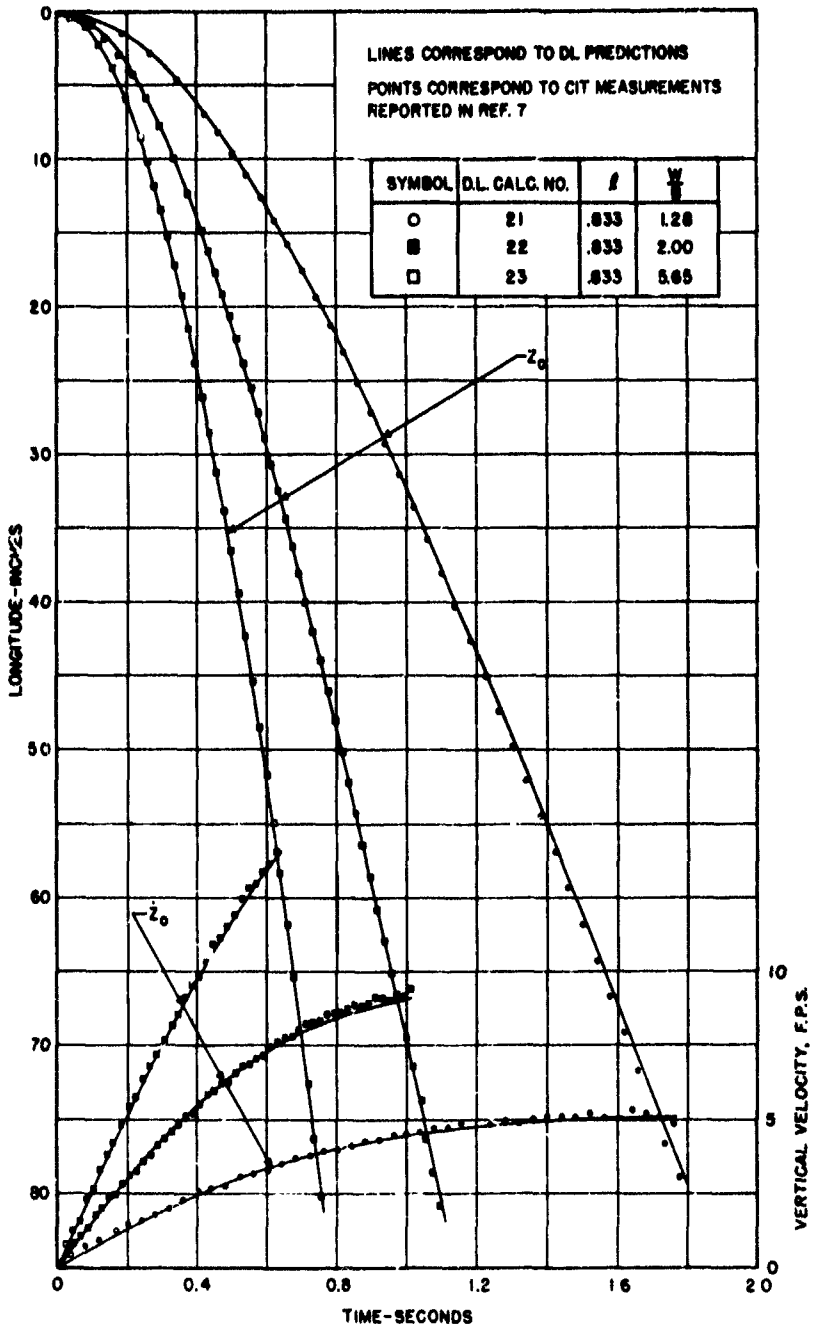

FIGURE 21. COMPARISON OF EXPERIMENTAL AND PREDICTED TRAJECTORIES FOR DL. CALCULATIONS NOS. 21, 22, 23

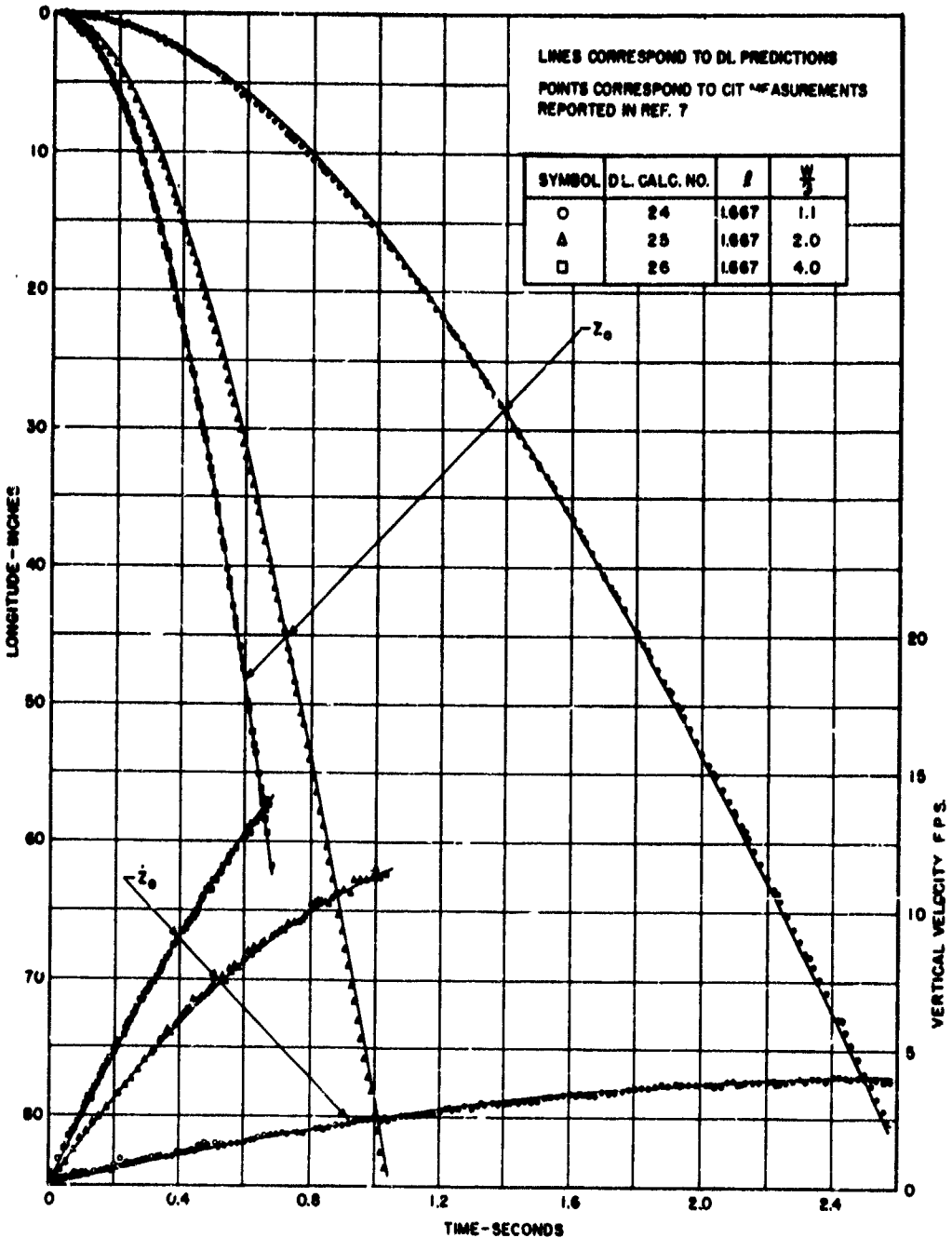

FIGURE 22. COMPARISON OF EXPERIMENTAL AND PREDICTED TRAJECTORIES FOR D.L. CALCULATIONS NOS 24, 25, 26

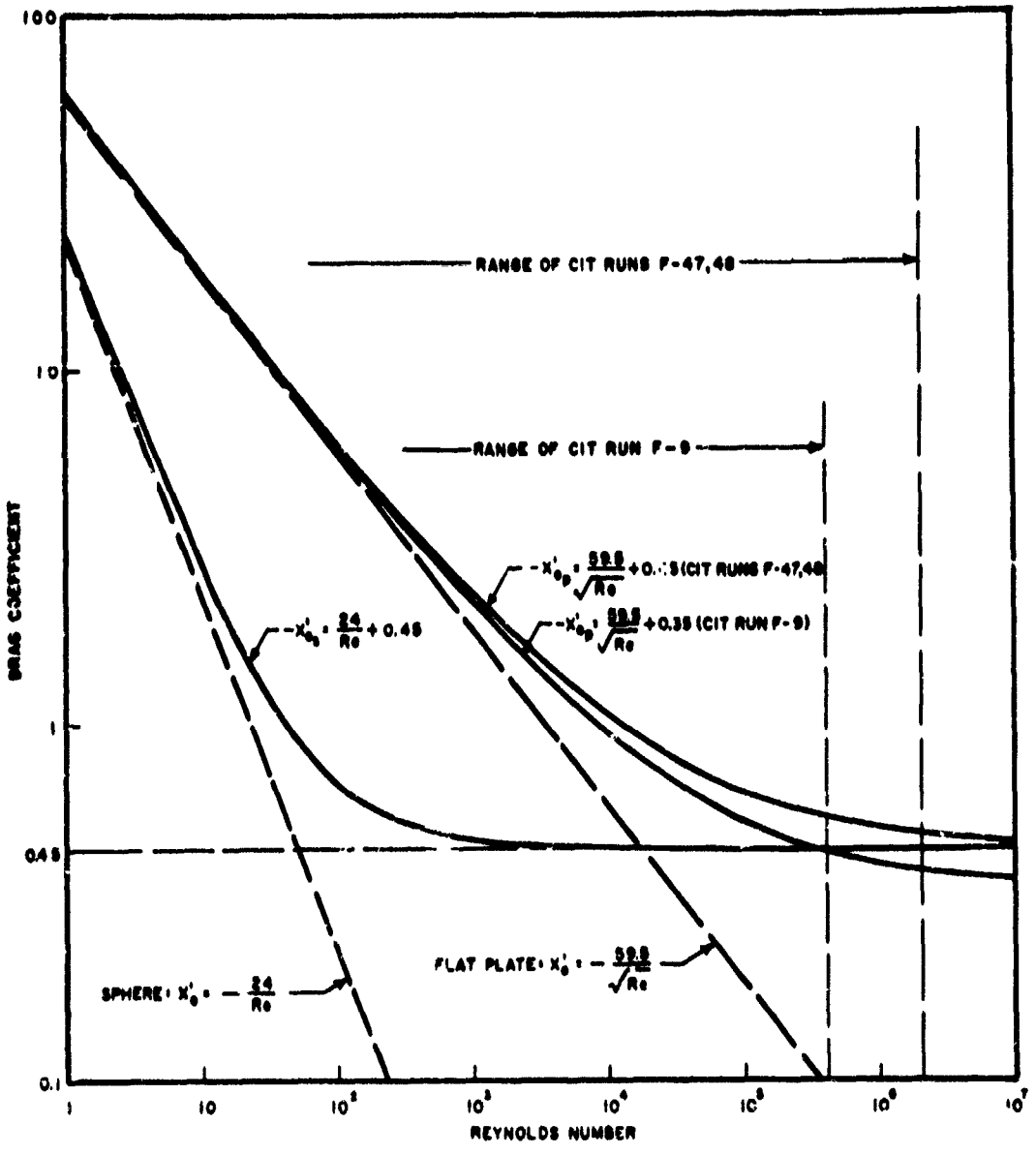

FIGURE 23. REYNOLDS NUMBER DEPENDENT DRAG COEFFICIENTS

DISTRIBUTION LIST

Copies

Alden Hydraulic Laboratory
Worcester Polytechnic Institute
Worcester 9, Massachusetts
1 Attn: Professor L. J. Hooper
Via: Office of Naval Research
Branch Office
Boston 10, Massachusetts

California Inst. of Technology
Pasadena, California
1 Attn: Hydrodynamics Laboratory
Via: Commanding Officer
Office of Naval Research
Branch Office
1030 East Green Street
Pasadena 1, California

1 Commanding Officer
Office of Naval Research
Branch Office
207 W. 24th Street
New York 11, N. Y.

General Dynamics/Convair
San Diego, California
1 Attn: Chief of Hydrodynamics
Via: Bureau of Naval Weapons
Representative
San Diego, California

Aerojet General Corporation
6352 N. Irwindale Avenue
Azusa, California
1 Attn: C. A. Gongwer
Via: Bureau of Naval Weapons
Representative
Azusa, California

Underwater Launch Department
Lockheed Missiles and Space Div.
Sunnyvale, California
1 Attn: R. W. Kermeen
Via: Bureau of Naval Weapons
Representative
Sunnyvale, California

Advanced Systems Engineering
Westinghouse Electric Corporation
Hendy Avenue
Sunnyvale, California
1 Attn: M. S. Macovsky
Via: Resident Inspector of
Naval Material
Sunnyvale, California

Goodyear Aircraft Corporation
Akron 15, Ohio
1 Attn: R. R. Fisher
Via: Bureau of Naval Weapons
Representative
Akron 15, Ohio

1 Applied Physics Laboratory
Johns Hopkins University
8621 Georgia Avenue
Silver Spring, Maryland

1 Cornell Aeronautical Lab Inc.
Buffalo 21, New York
Via: Bureau of Naval Weapons
c/o Cornell Aeronautical Lab
Buffalo 21, New York

Vidya, Incorporated
2626 Hanover Street
Stanford Industrial Park
Palo Alto, California
1 Attn: J. N. Nielsen
Via: Office of Naval Research
Resident Representative
Stanford University
Electronics Research Lab
Palo Alto, California

DISTRIBUTION LIST

Copies

Chief, Bureau of Naval Weapons
Department of the Navy
Washington 25, D.C.
3 Attn: Code RRRE-4
1 RAAD-3
1 RUTO-32
2 DLI-3
1 SP-22
1 RU-2

Commanding Officer and Director
David Taylor Model Basin
Carderock, Maryland
1 Attn: Hydrodynamics Laboratory

Commander
Naval Air Missile Test Center
1 Point Mugu, California

Commander
Naval Ordnance Test Station
Inyokern, China Lake
California
1 Attn: Technical Library

Commander
Naval Ordnance Test Station
Pasadena, California
1 Attn: Code P8074
1 P8O

Commander
Naval Ordnance Laboratory
White Oak, Silver Spring, Md.
1 Attn: Code BR
1 HL

Commanding Officer
Naval Underwater Ordnance Sta.
1 Newport, Rhode Island

Officer in Charge
Naval Aircraft Torpedo Unit
U. S. Naval Air Station
Quonset Point, Rhose Island
1 Attn: R. Crowell

Commanding Officer
Naval Torpedo Station
Keyport, Washington
1 Attn: J. Mason

Commander
Naval Weapons Laboratory
Dahlgren, Virginia
1 Attn: Technical Library

Chief of Naval Research
Department of the Navy
Washington 25, D. C.
1 Attn: Code 438

Ballistic Research Laboratory
Aberdeen Proving Grounds
1 Aberdeen, Maryland

Commander
Office of Aerospace Research
1 Washington 25, D. C.

Documents Service Center
ASTIA
Arlington Hall Station
Arlington 12, Virginia
Via: Chief,
Bureau of Naval Weapons (DLI-3)
10 Washington 25, D. C.

National Aeronautics and Space Adm
400 Maryland Ave., S. W.
4 Washington 25, D. C.
1 Attn: Code SP

Ordnance Research Laboratory
Pennsylvania State University
State College, Pennsylvania
1 Attn: Dr. G. F. Wislicenus
Via: Inspector of Naval Material
Southeastern District
Reading, Pennsyvania

Davidson Laboratory Report No. 898 UNCLASSIFIED

PREDICTION OF TRAJECTORIES
FOR AN UNDERWATER MISSILE

by Howard Dugoff, February 1963

Nonlinear motion equations were used to predict vertical planar trajectories of the Basic Finner Missile observed previously in underwater model experiments at California Institute of Technology. Values of the hydrodynamic coefficients appearing in the motion equations were obtained from Basic Finner experiments made previously at CIT, Bureau of Standards, and Davidson Laboratory. Coefficients also were estimated on theoretical grounds. The observed trajectories could not be predicted using experimental coefficients alone. However, theoretical coefficients yielded predictions that agreed well with the observed motions. Computed trajectories were particularly sensitive to independent changes in the values of the hydrodynamic static and damping derivative coefficients. However, when these values were kept consistent with relations expressing their physical interdependence, they could be varied over fairly wide ranges without appreciably affecting the predictions.

Davidson Laboratory Report No. 898 UNCLASSIFIED

PREDICTION OF TRAJECTORIES
FOR AN UNDERWATER MISSILE

by Howard Dugoff, February 1963

Nonlinear motion equations were used to predict vertical planar trajectories of the Basic Finner Missile observed previously in underwater model experiments at California Institute of Technology. Values of the hydrodynamic coefficients appearing in the motion equations were obtained from Basic Finner experiments made previously at CIT, Bureau of Standards, and Davidson Laboratory. Coefficients also were estimated on theoretical grounds. The observed trajectories could not be predicted using experimental coefficients alone. However, theoretical coefficients yielded predictions that agreed well with the observed motions. Computed trajectories were particularly sensitive to independent changes in the values of the hydrodynamic static and damping derivative coefficients. However, when these values were kept consistent with relations expressing their physical interdependence, they could be varied over fairly wide ranges without appreciably affecting the predictions.

Davidson Laboratory Report No. 896 UNCLASSIFIED

PREDICTION OF TRAJECTORIES
FOR AN UNDERWATER MISSILE

by Howard Dugoff, February 1963

Nonlinear motion equations were used to predict vertical planar trajectories of the Basic Finner Missile observed previously in underwater model experiments at California Institute of Technology. Values of the hydrodynamic coefficients appearing in the motion equations were obtained from Basic Finner experiments made previously at CIT, Bureau of Standards, and Davidson Laboratory. Coefficients also were estimated on theoretical grounds. The observed trajectories could not be predicted using experimental coefficients alone. However, theoretical coefficients yielded predictions that agreed well with the observed motions. Computed trajectories were particularly sensitive to independent changes in the values of the hydrodynamic static and damping derivative coefficients. However, when these values were kept consistent with relations expressing their physical interdependence, they could be varied over fairly wide ranges without appreciably affecting the predictions.

Davidson Laboratory Report No. 898 UNCLASSIFIED

PREDICTION OF TRAJECTORIES
FOR AN UNDERWATER MISSILE

by Howard Dugoff, February 1963

Nonlinear motion equations were used to predict vertical planar trajectories of the Basic Finner Missile observed previously in underwater model experiments at California Institute of Technology. Values of the hydrodynamic coefficients appearing in the motion equations were obtained from Basic Finner experiments made previously at CIT, Bureau of Standards, and Davidson Laboratory. Coefficients also were estimated on theoretical grounds. The observed trajectories could not be predicted using experimental coefficients alone. However, theoretical coefficients yielded predictions that agreed well with the observed motions. Computed trajectories were particularly sensitive to independent changes in the values of the hydrodynamic static and damping derivative coefficients. However, when these values were kept consistent with relations expressing their physical interdependence, they could be varied over fairly wide ranges without appreciably affecting the predictions.